Airborne LiDAR: A New Source of Traffic Flow Data

Dorota A. Grejner-Brzezinska, Ph.D., Charles Toth, Ph.D.
and Mark McCord, Ph.D.

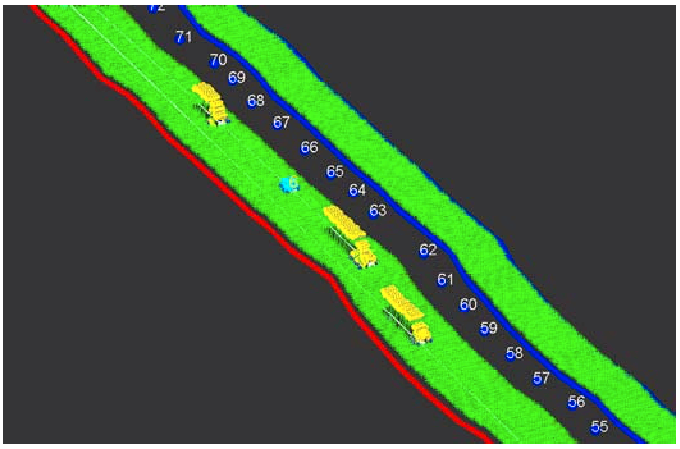

for the
Ohio Department of Transportation
Office of Research and Development

State Job Number ***134145***

October 2005

THE OHIO STATE UNIVERSITY

FHWA

RESEARCH & DEVELOPMENT

1. Report No.	2. Government Accession No.	3. Recipient's Catalog No.
FHWA/OH-2005/14		

4. Title and subtitle	5. Report Date
Airborne LiDAR: A New Source of Traffic Flow Data	***October 2005***
	6. Performing Organization Code

7. Author(s)	8. Performing Organization Report No.
Dorota A. Grejner-Brzezinska, Ph.D. ***Charles Toth, Ph.D.*** ***Mark McCord, Ph.D.***	
9. Performing Organization Name and Address	10. Work Unit No. (TRAIS)
The Ohio State University ***Department of Civil & Environmental Engineering & Geodetic Science*** ***Center for Mapping*** ***Columbus, Ohio 43212***	11. Contract or Grant No. ***134145***
	13. Type of Report and Period Covered
12. Sponsoring Agency Name and Address Ohio Department of Transportation 1980 West Broad Street Columbus, Ohio 43223	14. Sponsoring Agency Code

15. Supplementary Notes

16. Abstract

LiDAR (or airborne laser scanning) systems became a dominant player in high-precision spatial data acquisition to efficiently create DEM/DSM in the late 90's. With increasing point density, new systems are now able to support object extraction, such as extracting building and roads, from LiDAR data. The novel concept of this project was to use LiDAR data for traffic flow estimates. In a sense, extracting vehicles over transportation corridors represents the next step in complexity by adding the temporal component to the LiDAR data feature extraction process. The facts are that vehicles are moving at highway speeds and the scanning acquisition mode of the LiDAR certainly poses a serious challenge for the data extraction process. The OSU developed method and it implementation, the I_FLOW program, have demonstrated that LiDAR data contain valuable information to support vehicle extraction, including vehicle grouping and localizations. The classification performance showed strong evidence that the major vehicle categories can be efficiently separated. The I_FLOW program is ready for deployment.

17. Key Words	18. Distribution Statement
LiDAR, traffic flow	No restrictions. This document is available to the public through the National Technical Information Service, Springfield, Virginia 22161

19. Security Classif. (of this report)	20. Security Classif. (of this page)	21. No. of Pages	22. Price
Unclassified	Unclassified	***79***	

Form DOT F 1700.7 (8-72) **Reproduction of completed pages authorized**

Project title:

Airborne LiDAR: A New Source of Traffic Flow Data

SJN: 134145

Authors:

Dorota A. Grejner-Brzezinska, Ph.D., Charles Toth, Ph.D.
and Mark McCord, Ph.D.

Research Agency:
The Ohio State University

Report date: October 2005

Sponsoring Agency
Ohio Department of Transportation, Office of Aerial Engineering

Prepared in cooperation with the Ohio Department of Transportation and the U.S. Department of Transportation, Federal Highway Administration

Disclaimer

The contents of this report reflect the views of the authors who are responsible for the facts and the accuracy of the data presented herein. The contents do not necessarily reflect the official views or policies of the Ohio Department of Transportation or the Federal Highway Administration. This report does not constitute a standard, specification or regulation.

Acknowledgments

The authors thank the staff of the ODOT Office of Aerial Engineering for their contributions to this project. In particular, we want to express our gratitude to John Ray, Administrator, Office of Aerial Engineering, for his continuing support and coordination of the system acquisition and the field testing.

Table of content

1. INTRODUCTION

LiDAR (or airborne laser scanning) systems became a dominant player in high-precision spatial data acquisition in the late 90's. This new technology quickly established itself as the main source of surface information in commercial mapping, delivering surface data at decimeter-level vertical accuracy in an almost totally automated way.

Every indication is that transportation and other agencies will be deploying LiDAR systems over transportation corridors at an increasing rate in the future. The Ohio Department of Transportation is one the first agencies that already operates a state-of-the-art LiDAR system to support the Office of Aerial Engineering operations. Primarily for engineering purposes, the road surface is surveyed at sub-decimeter level accuracy. Vehicles on the road represent obstructions to the LiDAR pulses sent to reflect off the pavement. Therefore, a substantial amount of processing must be devoted to "removing the vehicle signals" to obtain the actual road surface. Rather than removing and discarding the signals, we suggest turning them into traffic flow information. This way, LiDAR surveys dedicated to surface extraction will soon be able to provide a valuable byproduct with little additional effort. Since the ODOT LiDAR system has been in operation, such data are already available to support the traffic flow extraction.

Acquiring flow data in a timely manner is essential for many transportation processes, especially for traffic monitoring and management. Ground-based systems typically use loop detectors and video cameras. These systems provide excellent data at a local scale, but consequently are less appropriate for monitoring flow patterns over longer road segments. Remote sensing sensors, especially airborne systems, however, show somewhat complimentary characteristics; namely that the acquired data can effectively support flow information extraction in a dynamic manner. Not only can vehicle counts and velocities be estimated, but also complex flow patterns such as slowdowns and intersection/ramp turning movements can be identified and quantified.

2. RESEARCH OBJECTIVES

The goal of this research is to investigate the feasibility of using LiDAR data collected over transportation corridors for extracting traffic flow information. The primary objectives of this research project were as follows:

- To develop and test techniques of identifying and extracting vehicles from LiDAR data.
- To create vehicle categories and to develop methods for automatic vehicle classification.
- To develop and test velocity estimation techniques by the vehicle category.
- To implement methods to test the effectiveness of using LiDAR intensity data to support the vehicle extraction, classification, and the velocity estimation processes.
- To develop a fusion technique to combine LiDAR and optical image data to improve the performance of the vehicle extraction and velocity estimation processes. This will also strongly support the road surface extraction process, a major interest to the Office of Aerial Engineering.
- To analyze the mutual benefits of combining the surface extraction and traffic flow extraction processes.
- To build a metrics to assess the performance of the surface and flow data extraction process with respect to various sensor configurations, such as LiDAR operational parameters, digital camera performance, flight conditions, georeferencing quality, etc.
- To assess the feasibility of real-time data extraction for real-time traffic management.
- To prepare a final report to document the findings of this research, and to provide meaningful data for future decision-making for traffic management purposes.

3. GENERAL DESCRIPTION OF RESEARCH

The feasibility of extracting vehicles from LiDAR data had been tested prior to the project (see References). Therefore, the project was to extend the investigation of the concept viability and then implement a prototype system that could directly support traffic management operations. Most of the effort went into algorithmic developments and software programming. The objective, to deliver a robust system that could support production at ODOT, posed a real difficulty for the research staff as it required software engineering skills beyond the usual level in research. The project benefited from the recently acquired Optech 30/70 ALTM LiDAR system that went into full operation about half way through the project. Three datasets, flown by the new LiDAR system, provided an excellent test database for both the program developments and testing.

4. RESULTS

To support the initial algorithmic research, data were provided by industrial partners; in particular, Woolpert LLC made available useful datasets. Later the new LiDAR system of the Aerial Engineering Office became the sole source of test data. The following three datasets were used:

- Toronto, CA, ODOT LiDAR system acceptance test flight, February 19, 2004.
- Ashtabula, OH, I-90 corridor mapping survey, November 16, 2004.
- Madison County, OH, calibration range dedicated test flight, Dec 4, 2004.

The data from these flights were primarily used for algorithmic tuning and software developments. The OSU developed program, called I_FLOW, represents the ultimate end result of the project. I_FLOW is able to input standard LiDAR data files in the standard format as they are output by REALM during normal processing and then extracts vehicles from LiDAR data, groups them into main vehicle categories, estimates velocity, and outputs a list of extracted vehicles with attribute information of time, location, and velocity. The program and detailed description of the results are provided in Appendices C and A. Using the imagery simultaneously collected by the ODOT DSS camera, a basic feasibility study was performed to assess the fusion of the two datasets to improve the quality, in particular, the velocity estimates, of the traffic flow extraction. Details are provided in Appendix B.

5. CONCLUSIONS

The I_FLOW program provides a complete implementation of all the algorithmic research results related to extracting and characterizing vehicles from LiDAR data that were developed in the project. The software has performed well all the three datasets recently acquired by the new ODOT LiDAR system. In addition, the execution time is also acceptable – LiDAR data come as tens of millions of points and handling such an amount of data is not an obvious task.

6. IMPLEMENTATION PLAN

The I_FLOW program is ready for installation in the OAE. The program description and the source code are included in Appendix C. If required, a short training course can be provided for ODOT personnel.

BIBLIOGRAPHY

1. Toth, C., Barsi A. and Lovas T.: Vehicle Recognition from LiDAR Data, *International Archives of Photogrammetry and Remote Sensing*, Vol. XXXIV, part 3/W13, pp. 163-166, 2004.
2. Grejner-Brzezinska D. and Toth C., 2003. Deriving Vehicle Topology and Attribute Information over Transportation Corridors from LIDAR Data, ION Annual Meeting, Albuquerque, NM, June 22-24, 2003.
3. Toth C., Grejner-Brzezinska D. and Lovas T.: Traffic Flow Estimates from LiDAR Data, Proc. ASPRS Annual Conference, May 5-9, pp. 203-212, CD ROM, 2003.
4. Toth, C., 2002. Airborne LIDAR Systems: Supporting Traffic Flow Estimates, 3rd International LIDAR Workshop, October 7-9, Columbus, Web.

APPENDIX A

1. Grejner-Brzezinska, D., Toth, C., Moafipoor, S. and Paska, E. 2004: Precise Vehicle Topology and Road Surface Modeling Derived from Airborne LiDAR Data**,** ION GNSS 2004, Long Beach, CA, September 21-24, 2004, CD-ROM.
2. Toth C, Grejner-Brzezinska D. and Moafipoor, S. 2004: Detecting Moving Targets from Airborne LiDAR Data, ION 2004 Annual Meeting, Dayton, OH, June 7-9, 2004, CD-ROM
3. Toth, C. and Grejner-Brzezinska, D., 2004: Vehicle Classification from LiDAR Data to Support Traffic Flow Estimates, Proc. of 3rd International Symposium on Mobile Mapping Technology, Kunming, China, March 29-31, 2004, CD-ROM.

Traffic flow parameter estimation and road surface modeling from airborne LiDAR data

Dorota Grejner-Brzezinska[1], Charles Toth[2], Eva Paska[1,2] and Shahram Moafipoor[1,2]

National Consortium for Remote Sensing in Transportation – Flows (NCRST-F)
The Ohio State University

[1] *Geodetic and Geoinformation Science*
470 Hitchcock Hall, 2070 Neil Avenue
Columbus, Ohio 43210
Tel: 641-292-8787; Fax: 614-292-2957

[2] *Center for Mapping*
1216 Kinnear Road, Columbus, OH 43212

e-mail: dbrzezinska@osu.edu

BIOGRAPHY

Dr. Dorota Brzezinska is an Associate Professor in Geodetic and Geoinformation Science, The Ohio State University (OSU). Prior to that, she was a Research Specialist at the OSU Center for Mapping. She received an MS in Surveying and Land Management from the Agricultural and Technical University of Olsztyn, Poland, and an MS and a Ph.D. in Geodesy from OSU. Her research interests cover precise kinematic positioning with GPS, precision orbit determination for GPS/LEO, GPS/INS integration, mobile mapping technology, and robust estimation techniques. Between 1990-1995 she was a Fulbright Fellow at OSU. She is the 2003-2005 Land Representative for the ION Council, chair of IAG Sub-Commission 4.1, *Multi-sensor Systems*, a co-chair of the IAG Study Group 4.1, *Pseudolite Applications in Positioning and Navigation*, and a chair of the Task Force 5.3.1, *Mobile Mapping Systems* of FIG WG 5.3.

Dr. Charles Toth is a Senior Research Scientist at the Ohio State University Center for Mapping. He received an MS in Electrical Engineering and a Ph.D. in Electrical Engineering and Geoinformation Sciences from the Technical University of Budapest, Hungary. His research expertise covers broad areas of 2D/3D signal processing, spatial information systems, high-resolution imaging, surface extraction, modeling, integratiion and calibration of multi-sensor systems, multi-sensor geospatial data acquisition systems, and mobile mapping technology. He is Chairing ISPRS WG I/2 on LiDAR and InSAR Systems and serves as the Director for the Photogrammetric Application Division of ASPRS.

Eva Paska graduated in June of 2001 from the Department of Surveying and Geoinformatics, Budapest University of Technology and Economics, Hungary, with an MS in Surveying and Geoinformatics Engineering. Between 2000 and 2002 she worked as an intern at The Ohio State University Center for Mapping. Since July 2002 she has been a graduate student at The Ohio State University, Department of Civil and Environmental Engineering and Geodetic Science. Her research interests cover image processing, LiDAR data processing/segmentation, and estimation techniques.

Mr. Shahram Moafipoor is a PhD student in the Department of Geodetics Science, The Tehran University, and currently he is a visiting scholar in the Department of Civil and Environmental Engineering and Geodetic Science, The Ohio State University. Prior to that, he was a researcher at National Cartography Center NCC, Iran. He obtained an MS degree in photogrammetry from Tehran University in Tehran, Iran in 1998 and B.Sc in surveying from Tehran University in Tehran, Iran in

1993. His research interests include navigation systems, aerial photography, and digital photogrammetry.

ABSTRACT

The National Consortium for Remote Sensing in Transportation-Flows (NCRST-F), led by The Ohio State University, and sponsored by the U.S. Department of Transportation and NASA, was established in 2001. Our partners in NCRST-F are the University of Arizona and George Mason University. The major focus of the OSU research team is to improve the efficiency of the transportation system by the integration of remotely sensed data with the traditional ground data to monitor and manage traffic flows. Our research team is concerned with the vehicle extraction and traffic pattern modeling based on airborne digital data, collected by frame cameras and LiDAR systems (Light Detection and Ranging). This paper is an extension of our earlier publications, where theoretical and practical studies on the feasibility of using LiDAR data and airborne imagery collected over the transportation corridors for estimation of traffic flow parameters were presented. In this contribution the actual example of traffic flow estimation obtained from high-accuracy data set, collected in February 2004 in Toronto, Canada is presented. In particular, vehicle extraction, classification into major categories, and velocity estimation, as a primary parameter describing the traffic flow, are discussed and analyzed.

The updated algorithms and methodology of extracting vehicle information together with the road surface modeling with LiDAR, precisely georeferenced by GPS/INS sensors, and augmented by LiDAR intensity information, are discussed. We demonstrate that our algorithms are fast and efficient and are capable of autonomous traffic flow information extraction. It is shown, however, that for better accuracy and reliability, a fusion of LiDAR with frame image data is desirable. Nonetheless, based on the high spatial density LiDAR data, we demonstrate that vehicle extraction and their coarse classification as well as estimation of flow can be efficiently performed in parallel to the efficient and automated road surface extraction and modeling.

1. INTRODUCTION

In recent years, remote sensing has made remarkable technological progress and has significantly expanded its application fields reaching science and engineering disciplines, formerly served exclusively by traditional tracking, positioning and mapping technologies. One of the examples is the traffic flow monitoring with airborne remote sensing methods, which in the past few years has been a major research focus of the National Consortium for Remote Sensing in Transportation-Flows (NCRST-F), led by The Ohio State University. Rapid technological advances that broadened the range of remote sensing applications stimulated the research community to reach beyond conventional uses of remote sensing, leading to the establishment of NCRST-F.

Transportation represents a major segment of the world's economy, and as such must be carefully monitored and planned, which require the most up-to-date, accurate and continuous methods of screening, mapping modeling and managing.

One of the important traffic measures is the ratio representing the number of vehicles per population sample. For example, there are more than 100 vehicles for every 100 people in the United States; the rate is about 50 and 25 in Western and Eastern Europe, respectively. On average (i.e., worldwide) the development of the transportation infrastructure, does not keep up with the growth of the number of vehicles and passenger-miles traveled, which emphasizes the necessity for better monitoring and more efficient traffic management methods. This, ultimately, requires better, faster, more reliable and continuous traffic data, which can by acquired with newer, better sensors and modern remote sensing techniques. Finally, only efficient traffic flow monitoring, supported by state-of-the-art technology and modeling methods may lead to effective, real-time traffic management.

To meet the demanding requirements of traffic flow monitoring and transportation management, the Consortium adopted the primary goals of improving the efficiency of the transportation system by integrating remotely sensed traffic flow data obtained from airborne and/or satellite platforms with traditional data collected on the ground.

Effective traffic monitoring and management require intelligent data acquisition and fusion from different sensors and platforms. The traditional technologies of traffic flow sensing, including inductive loop detectors, video cameras, roadside beacons, and travel probes, are based on fixed locations in the transportation network, and thus may not provide sufficient spatial and temporal resolutions. Although these detectors provide useful information locally, they generally do not provide sufficient coverage for traffic flows over larger areas. Airborne and spaceborne remote sensing technology, however, can provide data in large spatial extent with varying temporal and spatial resolutions. The primary objective of this research effort is the flow extraction from airborne platform data, while other members of NCRST-F use information generated by spaceborne platforms and sensors.

As part of the NCRST-F research effort, we conducted extensive investigations on using airborne LiDAR and digital imagery as a source of traffic flow data. Our initial studies supported by experimental tests confirmed that using LiDAR data and/or aerial imagery for the traffic flow estimation is feasible (see reference list for more details on the algorithms). This paper describes our currently used method of vehicle detection, extraction and tracking from both imagery and LiDAR, which forms the basis for traffic flow parameter estimation, including vehicle count, classification and vehicle velocity estimates. Vehicle extraction and classification are the basis of the vehicle density evaluation. Average vehicle density and speed, as well as traffic flow are the main parameters describing a traffic stream. In other words, the density is the number of vehicles traveling a predefined length of the road, while traffic flow represents the amount of vehicles traveling over a road segment in a given time period. Thus, speed multiplied by the density provides the traffic flow estimate.

This paper is the continuation of research presented earlier (Grejner-Brzezinska and Toth, 2002 and 2003a-b; Toth et al, 2003 a-b); new examples of traffic flow estimation together with its accuracy assessment are presented. The analyses are based on the high-density (2-4 points/m^2) LiDAR data collected on February 19, 2004 over the downtown Toronto area with the Optech ALTM 30/70 LiDAR system. The work presented in this paper is currently sponsored by the Ohio Department of Transportation (ODOT).

2. THE CONCEPT

The motivation for using LiDAR as a new source of traffic data follows from the success, measured in performance, of this technology in civilian mapping. In less than five years, LiDAR technology, illustrated in Figure 1, became the main source of surface information in topographic mapping. Although aimed at acquiring only surface points, the latest high-performance LiDAR systems can deliver very dense and accurate point clouds, and thus provide data for more sophisticated applications, such as object extraction, including traffic flow data collection over the transportation corridors. Recent advances in LiDAR technology, such as the availability of the intensity data of the reflected laser pulse, the increased number of recorded returns from a single laser beam (4 to 5), and the laser repetition rate approaching 100 kHz, support the expansion of the technology from simple surface extraction to more demanding feature extraction applications.

The primary advantages of LiDAR as an efficient and accurate mapping tool are: (1) the sensor is virtually independent on weather/cloud coverage and day/night conditions, (2) continuous (near continuous) data stream, (3) fast and accurate measurement of the road surface and structure that mainly depends on the quality of the direct georeferencing based on GPS/INS integration. The primary disadvantages are: (1) no object information and no texture since are available as LiDAR

data come in the form of a point cloud with X, Y, and Z spatial coordinates (this, however, changes as intensity information becomes available), (2) geometric distortions – shortening/elongation of moving objects (due to scanning), (3) limited spatial resolution – may change as pulse rate is increasing, and (4) high cost. It should be mentioned, however, that disadvantage (2) is effectively used in our research, as the velocity estimation is based on the vehicle elongation/contraction information, as explained in the sequel. It should be emphasized that the ultimate accuracy of LiDAR data is defined not only by the sensor quality, but primarily by the accuracy of the direct sensor orientation provided by GPS/INS, and the inter-sensor calibration of the GPS/INS/LiDAR system.

The price of LiDAR technology is still prohibitive for dedicated missions supporting only traffic monitoring. However, LiDAR data collected for routine infrastructure and topographic mapping applications over the transportation corridors can easily provide traffic flow information. For example, in order to determine the road surface and/or road infrastructure, the vehicles becomes obstacles that need to be removed. This information should not be discarded, however, but rather it should be directly converted to the traffic flow data. Collecting data over the transportation corridors during regular surveys offers a unique opportunity to obtain important data for transportation planners and managers at no additional cost. Data can be acquired also in transit while the system is flown between various mapping jobs.

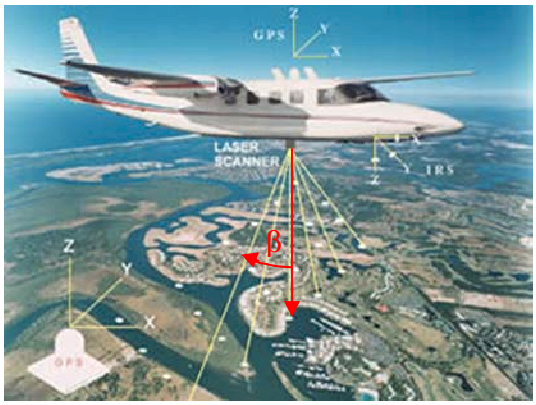

Figure 1. LiDAR data collection concept.

Figure 2 illustrates the workflow for the traffic flow extraction from LiDAR data. The primary tasks are: (1) input data pre-processing, (2) road surface extraction, (3) vehicle modeling, and (4) traffic flow estimation. The main steps needed for the velocity estimations, after the road surface was extracted and separated from the vehicles (see, Toth *et al.,* 2004) are (1) vehicle extraction, (2) primary parameterization of the vehicle's shape – vehicle modeling, (3) feature space selection – parameter optimization, and (4) vehicle classification. The next step in the semi-automated process, illustrated in Figure 2, is the vehicle velocity estimation followed by the traffic flow data computation, and finally, the accuracy assessment. The details of the road surface and vehicle extraction process can be found in (Toth *et al.,* 2004, 2003a-b; Grejner-Brzezinska and Toth, 2003a-b), and only an outline of the major processing steps is presented here for completeness.

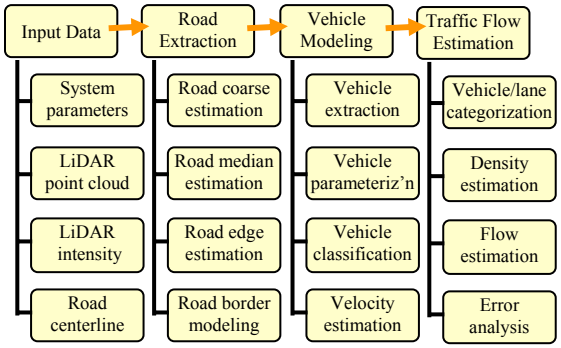

Figure 2. Data processing architecture.

The major steps of the road extraction process from LiDAR data are presented in Figure 3. The algorithms require the availability of the approximated spatial location of the road centerline (e.g., from a CAD/GIS database), to initiate the road extraction process. The results presented here are based on the analysis of the 3D LiDAR point cloud; however, an extension of our algorithms is currently pursued towards the inclusion of LiDAR intensity data.

The two principal algorithms of the road surface extraction are: (1) segmentation of LiDAR data to select flat surfaces (equation 1), and (2) analyzing LiDAR scan lines to locate straight line segments using the auto-

structure function (ASF) analysis (see Toth *et al.,* 2004 for more details).

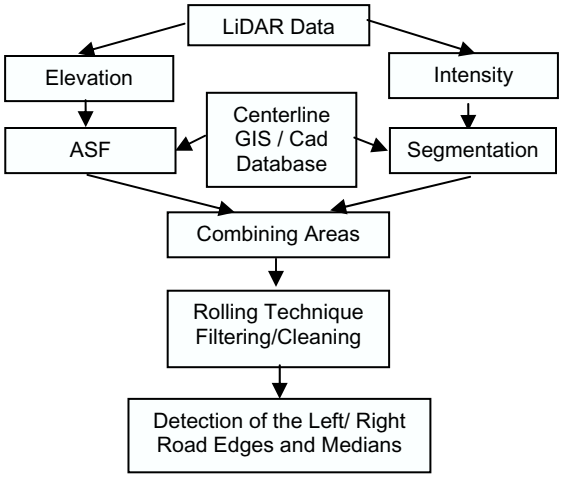

Figure 3. The road boundary extraction process (Toth et al., 2004)

The analysis of the normal vector, $\vec{n} = (A, B, C)$ selects the surface patches flagged as possible planar road segments, described by equation (1).

$$AX + BY + CZ + D = 0 \quad (1)$$

In a typical corridor mapping LiDAR mission, the scan lines correspond to the road cross profiles, offering wealth of information for the road surface detection process. The basic concept is to identify planar areas defined by the scan lines, which correspond to the road surface. There are several techniques of measuring the roughness and roughness length of a profile, such as auto-covariance, cross-correlation, variogram, texture analysis and the fractal method (Thomas, 1999). The correlation among the points along a profile, as a random variable, is selected in this paper, and the auto-covariance function or its modified equation, called structure function, is used in our investigation. For a profile of the length *L*, the structure function is defined as:

$$S(\tau) = \frac{1}{L-\tau} \int_0^{L-\tau} \{z(x) - z(x+\tau)\}^2 dx \quad (2)$$

where, *z(x)* and $z(x+\tau)$ are two elevations along the cross-profile, separated by a distance τ. This function is often normalized as the auto-structure function, called ASF:

$$ASF(\tau) = \frac{S(\tau)}{\max(S)} \quad (3)$$

The ASF function can be extended to determine 2D surface patches, but at the price of the increased computation requirements. The vehicles are natural obstacles for the ASF method when searching for flat surfaces on the road. Thus, close monitoring of the "affected" lines is needed, which naturally supports the vehicle extraction step.

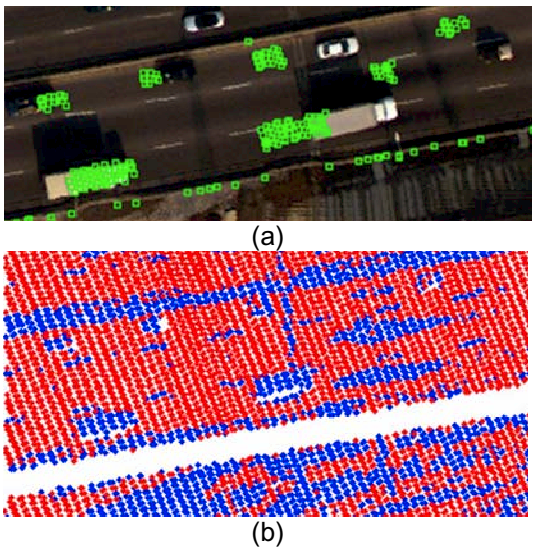

(a)

(b)

Figure 4. Road surface extraction based on intensity segmentation; (a) optical image (b) LiDAR intensity image.

The new generation of the LiDAR systems provides intensity data, which can be used as an additional source of information for the road extraction algorithm (see Figure 5 for the comparison of LiDAR intensity data with digital imagery). Although the intensity information is relative by nature, it can provide accurate local segmentation of the LiDAR data. For example, the road surface and vegetation along the road exhibit very different signal responses; thus, segmentation can be based on the relative intensity value. Figure 4 illustrates sample data segmented by a 15-35% intensity threshold value, showing a very good performance in extracting the road pavement and delineating the road

boundaries, road lanes, and the vehicles (which can be visually inspected by using the corresponding image data).

Once the road surface areas have been approximated from the elevation data and intensity (if available), a final consistency check using object space constraints should take place to determine and delineate the road. In this step a simple method called "rolling technique," based on signal auto-correlation is used. In essence, it corresponds to rolling a bar, parallel to the road direction, from the center of the road towards the edges; the rolling should stop at the road edges (zero slope), delineating the road boundaries.

The feasibility analysis of extracting vehicles and classifying them into main groups, such as passenger cars, multipurpose vehicles, and trucks, as well as all respective algorithms that we developed for these tasks are presented in (Grejner-Brzezinska and Toth, 2003a-b; Toth *et al.,* 2003a-b). In this paper the focus is primarily on the vehicle velocity estimation and its accuracy assessment.

3. TEST DATA, SENSOR PARAMETERS

The examples discussed in this paper are based on a high-density (2-4 points/m^2) LiDAR data set collected on February 19, 2004, over the downtown Toronto with the Optech ALTM 30/70 LiDAR system, simultaneously acquired with the 4K by 4K images (DDS digital camera system). Figure 5 shows an example of the LiDAR data, including elevation and intensity components, and the orthorectified RGB imagery for a selected segment of a freeway. The imaging sensors were equipped with the Applanix POS AV 510 integrated DGPS/IMU system.

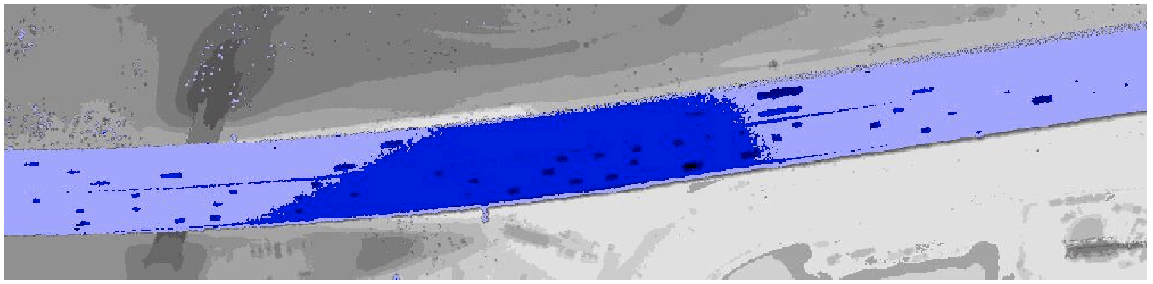

(a)

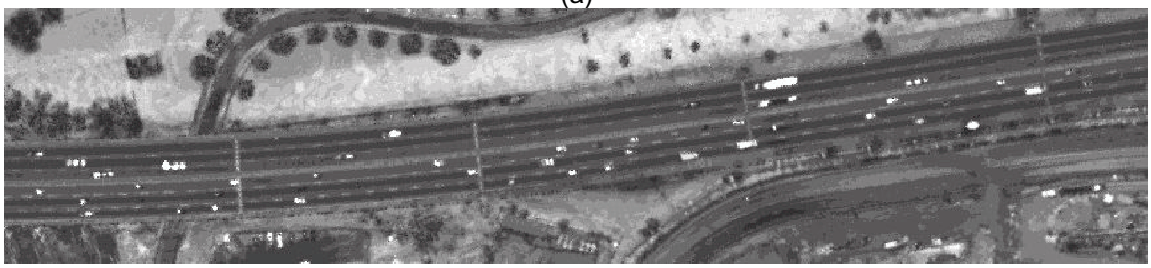

(b)

(c)

Figure 5. (a) LiDAR elevation data, (b) LiDAR intensity data, and (c) 4K by 4K digital camera ortho image of a freeway segment in downtown Toronto.

In general, laser sensors installed in the aircraft or helicopter can deliver range data at the cm-level accuracy. To obtain surface points with a comparable accuracy, however, the use of high-performance GPS/INS-based direct orientation system is mandatory. In addition, the scan angle of the rotating mirror needs to be known with high accuracy (new encoders can provide accuracy better than 1/1000 of the angle), where scan half-angle, β, is defined as an angle between the zenith and the outermost beams in the scan, as shown in Figure 1.

The error sources in the point determination from images and LiDAR measurements, in terms of the object space positioning accuracy, can be categorized into four main groups: (1) sensor platform position and attitude errors (navigation solution) – dominant part, as mentioned earlier, (2) inter-sensor calibration errors (boresight misalignment between the IMU and the sensor frames – angular errors), (3) sensor calibration errors, (4) miscellaneous errors, and (5) atmospheric effects.

σ_{XYZ} [m]	$\sigma_{\omega\phi\kappa}$ [arc sec]	$\sigma_{\omega\phi\kappa\text{-}b}$ [arc sec]	b [°]	RMSX [m]	RMS Y[m]	RMS Z[m]
0.05	10	10	0	0.073	0.073	0.051
			10	0.128	0.074	0.055
0.10	20	20	0	0.134	0.134	0.100
			10	0.170	0.135	0.103
0.20	30	30	0	0.313	0.313	0.300
			10	0.330	0.313	0.301

Table 1. Ground coordinate accuracies of LiDAR data with different navigation scenarios.

The coordinate accuracies achievable with state-of-the-art LiDAR systems at 600 m flying height are listed in Table 1 for different navigation performance levels (positioning, σ_{XYZ}, attitude, $\sigma_{\omega\phi\kappa}$, and boresight angle, $\sigma_{\omega\phi\kappa\text{-}b}$, accuracies), and for two different scan angles (0 and 10 degrees). The coordinate accuracy was assessed by error propagation based on the basic LiDAR equation (4).

$$r_{M,k} = r_{M,INS} + R^{M}_{INS}(R^{INS}_{L} \cdot r_{L} + b_{INS}) \quad (4)$$

Where

$r_{M,k}$ — 3D coordinates of point k in the mapping frame

$r_{M,INS}$ — 3D INS coordinates in the mapping frame

R^{M}_{INS} — rotation matrix between the INS frame and mapping frame, measured by GPS/INS

R^{INS}_{L} — boresight matrix between the laser frame and INS frame

r_{L} — 3D object coordinates in laser frame

b_{INS} — boresight offset component

For an easy comparison, the accuracy specifications for the two widely used GPS/INS systems, available commercially, POS AV 310 and 510, are presented in Table 2. According to the Applanix specification, the accuracy levels of the POS AV 510 direct georeferencing system in post-processing are 5 - 30 cm for the position; ~20 arc sec for roll and pitch; and ~30 arc sec for heading angle; see (http://www.applanix.com/html/products/prod_av_tech.html).

POS System	AV/DG 310	AV/DG 510
Absolute accuracy (Post processed)		
Position [m]	0.05-0.30	0.05-0.30
Velocity [m/s]	0.0075	0.005
Roll, Pitch [deg]	0.013	0.005
Heading [deg]	0.035	0.008
Relative accuracy		
Noise [deg/sqrt(hr)]	0.15	0.02
Drift [deg/hr]	0.5	0.1

Table 2. Specifications for POS AV 310 and 510 systems.

In our test flight, the GPS data were processed by the POSPac/POSGPS version 4.02. Table 3 lists the details of the GPS data quality and processing parameters.

Parameter	Magnitude
PDOP	Average = 1.9 Max = 2.7 Min = 1.3
Number of satellites	Average = 6 Max = 7 Min = 5
Baseline	Average = 11.8 km Max = 27.3 km Min = 0.1 km

Position standard deviation percentages	100.0 % between 0.00 - 0.10 m for East, North, Height
Estimate of average standard deviation	East: 0.02 m North: 0.025 m Height: 0.045 m
Fwd/Rev separation RMS Values	East: 0.013 m North: 0.024 m Height: 0.033 m

Table 3. GPS data quality and processing parameters.

4. VEHICLE VELOCITY ESTIMATION

In this section, the estimation of the vehicle velocity is discussed. Velocity, as already explained, is necessary for the traffic flow calculation, since the traffic flow is a product of the average vehicle velocity and the average vehicle density. Vehicle speed estimation from LiDAR is based on the vehicle elongation and shortening of the moving objects that are the effects of the scanning mode of the data acquisition.

Due to the continuous scanning nature of the LiDAR sensor and the motion of both the sensor and the vehicles, the length of the vehicles appears distorted in the LiDAR data set. In other words, the relative motion between the LiDAR sensor and the moving targets results in an elongated or shortened length of the vehicles. The cars are measured longer if they move in the same direction as LiDAR and shorter, if they move in the opposite direction. Exploiting the relationship between the LiDAR-measured and the actual lengths of the vehicles and the velocity of the sensor, the vehicle velocity can be expressed with the following formula (equation 5):

$$V_{vel\_along} = \frac{m-s}{m} \cdot V_{LiDAR}$$
$$V_{vel\_against} = \frac{s-m}{m} \cdot V_{LiDAR} \quad (5)$$

where V_{vel_along} / $V_{vel\_against}$ is the velocity of vehicle traveling along/against the LiDAR flying direction, V_{LiDAR} is the velocity of the LiDAR platform, m is the LiDAR-sensed vehicle length, and s is the true length of the vehicle. The LiDAR platform's speed is known with high accuracy, but the actual vehicle size is unknown. Moreover, the measured vehicle length from the LiDAR data may not be very accurate due to the errors in the vehicle representation: (1) the LiDAR pulse footprint size is not negligible, thus, the accuracy of the actual edge of the vehicle footprint determination depends on the size of the LiDAR footprint, (2) LIDAR point density; the distance between the points on the ground (object) limits the accurate length estimation, and (3) the shadow effect, which does not influence the length parameter estimation directly, but it makes the vehicle orientation more ambiguous and the width parameter estimation less accurate. For examples illustrating these problems see Figure 6 below.

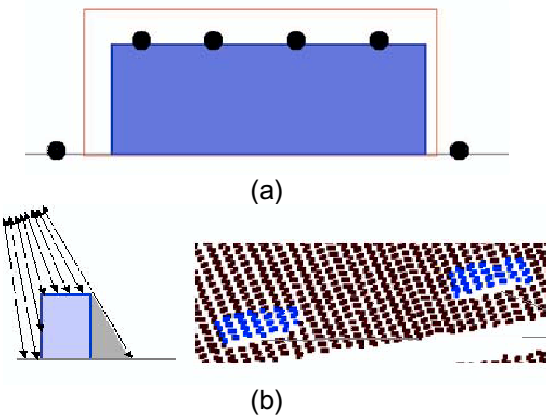

(a)

(b)

Figure 6. Limitations in accurate parameterization of LiDAR-sensed vehicles, (a) data density and footprint size, (b) shadow effect.

Our earlier study confirmed that all types of vehicles can be approximately classified into three main categories, for example:

passenger cars, multi-purpose cars, and trucks, and thus the actual vehicle length can be estimated as the average length within a category. Based on the statistics of the US vehicle market according to a study by Ramprakash (2003), the true length of, for example, passenger cars is between 4.36 and 5.23 m. These values are used in the example below.

Parameters			
V_{LiDAR} = 55 m/s			
$V_{VEH\ MIN}$ = 20 m/s		s_{MIN} = 4.36 m	
$V_{VEH\ MAX}$ = 32 m/s		s_{MAX} = 5.23 m	
True length	**Vehicle velocity**	**LiDAR-sensed length [m]**	
		Along	**Against**
s_{MIN}	$V_{VEH\ MIN}$	6.85	3.19
s_{MIN}	$V_{VEH\ MAX}$	10.42	2.75
s_{MAX}	$V_{VEH\ MIN}$	8.21	3.83
s_{MAX}	$V_{VEH\ MAX}$	12.50	3.30

Table 4. LiDAR-sensed lengths of passenger cars traveling on a freeway.

Some representative values of the elongated and shortened lengths of passenger cars that are sensed at typical sensor and vehicle relative speeds are shown in Table 4. The aircraft (LiDAR) speed was 55 m/s, and the car velocity ranges between the minimum and the maximum freeway speeds. In this scenario, the LiDAR-sensed length of the passenger cars moving in the flying direction falls between 6 and 13 meters, and 2.5 and 4 meters for the cars that move against the flying direction.

Table 5 shows the representative numbers for the velocity error at different LiDAR-sensed vehicle lengths. The vehicle velocity error is derived from the velocity range calculated from the statistical sample of the actual length. In other words, the velocity error is the difference between the velocities estimated for the average, the smallest and the highest vehicle length within the category. The vehicle measured lengths listed in Table 4 were used to estimate the values listed in Table 5. The velocity error can be minimized if the velocity calculation is based on the average true vehicle length in the category.

Parameters V_{LiDAR} = 55 m/s Statistical true Length [m]: Min = 4.36; Max = 5.23; Average = 4.78				
LiDAR-sensed Length [m]	**Estimated Velocity [m/s] calculated from Min Max and Average statistical true length**			**Velocity Error [m/s]**
	Min	Max	Ave	
3	24.93	40.88	32.91	7.97
7	21.76	13.90	17.33	3.93
10	31.02	26.23	28.63	2.40
15	39.01	35.82	37.41	1.60

Table 5. Errors in speed estimation due to the uncertainty in the true length size.

Figure 7 illustrates the vehicle velocity accuracy as a function of the LiDAR-sensed length. The estimation accuracy is rapidly decreasing due to the uncertainty in the true size, as the LiDAR-sensed length is getting shorter.

In summary, it can be concluded that the accuracy of the velocity estimation is better for vehicles traveling along the direction of the sensor motion, as their LiDAR-sensed measure is relatively long. Also, the uncertainty in the true vehicle length has less impact when the LiDAR-sensed length is longer. In a similar way, if the car is traveling in the direction opposite to LiDAR, its velocity estimate would be more accurate for lower speeds, since the shortening effect will be less severe.

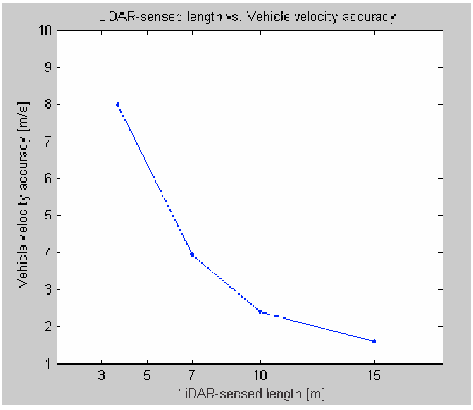

Figure 7. Velocity estimation accuracy as a function of LiDAR-sensed vehicle length.

To overcome the errors in the true vehicle length estimation due to generalization or possible misclassifications, the actual lengths of the vehicles should be determined from other sensory data, such as imagery collected simultaneously with the LiDAR point clouds. A single image does not provide the absolute size information, but the image sequence formation preserves the relative object size information. Although an extra effort, such as, using adequate matching technique is required to identify the same vehicles in the two data sets, the combination of the two data sets could eventually lead to the improved velocity estimation of the moving targets.

Figure 8 presents the vehicles extracted from the LiDAR data and overlaid on the orthoimage. LiDAR vehicle points are represented with green and red point clouds, corresponding to the motion along or against the flying direction, respectively. For referencing, some static objects, such as one point on the centerline and points at the guard rail are also marked in the figure. The matches of the corresponding vehicles in the two data sets are highlighted by rectangles with identical colors. Due to the different nature of the two data acquisition techniques, continuous scanning mode of the LiDAR sensor and instantaneous capturing of the imagery, the geo-locations and also the shapes of the corresponding vehicles differ in the two data sets. The approximate location of the LiDAR beam when the image was taken is marked by a triangle in Figure 8. Note that the LiDAR point clouds of the vehicles fall in front of the corresponding vehicles on the left side of the blue dotted line, and behind the corresponding vehicles on the right side of the line, as the LiDAR measured the vehicle either before or after the image was taken. Notice that the vehicles move in both directions. The positions of the matched vehicles can be estimated from both data sets, as the distance between the two locations can be computed from the time difference of the acquisitions (the LiDAR data come with GPS time tags and the camera exposure is known) and the average vehicle velocity.

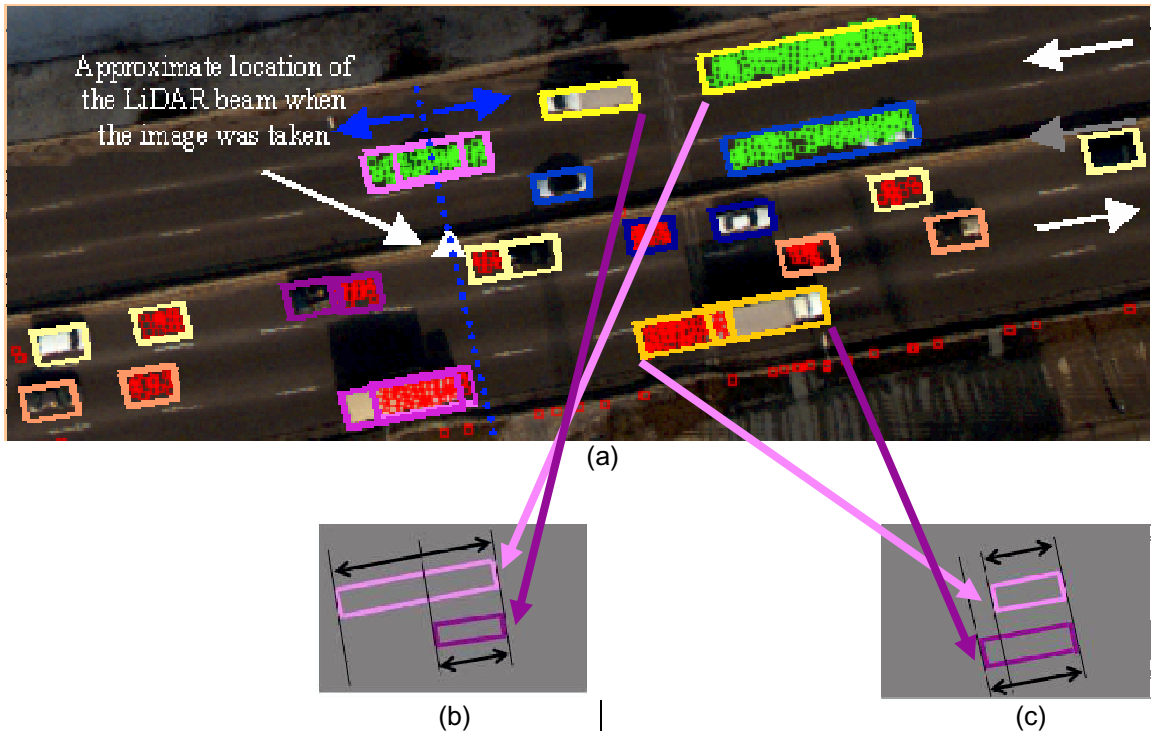

Figure 8. Vehicles extracted from the LiDAR data and overlaid on the orthoimage. Match of corresponding vehicles in the two data sets is marked with identical colors (a). Also shown are vehicle elongation (b) and vehicle shortening (c).

5. CONCLUSION

Estimating the velocity from LiDAR data based on extracted and broadly categorized vehicles produces moderate results. The speed of the larger vehicles can be fairly well approximated, but for smaller vehicles, especially these moving in the direction opposite to the LiDAR motion, the errors could become very significant. Thus, combining LiDAR with complementary sensor data, such as simultaneously collected imagery, can provide a good base for velocity estimation, which combined with the velocity extraction and categorization that provide the densities, will allow more reliable traffic flow parameter estimation.

6. ACKNOWLEDGEMENTS

This research was partially supported by the Ohio Department of Transportation. The authors would like to thank Optech International for providing the LiDAR datasets.

REFERENCES

Grejner-Brzezinska, D. A. and Toth, C. (2003a): Deriving Vehicle Topology and Attribute Information over Transportation Corridors from LiDAR Data, Proceedings, ION 59th Annual Meeting, June 23-25, Albuquerque, New Mexico, CD ROM, pp. 404-410.

Grejner-Brzezinska, D., C. Toth. (2003b): Airborne Remote Sensing: Redefining a Paradigm of Traffic Flow Monitoring, Proceedings, ION GPS/GNSS, Sept 9-12, Portland, Oregon, CD ROM.

Grejner-Brzezinska, D. A. and Toth, C., (2002): Modern Remote Sensing Techniques Supporting Traffic Flow Estimates, Proceedings, ION GPS, September 24-27, CD ROM, pp. 2423-2433.

Ramprakash, V.L., (2003): Detection and estimation of Vehicular Movement on Highways using a LiDAR sensor, MS.C. Thesis, The Ohio State University.

Thomas, T. R., (1999): *Rough Surfaces*, Imperial College Press, pp: 100-110.

Toth, C., Grejner-Brzezinska, D. and Lovas, T. (2003a): Traffic Flow Estimates from LiDAR Data, Proceedings, ASPRS Annual Conference, May 5-9, pp. 203-212, CD ROM.

Toth, C., Grejner-Brzezinska, D. A., Merry, C. (2003b): Supporting Traffic Flow Management with High-Definition Imagery, ISPRS Workshop on High Resolution Mapping from Space 2003, Hanover, Germany, October 6-8, CD ROM.

Toth, C. D. Brzezinska and S. Moafipoor (2004): Precise Vehicle Topology and Road Surface Modeling Derived from Airborne LiDAR Data, Proceedings ION NTM, June 7-9, Dayton, Ohio, CD ROM, pp. 402-408.

Precise Vehicle Topology and Road Surface Modeling Derived from Airborne LiDAR Data

Charles K. Toth[1], Dorota A.Grejner-Brzezinska[2] and Shahram Moafipoor[1]

[1] *Center for Mapping, The Ohio State University*
1216 Kinnear Road, Columbus, OH 43212

Tel: 614-292-7681; Fax: 614-292-8062
e-mail: toth@cfm.ohio-state.edu

[2]*Department of Civil and Environmental Engineering and Geodetic Science*
470 Hitchcock Hall, 2070 Neil Avenue

BIOGRAPHY

Dr. Charles Toth is a Senior Research Scientist at the Ohio State University Center for Mapping. He received an MS in Electrical Engineering and a Ph.D. in Electrical Engineering and Geoinformation Sciences from the Technical University of Budapest, Hungary. His research expertise covers broad areas of 2D/3D signal processing, spatial information systems, high-resolution imaging, surface extraction, modeling, integrating and calibrating of multi-sensor systems, multi-sensor geospatial data acquisition systems, and mobile mapping technology. He is Co-Chairing ISPRS WG II/2 on LiDAR and InSAR Systems and serves as the Assistant Director for the Photogrammetric Application Division of ASPRS.

Dr. Dorota Brzezinska is an Associate Professor in Geodetic and Geoinformation Science, The Ohio State University (OSU). Prior to that, she was a Research Specialist at the OSU Center for Mapping. She received an MS in Surveying and Land Management from the Agricultural and Technical University of Olsztyn, Poland, and an MS and a Ph.D. in Geodesy from OSU. Her research interests cover precise kinematic positioning with GPS, precision orbit determination for GPS/LEO, GPS/INS integration, mobile mapping technology, and robust estimation techniques. Between 1990-1995 she was a Fulbright Fellow at OSU. She is the 2003-2005 Land Representative for the ION Council, chair of IAG Sub-Commission 4.1, *Multi-sensor Systems*, a co-chair of the IAG Study Group 4.1, *Pseudolite Applications in Positioning and Navigation*, and a chair of the Task Force 5.3.1, *Mobile Mapping Systems* of FIG WG 5.3.

Mr. Shahram Moafipoor is a PhD student in the Department of Geodetics Science, The Tehran University, and currently he is a visiting scholar in the Department of Civil and Environmental Engineering and Geodetic Science, The Ohio State University. Prior to that, he was a researcher at National Cartography Center NCC, Iran. He obtained an MS degree in photogrammetry from Tehran University in Tehran, Iran in 1998 and B.Sc in surveying from Tehran University in Tehran, Iran in 1993. His research interests include navigation systems, aerial photography, and digital photogrammetry.

ABSTRACT

This paper represents the continuation of research presented earlier (Grejner-Brzezinska and Toth, 2002 and 2003a-b; Toth et al, 2003 a-b) referred to a theoretical and practical study on the feasibility of using LiDAR (Light Detection and Ranging) data and airborne imagery collected simultaneously over the transportation corridors for obtaining traffic flow estimates, such as (1) vehicle count estimates based on extracting vehicles from dense LiDAR point cloud and/or imagery, (2) classification of extracted vehicles into main categories, (3) velocity estimates based on modeling the vehicle categories and using sensor navigation data, and (4) intersection movement patterns.

In this paper, we present the updated algorithms and methodology of extracting the vehicle information together with the road surface modeling with precisely georeferenced (GPS/INS) LiDAR data, augmented by LiDAR intensity information. We demonstrate that intelligent algorithms that we developed are capable of fast and robust identification of the shapes (especially the vertical profiles of the vehicles), proving LiDAR's ability to preserve the vehicle geometry better, as compared to conventional image projection (again, primarily the vertical profile), where it can be significantly distorted. We prove that if LIDAR data of sufficient spatial density are available, vehicle extraction and their coarse classification can be efficiently performed in parallel to the efficient and automated road surface extraction and modeling.

1. INTRODUCTION

Federal and local government transportation management services monitor and control the traffic over the urban road network and the nation's highway system. These agencies collect data for both long-term planning and real-time traffic control. Real time information is usually gathered from many diverse sources, such as electronic sensors in the pavement (loop detectors), road tubes, ramp meter sensors, and video and digital cameras, which are sent to the traffic management center at various times. Most of this information is only recorded; a small part of it is analyzed in real-time and used for immediate traffic control and decision making. Commonly, the density and flow of traffic are the two main parameters for describing the traffic stream. In simple terms, the density is the number of vehicles occupying a road lane per unit length at a given time, while traffic flow represents the amount of vehicles traveling over a road segment in a given time period.

With the increasing number of vehicles entering the current transportation network annually, the importance of effective traffic management is becoming more crucial, because the construction of new roads is not keeping up with the volume of growing traffic. The key to better traffic management, however, is the access to better data and, of course, the capability for immediate processing of the data to provide a real-time response. Therefore, interest in new sensors that can provide large volumes of data in real-time is steadily growing. Airborne and spaceborne remote sensing technology can provide data in large spatial extent with varying temporal resolution. One of the distinctive characteristics of using remote sensing is that it can be deployed more or less anytime and anywhere – a definite advantage over the spatially local sensors. The installation and use of ground-based sensors disrupts traffic and endangers the crews.

LiDAR has become the primary surface extraction technology in mapping in the last five years. Its success is mainly due to the high-level of automation offered – the data can be literally used as acquired; the need for interactive processing is usually very limited. Mapping of the transportation infrastructure is primarily concerned with the static part of the object space. Vehicles, in particular the moving ones, pose a difficulty for processing: these objects should be removed during the processing. Instead of throwing away the removed objects, it could be advantageous to use these data to derive valuable information for traffic monitoring and management. An earlier research investigated the feasibility of extracting vehicles and classifying them into main groups, see (Grejner-Brzezinska *et. al*, 2003 and 2004; Toth et al, 2003b; Toth and Grejner-Brzezinska, 2004). Based on the success of the initial study, the decision was made to further investigate the approach and to develop a prototype of the concept. This paper reports additional research components not addressed in the initial phase.

2. SYSTEM DESIGN

The processing architecture of the system automatically extracting traffic flow from LiDAR data is shown in Fig. 1. The main processing steps are: (1) road surface extraction, (2) vehicle extraction, (3) primary parameterization of the vehicle shape – vehicle modeling, (4) feature space selection – parameter optimization, (5) vehicle classification, (6) vehicle velocity estimates, and (7) traffic flow data computation. The initial feasibility research on extracting flow data from LiDAR was focused on tasks (3-5). In this paper, the other tasks, which are the subject of ongoing research, are discussed. Section 3 is concerned with the road surface extraction. The primary objective is to determine the road boundaries while the complete surface modeling is omitted. Vehicle extraction is based on the availability of the road footprint and is discussed in Section 4. The aspects of vehicle velocity estimates are introduced in Section 5. Using an actual data set from a conventional LiDAR survey, traffic flow results are derived and discussed in Section 6. Finally, the conclusion and remarks are presented.

3. ROAD OUTLINE EXTRACTION

At a small scale roads are considered as linear features, while in large scale they are typically characterized by centerline and width parameters in 2D or by additional slope parameter in 3D. Furthermore, road details such as edge lines, median, fences, concrete dividers, shoulder lines, traffic signs, etc, are available at engineering scale mapping. The actual pavement surface is rarely modeled as the description using linear features is generally satisfactory.

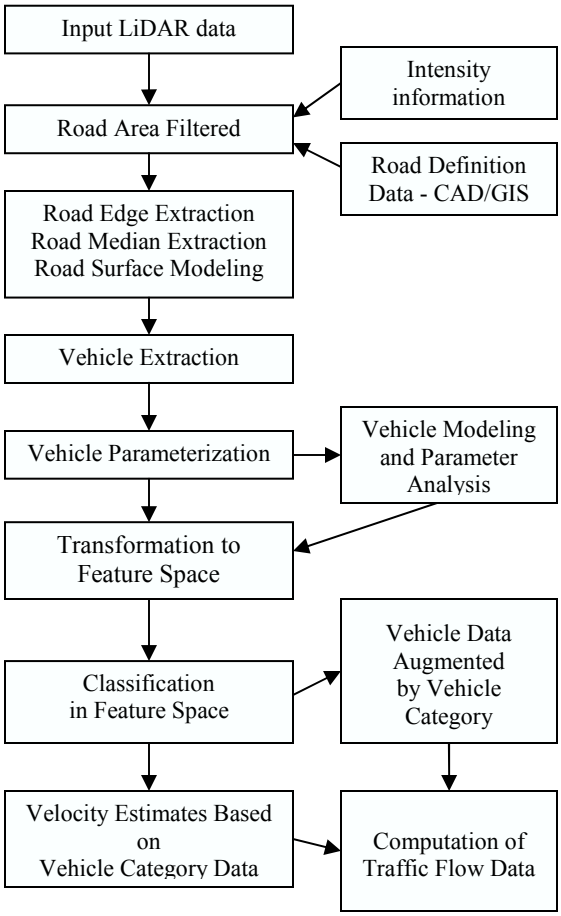

Figure 1. Data processing architecture

Methods for road extraction from remote sensed data are available and typically focused on linear feature extraction from satellite or airborne imagery. Extracting roads from LiDAR is a rather new approach (Hu and Tao, 2004). In both cases, however, the identification and coarse delineation of the road is the objective and no consideration is given to pavement level modeling. Also, these techniques are based on a general approach of not assuming the availability of any road data, such as a GIS or CAD database. In reality, this type of data is always available for the developed part of the world. Therefore, the road outline extraction process should be facilitated by using such data, which, in turn, changes the objective from finding roads in LiDAR data to realigning the road description based on the new measurement.

In our concept, the road outline and surface extraction, shown in Fig 2, assume the availability of coarse road data; at a minimum centerline information is needed (e.g.,. from a GIS database). Then the LiDAR point cloud, 3D points, and, depending on availability, LiDAR intensity form the input data. The use of intensity data is still in its infancy, but new systems already offer this capability and therefore are considered here. Approximated road areas/corridors can be separately analyzed based on both data sets and then results can be combined.

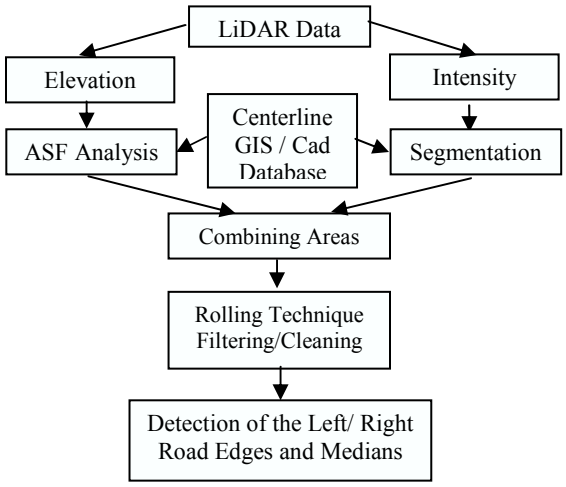

Figure 2. The road boundary extraction process

The strength of LiDAR data comes from the true 3D description of the object space, which offers a better object characterization and results in a better feature extraction performance. For our situation, corridor mapping, there are two apparent approaches: (1) segmentation of LiDAR data to find flat surfaces, and (2) analyzing LiDAR scanlines to find straight line segments. In the first case, points are grouped and small surface patches are fit to them, which are described by a plane representation, see Eq. 1.

$$AX + BY + CZ + D = 0 \quad (1)$$

Analyzing the normal vector, $\vec{n} = (A, B, C)$ the patches can be marked as possible road segments. Depending on the quality of the GIS/CAD road data, the road slope information should be used during the processing. If only horizontal data are available, the normal vector should be split into two components, along the road and across the road. The across the road component, which should describe a nearly horizontal surface, should be given higher weight in the segmentation. The along the road components can fluctuate more, but the rate of change should be consistent. This approach works well but is rather computation expensive.

Since roads are usually surveyed with perpendicular scanlines in a typical corridor mapping LiDAR mission, analyzing the road cross profiles as they are measured by consecutive scans provides a good alternative for road detection (changes in geometry are larger in that direction). In fact, this is the reason that roads are conventionally modeled by cross profiles. The basic concept is finding flat segments of the scanlines that correspond to road surfaces. There are several techniques for measuring the roughness and roughness length of a profile such as auto-covariance, cross-correlation, variogram, texture analysis and the fractal method (Thomas, 1999). The correlation between points on a profile, as a random variable, is chosen in this paper and the auto-covariance function or its modified equation called structure function is used in our investigation. For a profile of length *L*, the structure function is defined as:

$$S(\tau) = \frac{1}{L-\tau} \int_0^{L-\tau} \{z(x) - z(x+\tau)\}^2 \, dx \qquad (2)$$

where, *z(x)* and $z(x+\tau)$ are pairs of height values separated by a distance τ. This function is often normalized as the auto-structure function, called ASF:

$$ASF(\tau) = \frac{S(\tau)}{\max(S)} \qquad (3)$$

Figure 3 shows a few consecutive profile lines and the computed ASF functions. Although the ASF computation inherently implements some smoothing, a filtering of either the raw data or the derived ASF function is recommended, as the LiDAR data usually come with noise; typically 5 cm RMS.

The ASF function can be extended for surface patches (2D), but again at the price of increased computation requirements. In our experiences, both methods showed good results, as long as the roads to be identified had distinct geometry with respect to their surroundings. Thus, flat paved areas, such as parking lots and pedestrian walkways, cannot be reliably distinguished from roads. In addition, vehicles obviously cause problems, and therefore, the along the road pattern of the ASF function should be monitored to detect affected lines and they should be removed from the processing. If the scanlines are not perpendicular to the road centerline direction, cross profiles can be computed by interpolation before processing.

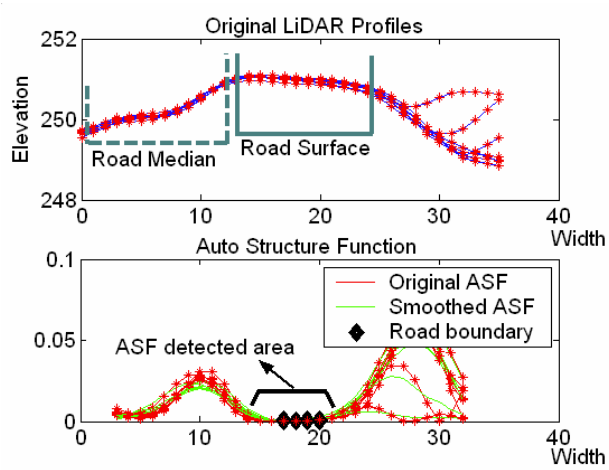

Figure 3. The road cross-profiles (top) and the computed ASF showing surface roughness (bottom).

As LiDAR intensity data are becoming widely available, they can be used as an additional source of information for the road extraction. Although the intensity information is relative by nature, it can provide for accurate local segmentation of LiDAR data. For example, the road surface and vegetation along the road exhibit very different signal response; thus segmentation can be based on the relative intensity value. Figure 4 depicts sample data segmented by a 40% intensity threshold value, showing a very good performance. Note the road centerline points, marked in blue, from the GIS/CAD data. The points erroneously segmented can be removed by basic morphology processing.

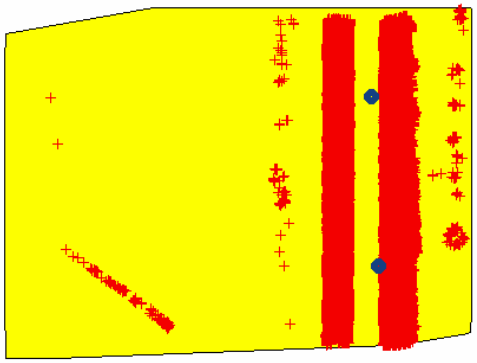

Figure 4. Road estimation based on intensity segmentation

Once the road surface areas have been approximated from elevation and intensity (if available) data, a final consistency check using object space constraints should take place to determine and delineate the road. At this point the

road direction and width are approximately known, and the objective is to determine the edge lines of the road. As the changes in road geometry are limited in the road direction, a similarity analysis is performed over smaller road segments, which is defined as a distance comparable to the road width. This technique is called rolling procedure and is based on auto-correlation – basically a virtual bar, parallel to the road direction is rolled from the center of the road towards the edges, see Fig. 5. The rolling of the bar is supposed to stop at the road edges, delineating the road boundaries.

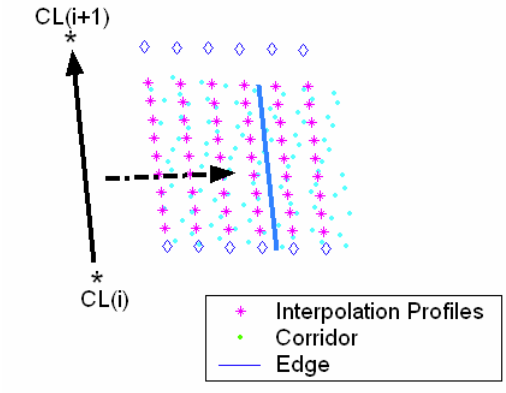

Figure 5. Rolling technique

The rolling process works with an overlap to achieve smooth road boundary delineation. Fig. 6 shows final road edges overlaid over the point cloud. The locations were independently formed on the left and right sides of the road.

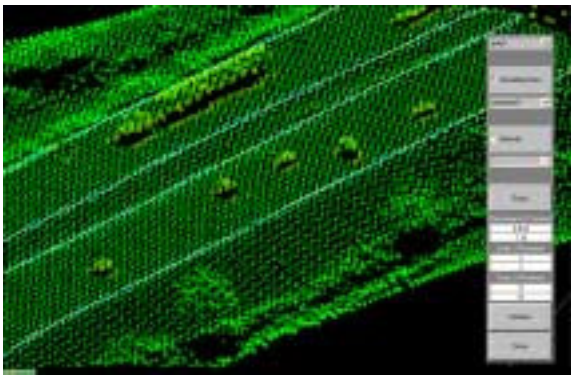

Figure 6. Road edges delineation

4. VEHICLE REMOVAL AND ROAD MODELING

Once the road boundaries are available, a simple thresholding can extract the vehicles; segments of the road between edge lines are approximated by a plane. To follow the changes in road surface orientation, the thresholding scheme should be adaptive, which guarantees that candidate points representing a vehicle will have true perpendicular height values with respect to the actual road surface – this way the very same vehicle description is obtained no matter whether the road is horizontal or of steep grade. Fig. 7 shows point clusters extracted as vehicle candidates. Note that besides the vehicles, there are other extracted objects that are definitely not vehicles, such as vegetation or guide rails on the side, and thus should be removed during subsequent processing.

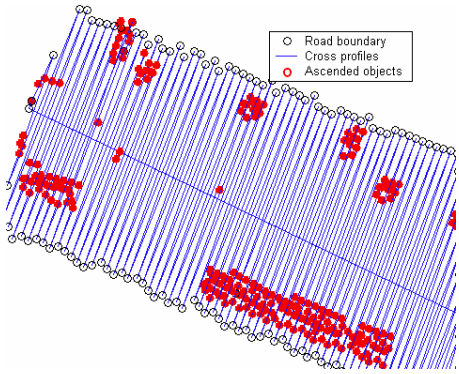

Figure 7. Thresholding the ascended points along the scanlines to detect vehicle objects

The vehicle candidate point clouds are modeled to support both vehicle classification and blunder detection – the removal of any raised objects that are not vehicles. As the current LiDAR point density, ranging typically between 1-5 points/m^2, and the relatively sizeable footprint size of the laser beam, usually in the range of 10-30 cm, cannot allow for very precise geometrical description of the vehicles, thus only coarse parameterization is possible of the vehicles. For instance, determining the 3D envelope of the vehicle points and then describing it by length, width and height(s) parameters. In addition, derived parameters, such as vehicle footprint size or volume, can be used. Figure 8 depicts vehicle points, showing both LiDAR scanlines and actual points.

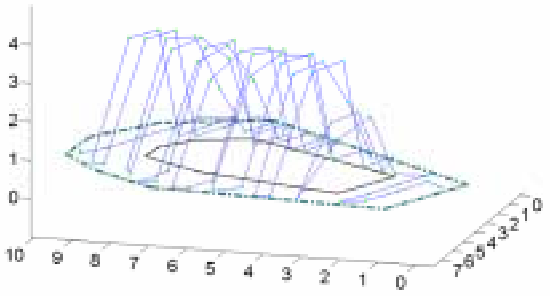

Figure 8. Vehicle points extracted with original scanlines overlaid.

Using the basic vehicle parameters, a blunder detection process is executed to remove all non-vehicle objects. Vehicle length varies as a function of the relative speed between a vehicle and the LiDAR sensor platform, but the width is invariant and thus provides the first criterion for blunder detection. Fig. 9 shows a concrete structure separating the two sides of the road that can be easily discarded, as its width falls below the minimum vehicle width and it has an unlikely long length. Additional filters are based on footprint size and volume.

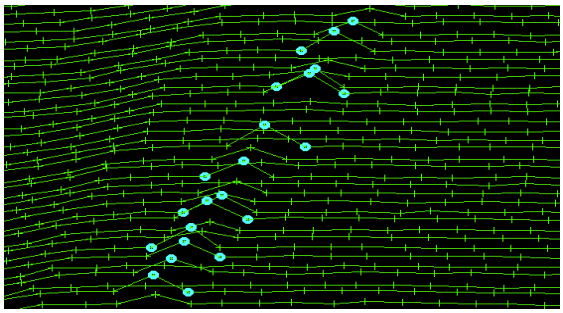

Figure 9. Concrete wall, a blunder object.

Once all the likely non-vehicle objects are removed, the next objective is the classification of the vehicles. The original vehicle parameter space, however, does not offer an efficient classification domain, as its dimensionality is high and the parameter correlation is unknown. Therefore, a Principal Component Analysis (PCA) is preferred to arrive at a reduced feature space where the classification takes place. A variety of parameter combinations have been tested such as using width, length, area and volume, or width, length and height profile; or only height profile, e.g., modeled by four values along the vehicle motion direction; and similar parameters augmented by average intensity values. Detailed results can be found in (Toth *et al.*, 2003b). Fig. 10 shows the 2D classification space, based on four parameter modeling, determined by a 72 vehicle training data set. The vehicle classes are passenger cars, trucks and all other vehicles.

The classification performance was tested on different data sets, and in general showed a good performance. From the three classifiers investigated, i.e., the rule-based, the Voronoi tessellation, and the neural network, the first one provided the best performance, consistently achieving about 98% success rate, see (Toth *et al.*, 2003a). It is important to note that the direction of the vehicle motion can also be recovered in some cases. Finally, the use of intensity data did not result in a better classification performance.

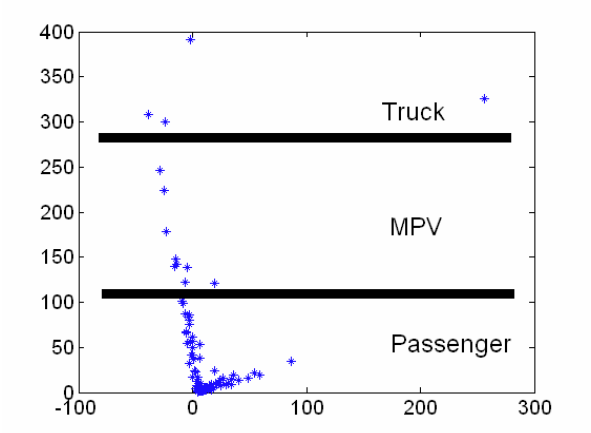

Figure 10. The PCA classification of the vehicles in the 2D space

5. VELOCITY ESTIMATES

The vehicle velocity is the second parameter needed to compute the traffic flow. The individual speed of each vehicle is usually not of interest, as only the average velocity of a group of vehicles is needed to obtain flow data. In the context of LiDAR, the dependency of the vehicle length with respect to the relative velocity between the object and the sensor forms the basis for speed estimation. Due to the continuous scanning, the vehicles appear shorter or longer in the relative motion direction. Equation (4) describes the relation between the actual size, *s*, and measured size, *m,* of the vehicles moving in both directions:

$$V_{veh} = \frac{m-s}{m} V_{LiDAR} \sin(\theta)\Big|_{along} \qquad (4)$$
$$V_{veh} = \frac{s-m}{m} V_{LiDAR} \sin(\theta)\Big|_{against}$$

where V_{LiDAR} is the velocity of LiDAR platform, V_{veh} is the vehicle velocity and θ is the intersection angle of LiDAR scan line and vehicle direction, usually small enough, so it can be ignored.

The determination of the vehicle direction is rather obvious, as vehicles always travel on the same side of the road. But, if needed, a simple statistics can show that on one side of the road the sensed length of the vehicles is longer than on the other one. Similarly, the LiDAR platform speed is known at high accuracy. The size parameters, however,

have significant errors. First, the LiDAR footprint has a non-negligible size. Then the LiDAR scanlines are separated by an even larger distance and thus setting a lower limit for the accuracy of the length estimation. Second, the actual vehicle size is unknown; only broad vehicle categories are determined in the classification phase. Therefore, only a size distribution is available for the computation. According to a study by Ramprakash, 2003, the percentage of the passenger car vehicle market share in the USA with corresponding length and height parameters is shown in Table 1.

Passenger car type	Share [%]	Average length [m]	Average height [m]
Small	27%	4.36	1.37
Mid size	49%	4.73	1.36
Large	9%	5.23	1.38
Luxury	15%	4.77	1.35
Average		**4.68 ± 0.35**	**1.36 ± 0.01**

Table 1. The basic statistics of the US passenger car vehicle market

Based on the average vehicle length, the velocity of a vehicle can be approximated and the accuracy of the length estimate can be derived from the vehicle category parameter distribution. Table 2 shows representative numbers for the velocity error at typical sensor and car relative speeds (aircraft speed was 55 m/s and the car speed ranged between minimum and maximum freeway speed). As expected, the estimation error is smaller if the vehicle and the LiDAR are moving in the same direction (the measured length is longer at smaller relative speed). Another interpretation is that the relative impact of the fixed size of the car length range is smaller if it is compared to longer measured values, see Eq. 4. Although the velocity accuracy estimates are poor, the average velocity of a group of vehicles can be estimated significantly better as vehicles usually move at comparable speed plus the averaging process has an error cancellation character.

Measured Length [m]	Velocity Accuracy [m/s]
3	9.6
7	3.0
10	2.0
15	1.3

Table 2. The velocity error estimates based on measured vehicle length.

6. DENSITY AND FLOW PARAMETERS

Based on the computed vehicle locations and class categories, as well as estimated velocities, various flow parameters can be derived. Flow is typically computed as a product of average vehicle density and average vehicle velocity. Density is usually derived after calculating the average spacing of vehicles along a given lane/road by Equation 5. Spacing is the distance between the vehicles moving in the same direction, as measured between corresponding points (front to front) of consecutive vehicles.

$$Average \quad Space = \frac{\sum Space \quad Between \quad Vehicles}{Number \quad of \quad Vehicles} \qquad (5)$$

To illustrate the traffic flow computation process, data from a high-density (2-4 points/m^2) LiDAR survey, acquired on February 19, 2004, over the downtown Toronto area with the Optech ALTM 30/70 system, were used. Fig. 11 shows a highway segment with vehicles extracted from the LiDAR data and overlaid on the orthoimage. Note that the LiDAR point cloud of the vehicles falls before the vehicles in the left side and after the vehicles on the right, respectively. A red mark shows the likely location of the LiDAR beam when the image was taken. For referencing, static objects were also overlaid – one point at the centerline and points at the guard rail.

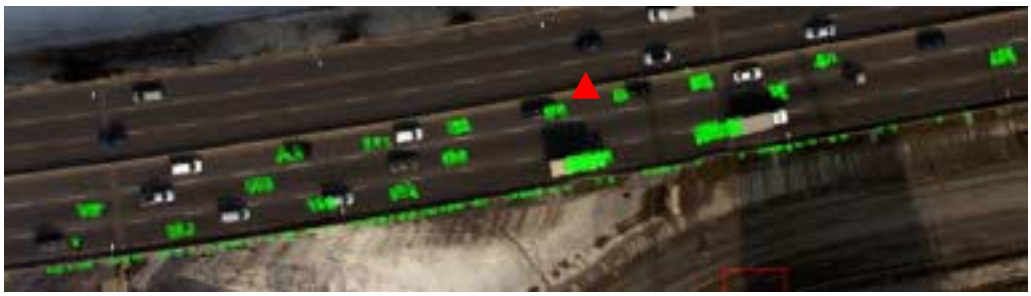

Figure 11. Vehciles extracted from LiDAR data overlaid on the orthoimage.

As the road is in a relatively flat area, only the horizontal components were used to compute the various flow parameters. The errors in spacing computation due to the non-instantaneous LiDAR data are ignored – this is acceptable if the relative speed of the vehicles is not changing rapidly. Table 3 lists the results, grouped by lane and road sides. Note that while vehicle velocity estimates are accurate to about 20%, the final flow has about 12% accuracy.

Lane No.	Space [m]	Vel. [mile/h]	Density [Veh/mile]	Flow [Veh/h]
L1	24.5	50	66	3234
L2	29.6	47	54	2646
L3	24.9	48	57	2793
Total	**8.7**	**49 ± 10**	**177 ± 0.2**	**8673 ± 1100**

Table 3: Traffic flow data

7. CONCLUSION

Our experiences with using LiDAR for obtaining traffic flow data have shown encouraging results. The developed concept and its prototype implementation proved that high-point density LiDAR can effectively support traffic monitoring and management by delivering a variety of traffic flow data. The proposed system represents an add-on capability to existing infrastructure airborne LiDAR mapping. Basically, this technique extracts the vehicles during the process of the road surface extraction and modeling, and uses them as a source for obtaining traffic flow. The recent introduction of the reflectance information is expected to further improve the road extraction process, while the vehicle classification seems to be unaffected by the availability of intensity data.

ACKNOWLEDGEMENTS

This research was partially supported by the NCRST-F program and by Ohio Department of Transportation. The authors would like to thank Woolpert LLC and Optech International for providing the LiDAR datasets.

REFERENCES

1. Grejner-Brzezinska D., Toth C and Paska E., (2003): Airborne Remote Sensing: Redefining a Paradigm of Traffic Flow Monitoring, ION GPS 2003, Portland, September 24-27, 2003, CD-ROM.
2. Grejner-Brzezinska D., Toth C and Paska E., (2004): Airborne Remote Sensing Supporting Traffic Flow Estimates, Proc. of 3rd International Symposium on Mobile Mapping Technology, Kunming, China, March 29-31, 2004, CD-ROM.
3. Hu, X., and Tao, V., (2004): Extraction of Streets in Dense Urban Area from Segmented LiDAR data, The 4th International Symposium of Mobile Mapping Technology, Kunming, China, March 29-31, 2004, CD-ROM.
4. Ramprakash, V.L., (2003): Detection and estimation of Vehicular Movement on Highways using a LiDAR sensor, MS.C. Thesis, The Ohio State University.
5. Thomas, T. R., (1999): *Rough Surfaces*, Imperial College Press, pp: 100-110.
6. Toth, C., Barsi A. and Lovas T., (2003a): Vehicle Recognition From LiDAR Data, *International Archives of Photogrammetry and Remote Sensing*, Vol. XXXIV, part 3/W13, pp. 163-166.
7. Toth C., Grejner-Brzezinska D. and Lovas T. (2003b): Traffic Flow Estimates from LiDAR Data, Proc. ASPRS Annual Conference, May 5-9, pp. 203-212, CD ROM.
8. Toth C., Grejner-Brzezinska D. and Merry C., (2003c): Supporting Traffic Flow Management with High-Definition Imagery, Proc. Of Joint ISPRS Workshop on High Resolution Mapping from Space 2003, Hannover, Germany, Oct 6-8, 2003, CD ROM.
9. Toth, C. and Grejner-Brzezinska, D., (2004): Vehicle Classification from LiDAR Data to Support Traffic Flow Estimates, Proc. of 3rd International Symposium on Mobile Mapping Technology, Kunming, China, March 29-31, 2004, CD-ROM.
10. Wehr, A. – Lohr U. (1999): Airborne Laser Scanning – and Introduction and Overview, *ISPRS Journal of Photogrammetry and Remote Sensing*, 54, pp. 68-82.

Vehicle Classification from LiDAR Data to Support Traffic Flow Estimates

Charles Toth[1] and Dorota Grejner-Brzezinska[2]
The Ohio State University
[1]Center for Mapping
1216 Kinnear Road, Columbus, OH 43212
[2]Department of Civil and Environmental Engineering and Geodetic Science
470 Hitchcock Hall, 2070 Neil Avenue, Columbus OH 43210
E-mail: toth@cfm.ohio-state.edu

KEY WORDS: LiDAR, vehicle extraction, classification

ABSTRACT:

In this paper we discuss the feasibility of using airborne LiDAR imagery data to support traffic flow parameter estimation, including primarily vehicle count estimates and vehicle classification, and to a less extent, velocity estimates. As a part of the classification task, we demonstrate the capability of LiDAR data to efficiently identify vehicles or vehicle categories by shape, especially by their vertical profile. We show that LiDAR offers the capability to better preserve the vehicle geometry, especially the vertical profile, as compared to optical imagery. During the projection process in optical imagery the vertical dimension is usually lost. Thus, a better vehicle classification/grouping was found from using dense LiDAR data. The identified and categorized vehicles can directly support the vehicle count estimation process. Experimental results are presented to validate the performance potential of the LiDAR data based vehicle extraction process.

1. INTRODUCTION

LiDAR is an emerging technology in the field of remote sensing that is capable of rapidly generating high-density, georeferenced digital elevation data with an accuracy equivalent to traditional land surveys, but significantly faster than traditional airborne surveys (Flood, 1999). Despite the initial high price, these systems have made remarkable market penetration, and recent technical and methodological advancements have further improved the capabilities of this remote sensing technology (Wehr and Lohr, 1999). In addition to the conventional Digital Surface/Elevation Model (DSM/DEM) products, the latest high-performance LiDAR systems can deliver very dense and accurate point clouds and thus provide data for more sophisticated applications. At the APSRS 2003 Annual Convention, Optech introduced the ALTM 30/70, a 70 kHz system and soon after that, LHS announced the 58 kHz version of its system. Both provide excellent support for high accuracy mapping. In reality, these developments make LiDAR technology capable of acquiring transportation application-specific information beyond conventional mapping, supporting tasks such as extracting moving objects. In this paper we investigate the potential of using airborne laser scanning technology for traffic monitoring and other transportation applications.

Road transportation systems have undergone considerable increases in complexity and at the same time traffic congestion has continued to increase. In particular, surface vehicle ownership and the use of vehicles are growing at rates much higher than the rate at which roads and other infrastructure are being expanded. Transportation authorities are increasingly turning to existing and new technologies to acquire timely spatial information of traffic flow to preserve mobility, improve road safety, and minimize congestion, pollution, and environmental impact (Zhao 1997). Besides the widely used conventional traffic data collection techniques, such as detection loops, roadside beacons, and travel probes, the state-of-the-art remote sensing technologies, such as LiDAR and high-resolution digital cameras can already provide traffic flow data over large areas without ground-based sensors. It is expected that the use of modern airborne sensors supported by state-of-the-art georeferencing and image-processing technologies will enable fast, reliable, and accurate data capture for traffic flow information retrieval with high spatial and temporal resolution. In particular, the following data could be supported: vehicle count/type, vehicle velocity and travel time estimation, origin-destination flows, highway densities (passenger car per unit distance per lane) and exit flow monitoring, intersection turning volumes, detection of congested/incident areas in real-time to support traffic redirection decision-making, platoon dispersion/condensation monitoring (which can be effectively accomplished only by remote sensing methods), and incident detection and response (Toth et. al., 2003a).

In this paper we investigate the feasibility of using LiDAR data for traffic flow estimates. In a sense, extracting vehicles over transportation corridors represents the next step in complexity by adding the temporal component to the LiDAR data feature extraction process. The facts are that vehicles are moving at highway speeds and the scanning acquisition mode of the LiDAR certainly poses a serious challenge for the data extraction process. Using data from regular LiDAR missions, it will be shown how vehicles can be extracted and then parameterized in a way that a robust classification of the vehicles is possible. The potential for determining vehicle speed estimates will be also addressed.

2. FLOW DATA

The research results discussed here have been accomplished through a multi-year multi-university effort supported by the joint sponsorship of the US Department of Transportation (USDOT) and NASA under the National Consortia on Remote Sensing for Transportation (NCRST). From the four major topics, the NCRST-F consortium is concerned with the

monitoring and managing of traffic flows, and with the intermodal transfer of goods, see (http://www.ncrst.org/research/ncrst-f/ncrst-f_home.html). Similar investigation with respect to using 4k by 4K direct digital imaging data can be found in Grejner-Brzezinska and Toth (2002, 2004). The major platforms currently used in the NCRST-F research activities are airborne, including fixed-wing aircraft, helicopter and UAVs, and spaceborne platforms. These platforms host a variety of sensors, but predominantly, frame or line CCDs, video cameras, multi/hyperspectral sensors and LiDAR (FDOT, 2002). This paper is concerned only with airborne platforms with LiDAR as the source for flow information. We discuss the use of LiDAR data for extracting moving vehicles over the transportation corridors and grouping them into broad classes. The method includes a filtering process of identifying vehicles, the selection of a parameterization to describe the LiDAR point cloud of a vehicle, the optimization of the parameter representation, and the classification process. Using three datasets obtained from typical LiDAR surveys, classification techniques have been tested to assess the performance of the vehicle groupings. Figure 1 shows a typical road segment with various vehicles clearly identifiable from the LiDAR point cloud, demonstrating the high level of spatial details provided by LiDAR.

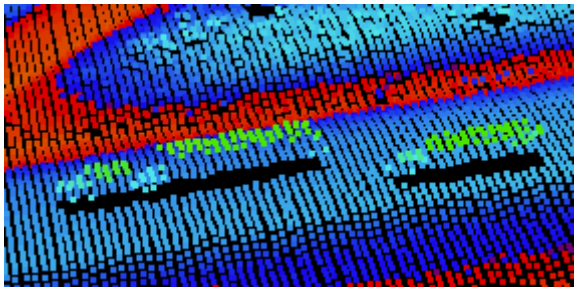

Figure 1. The LiDAR dataset captured over a freeway.

The ground-based data commonly available for traffic monitoring (such as detection loops, roadside beacons, travel probes and driver input) are spatially local in nature, while remotely sensed data have the capability of providing the spatial scale necessary for supporting effective (and real-time) traffic management. In the USA only about 25% of freeways in urban areas are subject to regular real-time traffic control by classical methods, which certainly indicates a need to implement new tools/methods to improve (enable) traffic management.

Important features that are unique to remote sensing in traffic monitoring include: (1) sensors are not attached to just one location (for example, tracking dangerous cargo or incidents), (2) sensors can be deployed during special events (natural disasters, evacuation), (3) provide superior spatial resolution, and (4) provide up-to-date traveller information, if applied in real-time. The major application areas where remote sensing can significantly contribute are (1) highway traffic monitoring, (2) highway traffic management, and (3) freight and intermodal analysis. The use of remote sensing can enhance the efficiency of many of the present practices used to determine the level of service; vehicle miles traveled (VMT), average annual daily traffic (AADT), and vehicle classifications and counts. Remote sensing can also help to determine passenger and freight flows at intermodal centers, and identify congestion points and patterns. Airborne or spaceborne imagery can improve spatial resolution, accuracy, and the visualization of traffic flows by the fusion of multisensor databases.

The motivation for the research presented here and the answer to the question of why LiDAR should be considered for this task at all, as its price tag seems to be overly high, is related to the following two facts:

- A great amount of LiDAR data is collected over transportation corridors and in urban areas with a dense road network. In these datasets, vehicles on the road represent obstructions to the LiDAR pulses as they are reflected back from the vehicles instead of the pavement. Therefore, a substantial amount of processing must be devoted to the "removal of the vehicle". Rather than removing and discarding the signals from vehicles, they can be turned into traffic flow information.
- Somewhat connected to the previous fact is that LiDAR systems can be turned on to collect data during transit, which accounts for substantial flying time. At almost no cost, a significant amount of data, rich in traffic flow information can be acquired. There is indication that transportation and other agencies will be deploying LiDAR systems over transportation corridors at an increasing rate in the future.

Finally, it should be noted here that LiDAR offers an advantage of all-weather and day-and-night imaging capability, compared to a panchromatic/color CCD, which is light and cloud-coverage dependent.

3. LIDAR DATA PROCESSING CONCEPT

The experimental data processing sequence is shown in Figure 2. In the first step, the input LiDAR data are filtered to reduce the point cloud to the road area (with some margin). The location of the road geometry is usually available from transportation agencies that maintain CAD or GIS databases. As either the accuracy of the road location information is limited or only centerline data are available, it is mandatory to perform a road-matching step. During this process, the crown lines of the road, on both sides for divided roads, are tracked from the LiDAR data. The process is driven by the road line description, and by running a moving window across the road line, the crown lines are estimated. As vegetation and man-made objects, such as vehicles, bridges and other structures, can obstruct the LiDAR pulse to reach the road surface, a subsequent processing step is necessary to check and, if possible, to restore the continuity of the road surface. This includes monitoring the directional changes of the road line, as well as the flatness of the road surface itself. Once the road crown lines have been estimated, the vehicle extraction is rather simple. Using a preset threshold, LiDAR points returned from vehicles can be easily separated from the road surface points. The actual thresholding is done in the surface normal direction, which is only critical for long vehicles traveling on steep roads. Where obstructions prevented the extraction of the road crown lines, obviously, there is no vehicle extraction. At this point, the extracted vehicles, as described by their location with time, can be passed to the transportation information system for further processing. The point distribution of the extracted vehicles

provides rich information for vehicle classification. An important aspect is the parameterization of the vehicle, discussed in detail in the next section. Once the vehicles are grouped into main categories, velocity estimates can be derived and subsequently used for overall vehicle flow data computation.

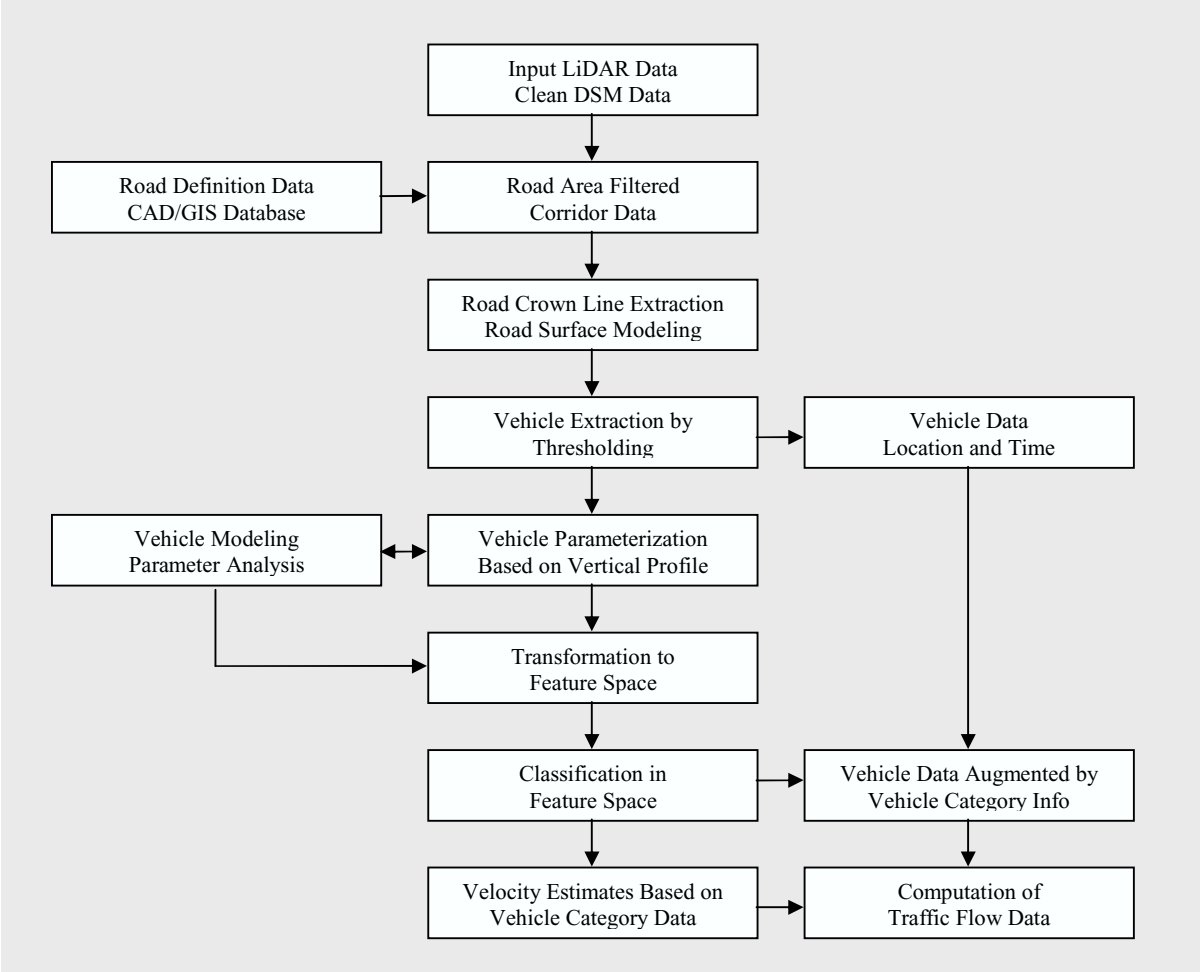

Figure 2. Design architecture and data processing flow.

4. VEHICLE PARAMETERIZATION

To distinguish major vehicle types, characteristic parameters have to be chosen. The difficulty, in short, is that the typical LiDAR point density is comparable to vehicle dimensions. Thus it is not trivial to identify surface areas of the vehicles at sufficient accuracy, let alone to recognize them at all. For instance, a small car traveling in the opposing direction to the laser scanner will have a large relative velocity between the sensor and object, resulting in few LiDAR points. The shape appears like a blob and gives rather limited clues about the actual shape of the vehicle (see Figure 1). With continuously increasing LiDAR point densities, the situation will certainly improve in the future. However, it is fair to say that model-based matching between the actual vehicle physical representation and the LiDAR points is not feasible at this point.

Another important aspect of the LiDAR input data is the relative velocity between the airborne data acquisition platform and the vehicles to be observed. The typical aircraft speed, known from the GPS/INS navigation solution, results in an average speed of the LiDAR sensor of about 200 km/h during surveys. This roughly translates into a relative velocity range of 100-300 km/h between the data acquisition platform and the observed moving objects. Figure 1 clearly shows the impact of the relative speed, as the vehicles traveling at faster relative speed (opposite direction) have smaller footprints, while the smaller relative velocity (airplane and vehicles are moving in the same direction) results in elongated vehicle footprints. For the extreme of zero relative velocity, such as the vehicle moving with the same ground speed as the aircraft, the LiDAR-sensed vehicle size would be infinite. The vehicle would become practically non-detectable.

Given the elongated shape of vehicles, the vertical profile along the travel direction is the most plausible feature to use to describe vehicles from LiDAR points (remember the density limitation of the LiDAR data). The profile can be approximated by various functions. For simplicity, in our

initial investigation we used a six-parameter representation that includes the size of the vehicle footprint and then four vertical parameters (average height values computed over the four equally sized regions) as shown in Figure 3.

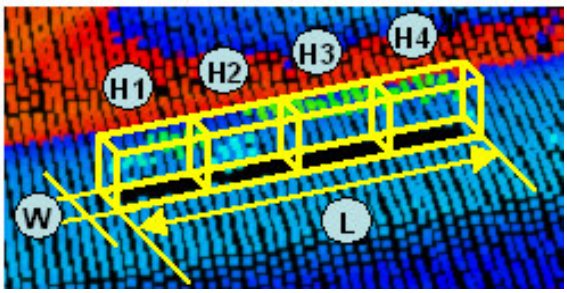

Figure 3. Parameterization of LiDAR points representing a vehicle.

To analyze the effectiveness of the six-parameter model, actual tests were conducted. Woolpert LLP from Dayton, Ohio provided a LiDAR dataset, obtained from flights done for regular mapping purposes. The point density was 1.5 point/m^2, which was certainly adequate for topographic mapping and could be considered at best minimal for vehicle identification. The LiDAR data covered a freeway section of State Route 35 (East of Dayton), packed with vehicles, and was used later as a training dataset for developing the classifiers. 72 vehicles were chosen and processed in an interactive way, the regions containing vehicles were selected by an operator and the vehicles were automatically extracted by the thresholding method presented earlier. All the vehicles were parameterized and then categorized into three main groups: passenger cars, MPVs (multi-purpose vehicles such as SUVs, minivans, light trucks), and trucks/18-wheelers.

To analyze parameter correlation and consequently to reduce the dimensionality of the parameter space, Principal Component Analysis (PCA) was then performed. PCA is an effective tool for handling data representation/classification problems, where there is a significant correlation among the parameters describing the object patterns. Using a training dataset, the correlation can be determined and a reduced parameter set can be defined that can both represent the information in a more compact way and can support an efficient classification in the reduced feature space. The clear advantage of the method is that it does not require any physical modeling of the data; of course, the selection of the input parameters has importance. Provided that a rich set of input parameters is defined, however, the method will effectively identify the redundancy and thus usually results in a quite reduced parameter representation. In our investigations the 72 vehicles provided a statistically meaningful dataset for the PCA process. In two sessions, the four- and six-parameter datasets were analyzed (height only and height with footprint size). The eigenvalues computed from the covariance matrix for the six-parameter model and ordered monotonically are shown in Table 1.

In analyzing the results, it is quite surprising to see that more than 98% percent of the original information content is preserved, if only the two largest eigenvalue components are used for data representation. To assess the classification performance, for which high information contents do not necessarily give guarantees, the 72 vehicles converted into the two-dimensional feature space as plotted in Figure 4. Cars are marked with ○, MPVs with +, and trucks with ⁎, respectively; vehicle direction with respect to sensor motion is coded in red and blue. Figure 5 shows the results, if only the height parameters (4) were used as input in the PCA.

	E1	E2	E3	E4	E5	E6
Eigenvalues (true values)	18.78	1.02	0.09	0.08	0.02	0.01
Eigenvalues (normalized)	93.87	5.09	0.45	0.41	0.11	0.07
Information content [%]	93.87	98.96	99.41	99.82	99.93	100

Tabel 1: The eigenvalues and information contents of the training data set, which consisted of 72 vehicles.

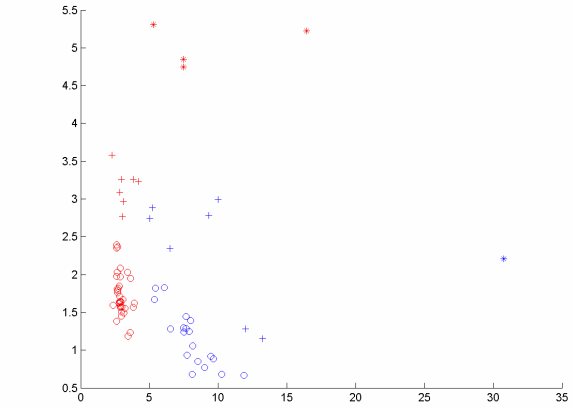

Figure 4. Vehicle distribution in the two-dimensional feature space (six-parameter input data-based PCA).

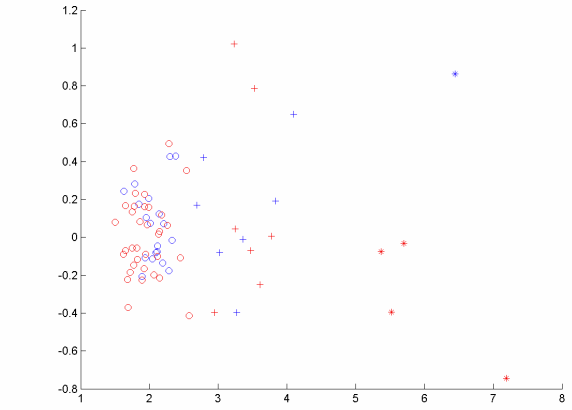

Figure 5. Vehicle distribution in the two-dimensional feature space, if only height parameters (4) were used in the PCA process.

By comparing Figures 4 and 5, it can be seen that vehicle categories can be effectively separated using solely vehicle height parameters. Obviously, not using the length information means that the vehicle travel directions become indistinguishable. Why the width has no significant impact is

probably explained by two facts. First, the variations between the three vehicle groups are rather small – the difference between the mean vehicle widths is about 0.5 m. Second, the footprint of the LiDAR, the area that one pulse will reach, is about 25 cm (diameter of the circle/ellipse). Given the spacing between the LiDAR pulses, which is at least 0.5 m, it is apparent that the measuring accuracy of the vehicle width is rather poor. Consequently the information content of this parameter is rather insignificant. The vehicle travel direction, however, can be recovered from the six-parameter model.

5. VEHICLE CLASSIFICATION

For vehicle classification, three methods were considered. The main goal is to classify the vehicles into the three main categories: passenger cars (P), multi-purpose vehicles (MPV) and trucks (T). Each category has two subclasses (along and against) considering the traffic direction relative to the flight direction. Therefore, the recognition process is expected to separate the vehicles into six groups, identified in Table 1.

ID	*Category*
1	P along
2	P against
3	MPV along
4	MPV against
5	T along
6	T against

Table 1. Vehicle categories used with the LiDAR data set.

The first method, a rule-based classifier, contains decision rules derived from the PCA transformed features. As depicted in Figure 6, a clear separation, in other words, clustering of samples with identical labels can be easily made between the groups by using straight lines. These lines are of course specified by two variables, which are determined by simple calculations.

For example, Category 1 (passenger cars traveling along the flight direction) is bounded by *Line A* and *C*, furthermore by the coordinate axis *x*. *Line A* can be defined by (1):

$$y = a_A x + b_A = \frac{0.5-3}{15}x + 3 \qquad (1)$$

where x and y are the two first principal components. Similarly *Line C* is defined by (2)

$$x = 4.5 \qquad (2)$$

The rule for the category is thereafter:

$$(y < -\frac{2.5}{15}x + 3)\ AND\ (x > 4.5)\ AND\ (y > 0) \qquad (3)$$

Category 3 (MPV traveling along the flight direction) represents a more complex cluster boundary, which can be described as:

$$(y > a_A x + b_A) AND (y < a_B x + b_B) AND (x > x_C) AND (y > c_D) AND (y > 0) \qquad (4)$$

where the indices show which parameters correspond to which lines.

The determination of all parameters and subsequent creating of all the rules is a rather straightforward task. However, the introduction of new observations (new features) usually requires the refinement of the rules. Applying the rules to an unknown feature vector is obviously simple and fast.

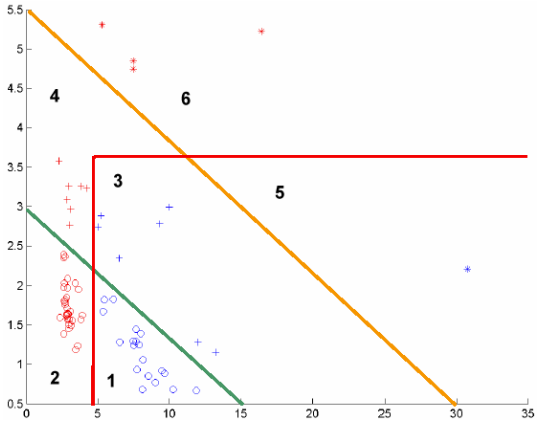

Figure 6. Segmentation of the two-dimensional feature space of the training vehicles

The second investigated classifier was a fundamental statistical technique: the minimum distance method. This classifier is based on a class description involving the class centers, which are calculated by averaging feature components of each class. An unknown pattern is classified by computing the distances between the pattern and all class centers and the smallest distance determines to which class the pattern will be classified. The distance calculation based on the Euclidean measure in our two-dimensional case is (Duda, 2001):

$$D_j = \sqrt{(x - \bar{x}_j)^2 + (y - \bar{y}_j)^2} \qquad (5)$$

where the class center of class j is given by $\bar{x}_j$ and $\bar{y}_j$. The classification is based on the evaluation of (6):

$$C = \arg\min_j (D_j) \quad j = 1, 2, \ldots 6 \qquad (6)$$

This method is simple and the algorithm processes rather quickly. As new vehicles are added to the training set, the class centers have to be recalculated, but the decision formula remains unchanged. Class centers and boundaries, which form a Voronoi tessellation, are shown in Figure 7.

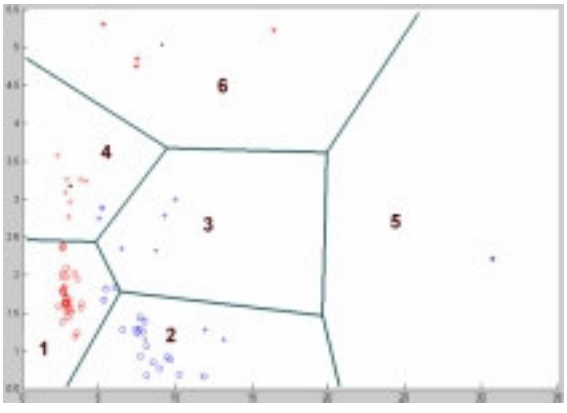

Figure 7. Segmentation of the two-dimensional feature space of training vehicles by the minimum-distance method (Voronoi tessellation).

The third method in the vehicle recognition investigation was based on an artificial neural network classifier. As it is commonly agreed (Brause, 1995; Rojas, 1993), most practical works require 3-layer feed-forward (back-propagation) neural networks; hence such a structure was implemented in our tests. The training method was the Levenberg-Marquard algorithm (Demuth, 1998), the maximal number of training steps (epochs) was 70, and the required error goal value was 0.1. The network error was calculated by the mean square error (MSE) method. At the end, the output of the neural network was rounded to the nearest integer. Further details on the neural network classifier can be found in (Toth et. al., 2003b).

The three developed vehicle recognition techniques were tested on the training data set of Ohio (1), on the data set containing vehicles from Ohio and Michigan, (2) and on combined dataset, including the Ontario data (3), provided by Optech. The first test (in-sample test) was only an internal check of the algorithms. Tables 2 and 3 show a performance comparison of the three techniques.

Data set (total number of vehicles)	*Rule-based*	*Minimum distance*	*Neural network*
Ohio (72 vehicles)	0 (0%)	8 (11.1%)	2 (2.8%)
Ohio + Michigan (87)	2 (2.3%)	12 (13.8%)	8 (9.2%)
Ohio + Michigan + Ontario (102)	2 (2%)	17 (16.7%)	16 (15.7%)

Table 2. The comparison of the three recognition techniques: vehicle count number of misclassification errors.

Data set (total number of vehicles)	*Rule-based*	*Minimum distance*	*Neural network*
Ohio (72 vehicles)	0 (0%)	4 (5.6%)	2 (2.8%)
Ohio + Michigan (87)	2 (2.3%)	8 (9.2%)	8 (9.2%)
Ohio + Michigan + Ontario (102)	2 (2.3%)	10 (9.8%)	14 (13.7%)

Table 3. The misclassification errors of the three methods, without considering the vehicle travel directions.

The rule-based method has perfectly identified the features, while the other two methods have small recognition errors. In all methods, the most frequent misclassification error type was the mismatch of the Ps and the MPVs in the along direction, since passenger cars can have shape and length very similar to MPVs. Ignoring the relative traveling direction, in other words classifying into three classes instead of six, the results are somewhat different as shown in Table 2.

The tests with the combined Ohio, Michigan and Ontario data show strong out-of-sample performance, which is a good indication of the applicability of the proposed vehicle recognition method. Obviously, more tests with a variety of data are needed to confirm the ultimate potential of using LiDAR data as a source for traffic flow estimates.

6. VELOCITY ESTIMATES

In simple terms, traffic flow over a road segment is defined as the product of the vehicle density and the average vehicle velocity. Therefore, estimating the speed of the vehicles is as important as counting and categorizing the vehicles, which was demonstrated in the previous section. In the following example, we will analyse how their velocity can be estimated. To extract vehicle velocities from LiDAR data, however, is not a simple task. Knowing the actual size of the vehicle, $\boldsymbol{s}$, and the LiDAR-measured size of the vehicle, $\boldsymbol{m}$, the vehicle speed can be expressed with respect to the LiDAR sensor speed as:

$$v_v = \frac{m - s}{m} \cdot v_l$$

where $\boldsymbol{v_v}$ is the estimated vehicle velocity and $\boldsymbol{v_l}$ is the speed of the LiDAR sensor. The difficulty of using this expression is that neither $\boldsymbol{s}$ nor $\boldsymbol{m}$ (the actual and the LiDAR-measured vehicle sizes) is known with sufficient accuracy. Only the LiDAR sensor speed is available with good accuracy. Clearly, the main vehicle categories provide some approximation of the vehicle size in the form of ranges. Unfortunately, except for the 18-wheelers, these intervals are overlapping. The accuracy of estimating $\boldsymbol{m}$ is, at minimum, limited by the footprint size of the LiDAR (Maas, 2002). In summary, individual vehicle velocities, in general, cannot be estimated at acceptable accuracy from LiDAR data; or, more precisely not from data acquired by current airborne laser scanners. The introduction of additional sensor data, such as simultaneously acquired imagery (Toth and Brzezinska, 2000b), however, can provide the missing vehicle size information and thus satisfactory velocity estimates can be achieved.

Without using additional sensory data, reasonable estimates can be obtained for specific situations such as large trucks or a platoon. For example, the vehicle category of the eighteen-wheelers can be characterized by a typical vehicle length with rather small variations in size. Thus, for such a truck travelling in the same direction as the LiDAR platform, the estimate of the vehicle speed could be determined at about 10% accuracy level under good conditions. For a platoon, statistical methods can provide a methodology for average speed estimation. For example, knowing the distribution of vehicle sizes of the main categories has the potential to estimate the average velocity of a larger group of the LiDAR-measured sizes with a reasonable confidence level, sufficient to derive flow data.

7. CONCLUSIONS

In this paper, the feasibility of using high-performance LiDAR data to derive traffic flow information has been studied. A simple model, built on the combination of vehicle shape and vehicle size, has shown robust performance for a sizeable population of vehicles extracted from two LiDAR datasets obtained from regular mapping airborne surveys. A principal component analysis performed on the six-parameter model resulted in a substantial reduction of the parameter space. Using only two of the largest eigenvalue components, not only could the three main vehicle groups be classified, but the vehicle travel direction could also be identified. The training set included 72 vehicles and the resultant classes in the two-dimensional parameter space. Three classification methods have been used and all of them have produced rather good results. Therefore, it is fair to say that LiDAR data can be efficiently used to support traffic flow applications. All three methods were able to recognize the vehicle categories with accuracy better than 80 %. This high recognition rate proves that a classifier designed and parameterized by an adequate training dataset can be successfully applied on other, unknown data sets. Furthermore, the results are even more encouraging, if the relatively modest LiDAR point density is factored in (1.5 point/m^2). State-of-the-art LiDAR systems can easily provide a 3-5 times denser point cloud and consequently better classification performance can be expected.

Estimating the velocity of the extracted and categorized vehicles, however, has produced mixed results. The speed for larger vehicles can be coarsely approximated, but there is no acceptable solution for estimating individual vehicle velocity exclusively from LIDAR data. Combining LIDAR with complementary sensor data, such as imagery, however, can provide a good base for velocity estimates and thus traffic flow data can be obtained.

In summary, the developed method has demonstrated that LiDAR data contain valuable information to support vehicle extraction, including vehicle grouping and localizations. The classification performance showed strong evidence that the major vehicle categories can be efficiently separated. With the anticipated improvements in LiDAR technology, such as denser point cloud and smaller pulse footprint, the classification efficiency is expected to increase. The price of LiDAR, however, is prohibitive at this point to support traffic monitoring applications. Nevertheless, collecting data over transportation corridors during regular surveys already offers a no-cost opportunity to obtain important traffic data. In addition, the advantage of the moving platform is that it can be freely deployed any time and anywhere.

8. ACKNOWLEDGEMENTS

This research was partially supported by the NCRST-F program. The authors would like to thank Tamas Lovas, PhD candidate from Budapest University of Technology and Economics and Vikram Ramprakash for their help in the data processing, and Woolpert LLC and Optech International for providing the LiDAR datasets.

9. REFERENCES

Baltsavias, E. P. – Gruen, A. – L. V. Gool (Eds.) (2001): Automatic Extraction of Man-Made Objects from Aerial and Space Images (III), Alkema Publishers, Lisse

Brause, R. (1995): Neuronale Netze, B. G. Teubner, Stuttgart

Demuth, H. – Beale, M. (1998): Neural Network Toolbox, Matlab User's Guide, The MathWorks, Natick

Duda, R. O. – Hart, P. E. – Stork, D. G. (2001): Pattern Classification, Wiley, New York

FDOT (2002). Achievements of the DOT-NASA Joint Program on Remote Sensing and Spatial Information Technologieshttp://www.ncgia.ucsb.edu/ncrst/synthesis/SynthRep2002/).

Flood, M. (1999): Commercial Development Of Airborne Laser Altimetry – A Review Of The Commercial Instrument Market And Its Projected Growth, *International Archives of Photogrammetry and Remote Sensing*, Mapping Structure and topography by Airborne and Spaceborne Lasers, Vol. XXXII, part 3/W14, pp. 13-20.

Grejner-Brzezinska, D. A. – Toth, Ch.K. (2002). Modern Remote Sensing Techniques Supporting Traffic Flow Estimates, Proceedings of the International Technical Meeting of The Institute of Navigation, 24-27 September, 2002, Portland, OR, CD-ROM, pp. 2423-2433.

Grejner-Brzezinska, D. A. – Toth, Ch.K. (2004). Airborne Remote Sensing Supporting Traffic Flow Estimates, in this proceedings.

Lillesand, T. M. – Kiefer, R. W. (1994): Remote Sensing and Image Interpretation, Wiley, New York

Pitas, I. (2000): Digital Image Algorithms and Applications, John Wiley & Sons, Inc.

Rojas, R. (1993): Theorie der neuronalen Netze – Eine systematische Einführung, Springer Verlag, Berlin

Russ, J. C. (1995): The Image Processing Handbook, CRC Press, Boca Raton

Toth C. – Grejner-Brzezinska D. – Lovas T. (2003a): Traffic Flow Estimates from LiDAR Data, Proc. ASPRS Annual Conference, May 5-9, pp. 203-212, CD ROM.

Toth C. – Grejner-Brzezinska D. – Merry C. (2003b): Supporting Traffic Flow Management with High-Definition Imagery, Proceedings of ISPRS/EARSeL Joint Workshop on High Resolution Mapping from Space 2003, Oct 6-8, Hannover, Germany, CD-ROM.

Toth C. – Barsi A. – Lovas T. (2003c): Vehicle Recognition from LiDAR Data, *International Archives of Photogrammetry and Remote Sensing*, Information from Imagery, Vol. XXXIV, part 3/W13, pp. 162-166.

Wehr A. – Lohr U. (1999): Airborne Laser Scanning – and Introduction and Overview, *ISPRS Journal of Photogrammetry and Remote Sensing*, 54, pp.68-82.

Zhao, Y. (1997): Vehicle Location and Navigation Systems, Artech House, Inc., Boston.

APPENDIX B

1. Toth C. and Grejner-Brzezinska D.: Traffic Flow Estimation From Airborne Imaging Sensors: A Performance Analysis, Proc. of Joint ISPRS Workshop on High Resolution Earth Imaging and Geospatial Information, Hannover, Germany, May 17-20, 2005, CD ROM.
2. Paska E. and Toth C. 2005: Vehicle Velocity Estimation from Airborne Imagery and LiDAR, Proc. ASPRS 2005 Annual Conference, Baltimore, MD, March 7-11, CD-ROM

TRAFFIC FLOW ESTIMATION FROM AIRBORNE IMAGING SENSORS: A PERFORMANCE ANALYSIS

C. K. Toth[a], D. Grejner-Brzezinska[b]

[a]OSU, Center for Mapping, 1216 Kinnear Road, Columbus, OH 43212-1154, USA – toth@cfm.ohio-state.edu
[b]OSU, Department of Civil and Environmental Engineering and Geodetic Science, Columbus, USA

Commission I and IV, WG I/1, WG 1/3, WG I/5, WG IV/2, WG IV/5

KEY WORDS: LiDAR, digital camera, vehicle extraction, traffic flow

ABSTRACT:

Recent developments in airborne sensor technologies have led to not only improved mapping performance, but have opened up a series of new applications. Enhanced spatial and temporal resolution can now allow for effectively detecting and describing moving objects for the first time. Vehicles, moving or standing, used to be problematic during the traditional mapping process; they needed to be detected and removed during the surface and/or object extraction process. From a traffic monitoring and management perspective, however, these objects are of high interest. The number of vehicles, their location and velocity as well as additional properties, such as vehicle type, size or weight, represents the essential base data for traffic flow description and modeling. Research has shown that vehicles can be extracted, counted and tracked from image sequences and that LiDAR data can provide an effective coarse categorization of vehicles in a highly automated way.

An analysis of the performance on the traffic flow estimation process for a typical state-of-the-art airborne sensor suite, composed of a LiDAR and a digital camera is presented. To assess the absolute performance, a dedicated test flight over a calibration range was conducted. The test area had specific ground targets that are equally identifiable and can be accurately positioned in both LiDAR data and imagery. In addition, a moving target was used to assess the size measuring performance of the moving object extraction process. The results confirmed that high-performance airborne sensors can provide quality data for traffic flow information extraction.

1. INTRODUCTION

Transportation represents a major segment of the world's economy, and as such must be carefully monitored and planned. This requires the most up-to-date, accurate and continuous methods for screening and mapping for effective modeling and management. Traditionally, permanent installations provide mostly real time information usually gathered from many diverse sources, such as electronic sensors in the pavement (loop detectors), road tubes, ramp meter sensors, and video and digital cameras. Data from these sensors are sent to the traffic management center at various times. Most of this information is only recorded; a small part of it is analyzed in real-time and used for immediate traffic control and decision-making. Furthermore, the installation and use of ground-based sensors disrupts traffic and endangers the crews. The major focus of this research effort, in general, is to improve the efficiency of the transportation system by the integration of remotely sensed data with the traditional ground data to monitor and manage traffic flows.

The National Consortium for Remote Sensing in Transportation-Flows (NCRST-F), led by The Ohio State University, and sponsored by the U.S. Department of Transportation and NASA, was established in 2001. Our partners in NCRST-F are the University of Arizona and George Mason University. As mentioned earlier, the major focus of the OSU research team is to improve the efficiency of the transportation system by the integration of remotely sensed data with traditional ground data to monitor and manage traffic flows. Our research team is concerned with the vehicle extraction and traffic pattern modeling based on airborne digital data that is collected by medium-format frame cameras and LiDAR systems. This paper is an extension of our earlier publications, where theoretical and practical studies on the feasibility of using LiDAR data and airborne imagery collected over the transportation corridors for estimation of traffic flow parameters, were presented.

The driving force behind this research effort is opportunity mapping. A fairly large percentage of geospatial data acquisition is done over urban areas with a substantial road network, where the vehicles become obstacles that need to be removed. In particular this is the case for road surface and/or road infrastructure mapping. This information should not be discarded, however, but rather the data should be directly converted to traffic flow data. Collecting data over the transportation corridors during regular surveys offers a unique opportunity to obtain important data for transportation planners and managers at practically no additional cost. Data can be acquired also in transit while the system is flown between various mapping jobs. Medium format cameras have become standard companion sensors for LiDAR, providing simultaneous visual image coverage and thus this imagery can be also used to support traffic flow extraction.

In this contribution the actual example of traffic flow estimation, along with performance validation obtained from high-accuracy datasets collected in late 2005 in Ohio, USA is presented. In particular, vehicle extraction, velocity estimation supported by fusion of LiDAR and image data, as primary parameters describing the traffic flow, are discussed and analyzed.

2. TRAFFIC FLOW

For highway planning and traffic management purposes, each road segment is characterized by its traffic flow. Flow can be defined as the number of vehicles passing a given

point on a highway during a given period of time, such as vehicles per hour. Flow is one of the primary elements of traffic stream description besides density and speed. The three basic parameters of traffic stream are related to each other by the following relation: flow is the product of speed and density. The two basic types of mathematical models for describing traffic flow are the macroscopic and microscopic models. While macroscopic models are concerned with describing the flow-density relationship for a group of vehicles, microscopic models describe the flow by tracking individual vehicles using car-following logic. The relationship between flow and density is frequently used in freeway traffic management to control the density in an effort to optimize productivity (flow). The relationship between speed and flow could be used for design purposes, as it defines the trade-off between the level of service on a road facility (as expressed by the speed) and the productivity (as defined by the flow). Traffic control is aimed at managing and controlling the movement of traffic on streets, highways, and freeways in an attempt to optimize the use of such facilities. Traffic control service, in general, is responsible for collecting real-time traffic data from the field and then processing the data into useful information (Chowdhury and Sadek, 2003).

Traffic flow is a generic term used to describe vehicle movement and volume over a transportation network. Two of the most important traffic measures produced by state DOTs and other transportation agencies around the world are AADT and VMT (Pline Ed., 1992). Average annual daily traffic (AADT) is produced to represent the vehicle flow over a highway segment on an average day of the year. Vehicle miles traveled (VMT) indicates travel over the entire highway system and is used to indicate mobility patterns and travel trends. VMT is also used as an indicator for allocation of highway resources. Flow data are generally obtained by ground-based equipment, such as loop detectors or road tubes, which are fixed to a location and are deployable as needed. In the latter case, the sample data are collected from road tubes placed in the traveled portion of the road, disrupting traffic and endangering the crews when placing or collecting the tubes. Using satellites and air-based platforms, the survey/control crews can cover large areas, access remote highways, and carry sensors that can collect data from safe and non-disruptive off-the-road locations. The imagery collects "snapshots" of traffic over large areas at an instant of time or a sequence of snapshots over smaller areas, whereas traditional data collection observes vehicles at a point on the highway over much longer time intervals (McCord *et al*., 2003).

3. TRAFFIC FLOW FROM AIRBORNE SENSORS

The idea of using remote sensing for obtaining traffic flow data comes from two directions. First, a demand for finding new data sources to support and improve traffic flow monitoring and management inspired a research initiative on using remote sensed data in transportation. Second, the transition of the last few years from analog airborne imaging systems to fully digital multi-sensory imaging suites supported by high-performance direct georeferencing has provided the enabling technology needed for effective detection of moving targets.

Initial research focused on extracting traffic flow data from aerial and satellite imagery, see (Toth et al., 2003b; Merry *et. al*, 1999; Grejner-Brzezinska and Toth, 2002 and 2003b). Later, theoretical and practical studies were carried out on the feasibility of using LiDAR data to obtain traffic flow estimates, see (Toth *et. al*, 2003a and 2004; Ramprakash 2003; Grejner-Brzezinska and Toth, 2003a). These papers describe methods for vehicle detection, extraction, and tracking from both imagery and LiDAR, which form the basis for traffic flow parameter estimation, such as vehicle count, classification and vehicle velocity estimates.

3.1 Flow Data from LiDAR

A LiDAR point cloud offers explicit three-dimensional information of the object space and consequently provides an excellent basis for shape-based feature extraction. Furthermore, road surfaces have simple geometry and to some extent that applies to the vehicles; therefore, the vehicle extraction not only can be automated, but it can be done at a rather high performance level. Typically, a vegetation canopy over roads could pose some difficulty, although multiple returns from the LiDAR pulse can mitigate this problem. Obviously, the LiDAR point density plays a key role in the vehicle extraction performance and all the follow-on processing steps. Extended experiments proved that from 2-3 points/m^2 density, the vehicle extraction becomes robust and there is not much improvement beyond 5 points/m^2. A vehicle at 7 points/m^2 is shown in Figure 1. For vehicle classification, the situation is different, as the higher point density is essential to differentiate among vehicle categories. At the 2-5 points/m^2 density range, only major vehicle classes, such as cars, trucks and the remaining other vehicles could be classified at an acceptable success rate (Toth and Grejner-Brzezinska, 2004b). The 15-20 vehicle category based classification used by most transportation agencies requires substantially higher densities that is not routinely achieved in current airborne LiDAR practice (terrestrial laser scanning can easily provide that point density). The velocity of vehicles can be estimated from the motion artifact in LiDAR data due to the scanning pattern and the relative velocity of the sensor and the moving targets. The difficulty is that the true vehicle size is unknown and only the class mean or median data can be used, resulting in rather poor velocity estimates. The effect of the weak velocity data measures could be reduced, if the average velocity is computed for a larger group of vehicles (Toth *et al*, 2004b).

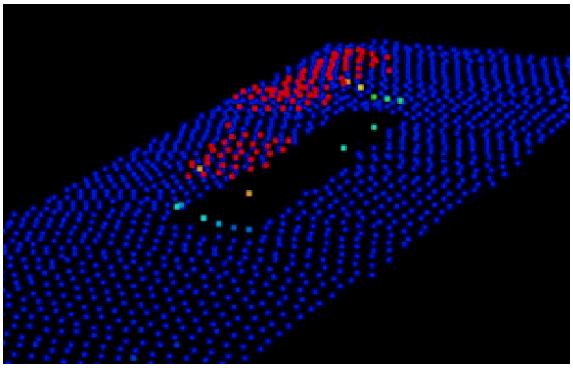

Figure 1. Vehicle close-up from LiDAR.

3.2 Flow From frame Imagery

Vehicle detection and tracking from reconnaissance and to a less extent conventional airborne surveying imagery has been

a well-established research field for several decades. Developments have been mostly fueled by defense applications. Even a short overview of the available methods/techniques from this field would go beyond the size limitation of this paper. The approach we selected for our research is based on using orthorectified imagery. Furthermore, only medium format digital cameras, with a typical 4K by 4K sensor resolution were considered, such as the DSS system from Applanix. The image scale varied between 1:6,000 and 1:20,000 (in ground resolution terms, the GSD was in the 7-25 cm range). The creation of orthoimages imposes certain requirements, such as the availability of good surface data, either from a past mission or simultaneously acquired with the imagery and good direct sensor orientation data, but the benefits are irresistible. Most importantly, the vehicle shape in the horizontal footprint is preserved at true object scale. For overlapping images, the detection of moving vehicles (as well as any moving targets) can be accomplished by a simple image subtraction, as shown in Figure 2, while detection of non-moving vehicles is a much more complex task. Both processes can be supported by available road geometry data, such as road centerline or edge lines. Test images acquired from helicopter and fixed-winged aircraft were used to monitor traffic flow over road segments and to determine turning volume at intersections. Results showed good performance for extracting moving vehicles (Grejner-Brzezinska *et al*, 2004; Paska and Toth, 2004; Paska and Toth, 2005). Vehicle tracking, however, still needs more research, as the implemented solution produced unreliable results, which is partially due to the slow image acquisition rate (0.2-0.3 images/s) and/or lack of adequate overlap (Toth and Grejner-Brzezinska, 2004).

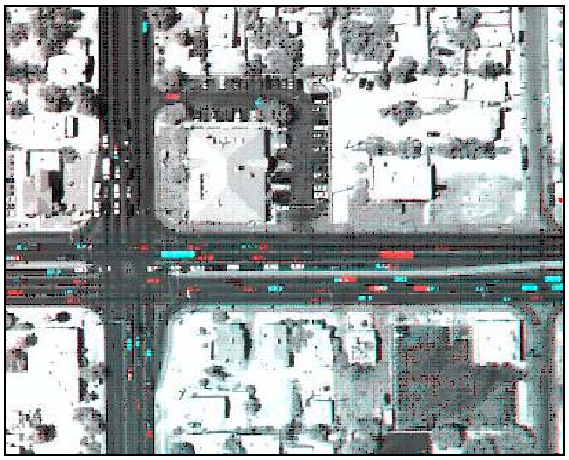

Figure 2. Detecting moving objects in the ortho domain.

3.3 Comparing Flow Data Obtained by LiDAR and Frame Imagery

The performance of LiDAR and image based traffic flow extraction depends on a variety of factors, such as sensor specification, sensor platform, data acquisition pattern, sensor calibration, sensor inter-calibration, direct georeferencing performance and feature extraction performance that could be further broken down into vehicle detection, vehicle parameterization/classification, and velocity estimation. Ignoring the common and non traffic flow specific aspects, a simple performance matrix is provided in Table I, where the parameters reflect the cumulative results from a wide spectrum of airborne tests within a time span of about three years. The sensor instrumentation included older 10 kHz and 33 kHz LiDAR systems and a new ALTM 30/70, a BigShot 4K by 4K digital camera and DSS systems. The direct georeferencing of the imaging sensors was supported by several geodetic grade IMUs and GPS receivers. Table 1 is intended only for orientation purposes, as it cannot account for several factors of various flight and sensor configurations, such as LiDAR point density or image data rate/overlap, processing and interpretation details, such as feature extraction performance, image artifacts, or absolute vs. relative accuracy performance. Nevertheless, Table I clearly shows the main trends, namely, that LiDAR is very effective at vehicle extraction and coarse classification, but is less adequate for velocity estimation. Imagery has just the opposite pattern; it is less effective for vehicle extraction, but once vehicles are extracted and tracked, the velocity estimation is rather good. Since flow is the product of vehicle counts and velocity, the end results are comparable for both sensors.

Sensor	**LiDAR**	**Digital Camera**	
Platform	**Airplane**	**Airplane**	**Helicopter**
Performance	**[%]**	**[%]**	**[%]**
Vehicle extraction			
Vehicles moving	95+	90+	95+
Vehicles not in motion	95+	80+	80+
Vehicle classification into three major classes	99+	60+	70+
Vehicle tracking	Not feasible	<50	60+
Error (typical)			
Velocity estimation	20-40	<20	<10
Flow computation	10-20	<10	< 5

Table 1. Performance of various traffic flow extraction tasks with respect to sensors and platforms.

4. COMBINING LIDAR AND IMAGERY

The recent trend in airborne surveying, the simultaneous data acquisition of LiDAR with medium format digital camera, allows for the fusion of both the sensor-level data and the results/features extracted from the two datasets. As discussed in the previous section, both sensors are capable of providing vehicle counts and velocity estimates, however, in varying quality. Since their limitations and strengths are complementary, they can support each other and their fusion could lead to better traffic flow estimation. Therefore, the next step in our research should be to combine the LiDAR outstanding vehicle extraction performance with the excellent velocity estimation of the optical imagery. Thus, the objective of this discussion is to assess how the velocity of moving objects extracted from LiDAR can be better estimated by using imagery.

To overcome the errors in the true vehicle length estimation in the LiDAR data due to generalization or possible misclassifications, the actual length of the vehicle must be determined from other sensory data, such as imagery collected simultaneously with the LiDAR data. Though a single image does not provide the absolute size information, the image may preserve the relative object size information, such as the width/height ratio of a vehicle. Although an extra effort, such as using an adequate matching technique, is

required to identify the identical vehicles in the two datasets, the combination of the two datasets could eventually lead to an improved velocity estimation of the moving vehicles (Paska and Toth, 2005).

Figure 3 shows extracted vehicles from LiDAR data, as they are overlaid on an orthoimage formed from a simultaneously acquired image. LiDAR vehicle points are represented in green and red, corresponding to the motion along or against the flying direction, respectively. For referencing, some static objects, such as one point on the centerline and points at the guard rail, are also marked in the figure. This figure illustrates: (1) the elongated (when vehicles are moving along the flying direction) and shortened (when vehicles are moving against the flying direction) lengths of the moving objects, as sensed by the LiDAR, and (2) the relationship between corresponding vehicles on the imagery and in the LiDAR data. The matches of the corresponding vehicles in the two datasets are highlighted by rectangles with identical colors. Due to the different nature of the two data acquisition techniques, the continuous scanning mode of the LiDAR sensor and instantaneous capturing of frame imagery, the locations and also the shapes of the corresponding vehicles differ in the two datasets. The white triangle in Figure 1 shows the approximate location of the LiDAR beam when the image was taken.

Vehicles can be sorted into four categories based on their direction and the relation of their positions in the LiDAR and imagery data: (1) vehicles traveling along the flying direction and scanned before the image acquisition (in Figure 1 they are in the upper lanes and to the right from the triangle sign), (2) vehicles traveling along the flying direction and scanned after the image acquisition (in Figure 2 they are to the left from the triangle sign), (3) vehicles traveling against the flying direction and scanned before the image acquisition (in Figure 1 they are in the lower lanes and to the right of the triangle sign), and (4) vehicles traveling against the flying direction and scanned after the image acquisition (in Figure 1 they are to the left of the triangle sign).

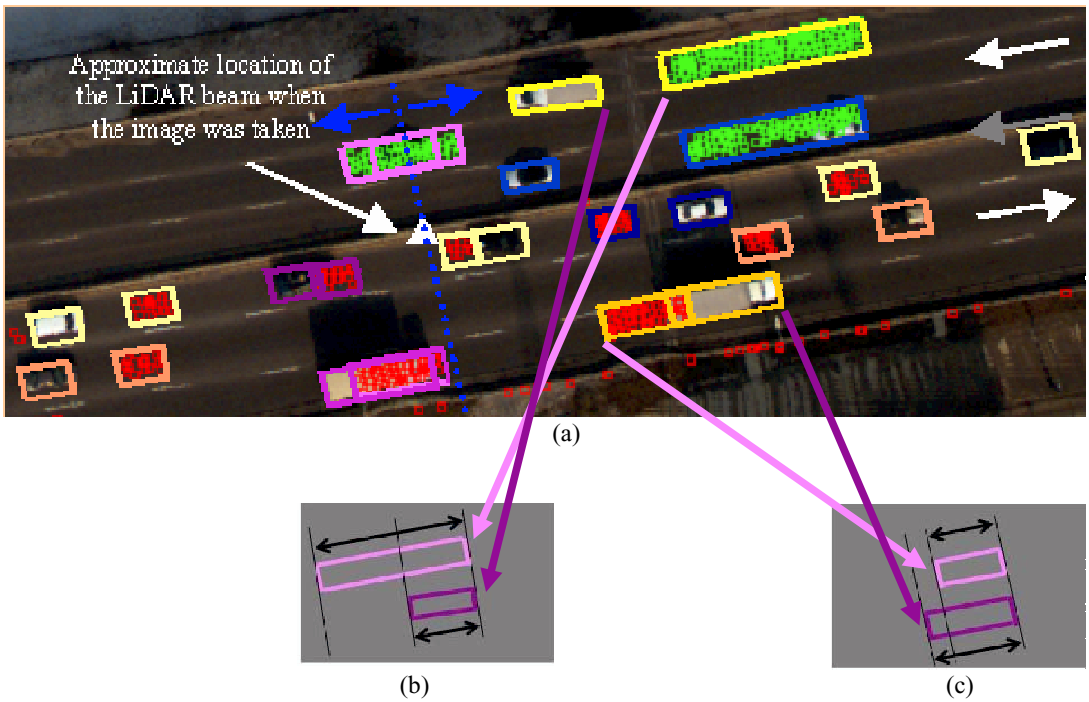

Figure 3. Vehicles extracted from the LiDAR data and overlaid on the orthoimage;
(a) match of corresponding vehicles in the two datasets is marked with identical colors.
Also shown are (b) vehicle elongation, and (c) vehicle shortening.

Note that the LiDAR point clouds of the vehicles fall in front of the corresponding vehicles on the left side of the blue dotted line and behind the corresponding vehicles on the right side of the line. This is because the LiDAR measured the vehicle either before or after the image was taken. Based on the known relative positions of corresponding vehicles, search areas for a matching procedure can be determined. The acquisition time of each LiDAR point, as well as the image capture time, is recorded in GPS seconds. The possible relative distance between the image and LiDAR vehicle positions could be calculated from the vehicle velocity and the acquisition time of the image and the LiDAR vehicle points (coarse vehicle velocity approximations could be obtained from vehicle velocity computation from image sequences or the minimum and maximum speed limits of the actual road and so on). Note in Figure 3 that the relative distance between corresponding vehicles is getting larger the farther from the triangle sign. Similarly, the difference between the data acquisition time of the LiDAR sensor and digital camera is also getting larger. The difficulty of matching can be substantially reduced with higher image acquisition rates that can be easily achieved with modern digital cameras. Since the road surface, as well as the image sensor plane on the airborne platform is usually horizontal, the width/height ratio of a vehicle is fairly accurate with respect to, for example, the LiDAR point horizontal positional accuracy. Thus, the LiDAR-sensed vehicle width

can be used to determine the vehicle true length by using the width/height ratio obtained from the image.

5. PERFORMANCE EVALUATION

To check the performance of the combined LiDAR and image traffic flow extraction, as well as validate the LiDAR only or image only estimates, a dedicated test flight was organized in late 2004. The Madison County, Ohio, test range that includes a dense network of permanently installed signalized ground controls to support airborne surveys was temporarily extended by using LiDAR-specific targets, shown in Figure 4, that could be also used for image control (Csanyi *et al*., 2005). In addition, there was a "moving" target, the OSU Center for Mapping GPSVan (He *et al.*, 1994), a vehicle equipped with high performance GPS/IMU hardware. This vehicle, shown in Figure 4, was constantly moving in the test area and was mapped by both sensors several times under various sensor settings, such as the LiDAR system was operated at various pulse rates during repeated passes over the calibration range. This served several purposes. Most importantly, the impact of the point density for the vehicle extraction, classification and velocity estimation was assessed. This also provided valuable data to assess the impact of the various pulse rates on the overall accuracy of the system, with and without ground controls. The airborne sensor suite included an ALTM 30/70 LiDAR system and a DSS digital camera. The LiDAR system was operated at 33, 50 and 70 kHz pulse rates, resulting in point densities ranging from 3 to 8 points/m^2. The digital camera had a GSD range of 10-15 cm.

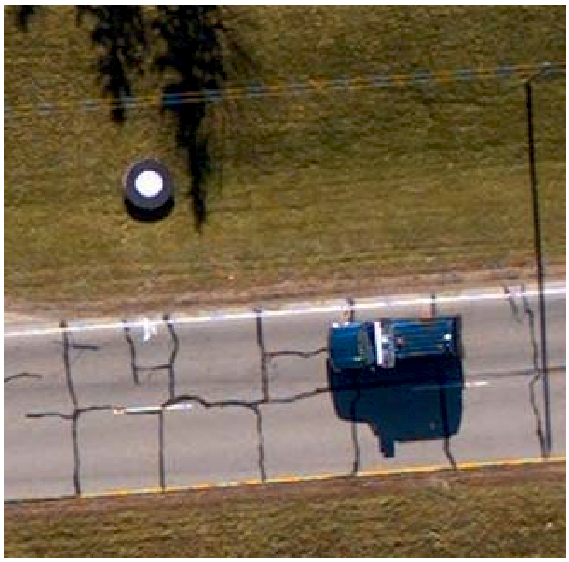

Figure 4. LiDAR target and the GPSVan.

Table 2 shows a representative set of measurements of the LiDAR sensor as it mapped the GPSVan at various pulse rates. As expected, the accuracy of the vehicle size, as measured by the smallest rectangle fitted to the vehicle points, depends on the point density, which, in turn, is basically a function of the pulse rate for a given flying height. Clearly, the vehicle width is fairly underestimated at lower point densities. The smaller size is a combined effect of the point density, laser pulse divergence and point pattern. The image measurements for the width/length ratios, however, show a good stability. The vehicle velocity estimates, shown in Table 3, illustrate that the larger error was introduced by the incorrect vehicle length. The GPSVan has a true length of 5.5 m but falls into the other vehicle category with a class length value of 4.7 m. This length could be effectively decreased by the vehicle length estimation from the LiDAR-measured width by using the image measured width/length ratio. The statistics, shown for the cases when the vehicle and the LiDAR traveled in the same direction (shaded area in Table 3) clearly indicate that accuracy of the true length-based velocity estimation can be achieved for the combined LiDAR and image solution. The opposite direction case has a smaller improvement, (with statistics of estimated bias and variance of 2.39 and 1.73, respectively). However, it is still important as it helps to obtain a better overall error in velocity when the average velocity of a group of vehicles is computed. Further discussion of the error characteristics of the LiDAR-based length and velocity estimation is in (Paska and Toth, 2005).

6. SUMMARY

Earlier research results demonstrated that airborne remote sensing based on state-of-the-art LiDAR and digital camera systems could provide valuable traffic flow data that can effectively support traffic monitoring and management. In particular, LiDAR has proven to be a good source of vehicle extraction and course classification, while digital imagery excels with better velocity estimation performance. In this paper, an initial analysis was provided to assess the overall performance gain in traffic flow estimation, if LiDAR and digital imagery were combined at the feature level.

Vehicle velocity estimation from LiDAR is based on the vehicle elongation and shortening of the moving objects due to the scanning mode of the data acquisition. The accuracy of vehicle velocity estimation depends on the vehicle's direction, true length, relative velocity between sensor and object, and on how accurately the true and LiDAR-sensed vehicle length could be estimated. The actual vehicle size is unknown in practice, and thus, the true length of the vehicles must be estimated from either the basic statistics of the vehicle categories, that can be determined after classifying the extracted vehicles, or by using additional information. To overcome the errors in the true vehicle length estimation due to generalization or possible misclassifications, the actual length of the vehicles was determined by using scale information from imagery collected simultaneously with the LiDAR. Initial results have shown that combining LiDAR with complementary sensor data, such as simultaneously collected imagery, can provide a better base for velocity estimation and thus allows for more reliable traffic flow parameter determination.

This discussion in a broader sense addresses the problem of mapping moving objects, which is an emerging field in geospatial science. Obviously, transportation, and in particular, traffic management needs this data, but rapid/emergency mapping also demand this type of geospatial data acquisition and processing. Our investigations provide an insight into the difficulty of mapping moving objects and clearly indicate that only multisensory systems can adequately solve the problem of collecting high spatial and temporal resolution geospatial data in a preferable highly redundant manner.

LiDAR sensor parameters						Vehicle measurements					Image-based correction	
Strip number	PRF [kHz]	Scan angle[°]	Spacing between profiles [m]	Point spacing in profiles [m]	Point density [pts/m^2]	Vehicle direction with respect to LiDAR platform	LiDAR-measured vehicle length [m]	LiDAR-measured vehicle width [m]	Ideal LiDAR vehicle length [m] (based on GPS)	Number of points per vehicle	Image-measured length/width ration	Vehicle length from image ratio and LiDAR width
5	33	10	0.52	0.50	2.9	+	8.37	1.81	8.87	51	2.95	5.34
12	33	10	0.48	0.50	4.0	+	10.52	2.01	10.52	81	2.83	5.69
9	33	20	0.71	0.70	1.8	-	3.40	1.59	4.02	15	2.85	4.53
11	50	10	0.40	0.40	6.1	+	9.40	1.99	9.48	95	2.83	5.63
13	50	20	0.55	0.65	3.2	+	9.70	1.86	10.33	51	2.91	5.41
14	50	20	0.58	0.60	2.8	-	3.68	1.85	4.13	22	2.85	5.27
10	50	20	0.55	0.55	3.1	0	5.25	1.72	5.55	27	2.97	5.11
4	70	10	0.35	0.35	8.2	+	7.85	1.90	7.95	120	2.89	5.49
8	70	20	0.50	0.50	4.1	-	3.89	1.88	4.10	31	2.84	5.34
											2.88	
											0.05	

Table 2. Vehicle length and width measurement from LiDAR and length estimation based on combined LiDAR and image data.

Strip number	Vehicle velocity computed from different vehicle length measurements [m/s]						GPS velocity
	Using vehicle class length (4.7 m)		Derived from LiDAR width using image ratio		True vehicle length (5.55 m)		Reference
	Velocity	Difference	Velocity	Difference	Velocity	Difference	
5	19.75	-3.90	21.22	0.59	25.71	2.06	21.81
12	23.85	-4.16	23.18	0.59	27.93	-0.08	23.77
9	33.31	-0.18	17.51	2.45	20.14	-13.35	19.96
11	21.94	-4.58	21.48	0.73	26.79	0.27	22.21
13	21.71	-2.77	22.45	0.94	26.16	1.68	23.39
14	26.85	3.37	22.83	-4.82	14.64	-8.84	18.01
10	2.85	-5.15	1.33	-1.26	5.22	-2.78	0.07
4	15.15	-5.28	15.55	-0.08	20.75	0.32	15.47
8	23.11	7.87	20.18	-1.03	11.28	-3.96	19.15
		4.14		**0.58**		**0.88**	
		0.93		**0.32**		**0.91**	

Table 3. Velocity estimation performance for various sensor settings for LiDAR-only and for combined LiDAR and image data.

ACKNOWLEDGEMENTS

This research was partially supported by the NCRST-F and by the Ohio Department of Transportation. The authors would like to thank Eva Paska, PhD candidate student at the Department of Civil and Environmental Engineering and Geodetic Science, The Ohio State University for her help in the data processing.

REFERENCES

Chowdhury, M. A. – Sadek, A., 2003. Fundamentals of intelligent transportation system planning, Artech House Publishers.

Csanyi, N. – Toth, C. – Grejner-Brzezinska, D. – Ray, J., 2005. Improving LiDAR Data Accuracy Using LiDAR-Specific Ground Targets, ASPRS Annual Conference, Baltimore, MD, March 7-11, CD-ROM.

Grejner-Brzezinska, D. A. – Toth, C., 2002. Modern Remote Sensing Techniques Supporting Traffic Flow Estimates, Proceedings, ION GPS, September 24-27, CD ROM, pp. 2423-2433.

Grejner-Brzezinska, D. A. – Toth, C., 2003a. Deriving Vehicle Topology and Attribute Information over Transportation Corridors from LiDAR Data, Proceedings, ION 59th Annual Meeting, June 23-25, Albuquerque, New Mexico, CD ROM, pp. 404-410.

Grejner-Brzezinska, D. A. – Toth, C., 2003b. Airborne Remote Sensing: Redefining a Paradigm of Traffic Flow Monitoring, Proceedings, ION GPS/GNSS, Sept 9-12, Portland, Oregon, CD ROM.

Grejner-Brzezinska, D. – Toth, C. – Paska, E., 2004. Airborne Remote Sensing Supporting Traffic Flow Estimates, Proc. of 3rd International Symposium on Mobile Mapping Technology, Kunming, China, March 29-31, 2004, CD-ROM.

He, G.P. – Novak, K. – Tang, W., 1994. The Accuracy of Features Positioned with the GPSVan, Symp. ISPRS Comm. II Symposium, Vol. 30, Part 2, pp. 480-486.

McCord, M. – Goel, P. – Jiang, Z. – Coifman, B. – Yang, Y. – Merry, C., 2002. Improving AADT and VDT Estimation With High-Resolution Satellite Imagery, Pecora 15/Land Satellite Information IV/ISPRS Commission I/FIEOS 2002 Conference Proceedings.

Merry, C.J. – McCord, M.R. – Goel, P.K., 1999. Satellite data use for traffic monitoring, Proceedings of the 14th William T. Pecora Memorial Remote Sensing Symposium (CD-ROM), 6-10 December, Denver, Colorado, pp. 183-190.

Paska, E. – Toth, C., 2004. A Performance Analysis on Vehicle Detection from Remotely Sensed Imagery, Proceedings of the ASPRS Annual Conference, Denver, May 23-28, CD-ROM.

Paska, E. – Toth, C., 2005. Vehicle Velocity Estimation from Airborne Imagery and LiDAR, ASPRS Annual Conference, Baltimore, Maryland, CD ROM.

Pline, J.L., 1992. Transportation and Traffic Engineering Handbook, 4th Edition, Prentice Hall.

Ramprakash, V.L., 2003. Detection and estimation of Vehicular Movement on Highways using a LiDAR sensor, MS.C. Thesis, The Ohio State University.

Toth, C. – Grejner-Brzezinska, D. – Lovas, T., 2003a. Traffic Flow Estimates from LiDAR Data, Proceedings, ASPRS Annual Conference, May 5-9, pp. 203-212, CD ROM.

Toth, C. – Grejner-Brzezinska, D. A. – Merry, C., 2003b. Supporting Traffic Flow Management with High-Definition Imagery, ISPRS Workshop on High Resolution Mapping from Space 2003, Hanover, Germany, October 6-8, CD ROM.

Toth, C. – Grejner-Brzezinska, D., 2004a. Vehicle Classification from LiDAR Data to Support Traffic Flow Estimates, Proc. of 3rd International Symposium on Mobile Mapping Technology, Kunming, China, March 29-31, 2004, CD-ROM.

Toth C. – Brzezinska, D. – Moafipoor, S., 2004b. Precise Vehicle Topology and Road Surface Modeling Derived from Airborne LiDAR Data, The 60th Annual Meeting of ION 2004, Dayton, OH, June 7-9, 2004. CD-ROM.

Toth, C. – Grejner-Brzezinska, D. A., 2004c. Traffic Management With State-Of-The-Art Airborne Imaging Sensors, *International Archives of Photogrammetry and Remote Sensing*, Vol. XXXIV, Part B2, pp. 897-904, 2000pp. 848-843.

Vehicle Velocity Estimation from Airborne Imagery and LiDAR

Eva Paska and Charles K. Toth
Center for Mapping
The Ohio State University
1216 Kinnear Road, Columbus, OH 43212-1154
E-mail: eva-paska@cfm.ohio-state.edu

ABSTRACT

This paper addresses vehicle velocity estimation methods based on aerial imagery and/or LiDAR. The precondition of the velocity estimation is the availability of vehicles, extracted, adequately described, and tracked, which can be accomplished from both data sources. In previous works, vehicle detection and tracking techniques were described for both data types. Tracked vehicles can serve as input to more complex processing tasks, such as estimating velocity profiles of individual vehicles or monitoring traffic dynamics in short term. The recent trend in airborne surveying, the simultaneous data acquisition of LiDAR with digital camera, however, allows for improved velocity estimation of moving targets by combining datasets acquired by the two technologies from the same flight. Both data are capable of providing velocity estimates, however, in varying quality. As their limitations and strengths are complementary, they can support each other and their fusion could lead to better velocity estimation. The objective of this discussion is to assess how the velocity of moving objects extracted over transportation corridors from LiDAR and imagery can be estimated.

INTRODUCTION

A demand for finding new data sources in order to support and improve traffic flow monitoring and management inspired a research initiative on using remote sensed data in transportation. Supported by the National Consortium for Remote Sensing in Transportation - Flows (NCRST-F) research efforts first focused on extracting traffic flow data from aerial and satellite imagery, see (Toth et al., 2003b; Grejner-Brzezinska and Toth, 2002 and 2003b; Paska and Toth, 2004). Later, theoretical and practical studies were carried out on the feasibility of using LiDAR data to obtain traffic flow estimates, see (Toth et al., 2003a and 2004; Grejner-Brzezinska and Toth, 2003a). These papers describe methods for vehicle detection, extraction, and tracking from both imagery and LiDAR, which form the basis for traffic flow parameter estimation, such as vehicle count, classification and vehicle velocity estimates. Based on these experiences, the next step in research should be the fusion of results extracted from the two datasets, acquired simultaneously from the same flight. In this paper, the estimation of vehicle velocities from the two data types is discussed; the focus is on how the two data types can support each other in order to obtain better vehicle velocity estimates. More importantly, an accuracy assessment of the speed approximation is carried out. The analyses presented in the paper are based on a high-density (2-4 points/m^2) LiDAR dataset and 4k by 4k digital imagery acquired on February 19, 2004, over the downtown Toronto area with the Optech ALTM 30/70 LiDAR system and DSS digital camera, respectively.

TRAFFIC FLOW

For highway planning and traffic management purposes, each road segment is characterized by its traffic flow. Flow can be defined as the number of vehicles passing a given point on a highway during a given period of time, typically one hour (vehicles per hour). Flow is one of the primary elements of traffic stream besides density, and speed. The three basic parameters of traffic stream are related to each other by the following equation: flow = speed x density. The two types of mathematical models for describing traffic flow are the macroscopic and microscopic models. While macroscopic models are concerned with describing the flow-density relationship for a group of vehicles, microscopic models describe the flow by

tracking individual vehicles using car-following logic. The relationship between flow and density is frequently used in freeway traffic management to control the density in an effort to optimize productivity (flow). The relationship between speed and flow could be used for design purposes as it defines the trade-off between the level of service on a road facility (as expressed by the speed), and the productivity (as defined by the flow). Traffic control is aimed at managing and controlling the movement of traffic on streets, highways, and freeways in an attempt to optimize the use of such facilities. Traffic control service, in general, is responsible for collecting real-time traffic data from the field and then processing the data into useful information.

Transportation represents a major segment of the world's economy, and as such must be carefully monitored and planned, which requires the most up-to-date, accurate and continuous methods of screening, mapping modeling, and managing. The major focus of this research effort, in general, is to improve the efficiency of the transportation system by the integration of remotely sensed data with the traditional ground data to monitor and manage traffic flows. The research presented here is concerned with the vehicle extraction and traffic pattern modeling based on airborne digital data, collected by frame cameras and LiDAR systems.

CONCEPT OF VEHICLE VELOCITY ESTIMATION FROM IMAGERY AND LIDAR

In this section, the estimation of the vehicle velocity is discussed and suggestions for combining datasets acquired by the two technologies from the same flight are offered. Velocity, as already explained, is necessary for the traffic flow calculation, since the traffic flow is a product of the average vehicle velocity and the average vehicle density.

Vehicle velocity estimation for the extracted vehicles requires adequate tracking data for imagery and precise timing for LiDAR data. When tracking a vehicle in a sequence of images, its position is computed for each image frame. From these data, the traveled distance between two epochs, defined in image acquisition time, and therefore average speed can be computed. The different characters of LiDAR imply a different approach in order to obtain vehicle velocity information. Vehicle speed estimation from LiDAR is based on the vehicle elongation/shortening of the moving objects that is due to the scanning mode of the data acquisition. Due to the continuous scanning of the LiDAR sensor and the motion of both the sensor and vehicles, vehicles appear distorted in LiDAR datasets. The relative motion between the LiDAR sensor and moving targets results in an elongated or shortened length of the vehicles. Some representative values of the elongated and shortened lengths of passenger cars that are sensed at typical sensor and vehicle relative speeds are shown in Table 1. The aircraft (LiDAR) speed was 55 m/s, and the car velocity was set to minimum and maximum freeway speeds. In this scenario, the LiDAR-sensed length of the passenger cars moving in the flying direction falls between 6 and 13 meters, and 2.5 and 4 meters for the cars that move against the flying direction.

Parameters V_{LiDAR} = 55 m/s $V_{VEH\ MIN}$ = 20 m/s s_{MIN} = 4.36 m $V_{VEH\ MAX}$ = 32 m/s s_{MAX} = 5.23 m			
True length	Vehicle velocity	LiDAR-sensed length [m]	
		Along	Against
s_{MIN}	$V_{VEH\ MIN}$	6.85	3.19
s_{MIN}	$V_{VEH\ MAX}$	10.42	2.75
s_{MAX}	$V_{VEH\ MIN}$	8.21	3.83
s_{MAX}	$V_{VEH\ MAX}$	12.50	3.30

Table 1. LiDAR-sensed lengths of passenger cars traveling on a freeway.

Exploiting the relationship between the measured length and true length of the vehicle, the vehicle velocity with respect to the LiDAR platform velocity can be expressed with the following formula (1):

$$V_{vel\_along} = \frac{m-s}{m} \cdot V_{LiDAR}$$
$$V_{vel\_against} = \frac{s-m}{m} \cdot V_{LiDAR} \quad (1)$$

where (assuming constant speeds for short periods) V_{vel_along} / $V_{vel\_against}$ is the velocity of the vehicle traveling along/against the LiDAR flying direction, V_{LiDAR} is the velocity of the LiDAR platform, m is the LiDAR-sensed vehicle length, and s is the true length of the vehicle. The LiDAR platform's speed is known with high accuracy; the measured vehicle length from the LiDAR data may not be very accurate due to the errors in the vehicle representation. The actual vehicle size is unknown in practice, and thus, the true lengths of the vehicles must be estimated from the basic statistics of the vehicle categories, such as after classifying the extracted vehicles. Our earlier studies confirmed that all types of vehicles can be easily classified into three main categories, for example, passenger cars, multi-purpose cars, and trucks. Consequently, the actual vehicle length can be estimated as the average length within a category. Based on the statistics of the US vehicle market according to a study by Ramprakash (2003), the true length of passenger cars, for example, is between 4.36 and 5.23 m. To overcome the errors in the true vehicle length estimation due to generalization or possible misclassifications, the actual length of the vehicle must be determined from other sensory data, such as imagery collected simultaneously with the LiDAR point clouds. Though a single image does not provide the absolute size information, the image sequence formation preserves the relative object size information. Although an extra effort, such as using an adequate matching technique, is required to identify the identical vehicles in the two datasets, the combination of the two datasets could eventually lead to an improved velocity estimation of the moving vehicles.

Figure 1 shows extracted vehicles from LiDAR data as they are overlaid on an orthoimage. LiDAR vehicle points are represented in green and red, corresponding to the motion along or against the flying direction, respectively. For referencing, some static objects, such as one point on the centerline and points at the guard rail, are also marked in the figure. This figure illustrates: (1) the elongated (when vehicles moving along the flying direction) and shortened (when vehicles moving against the flying direction) lengths of the moving objects, and (2) the relationship between corresponding vehicles on the imagery and in the LiDAR data. The matches of the corresponding vehicles in the two datasets are highlighted by rectangles with identical colors. Due to the different nature of the two data acquisition techniques, continuous scanning mode of the LiDAR sensor and instantaneous capturing of the imagery, the geo-locations and also the shapes of the corresponding vehicles differ in the two datasets. The white triangle in Figure 1 shows the approximated location of the LiDAR beam when the image was taken.

Vehicles can be sorted into four categories based on their direction and the relation of their positions in the LiDAR and imagery data: (1) vehicles traveling along the flying direction and scanned before the image acquisition (in Figure 1 they are in the upper lanes and right from the triangle sign), (2) vehicles traveling along the flying direction and scanned after the image acquisition (in Figure 1 they are left from the triangle sign), (3) vehicles traveling against the flying direction and scanned before the image acquisition (in Figure 1 they are in the lower lanes and right from the triangle sign), and (4) vehicles traveling against the flying direction and scanned after the image acquisition (in Figure 1 they are left from the triangle sign).

Direction of vehicle	**Vehicle scanned**		**Vehicle in LiDAR data**
Along	Before	the image acquisition	is behind the corresponding vehicle on image
Against	Before		
Along	After		is in front of the corresponding vehicle on image
Against	After		

Table 2. Relative positions of corresponding vehicles in imagery and LiDAR data.

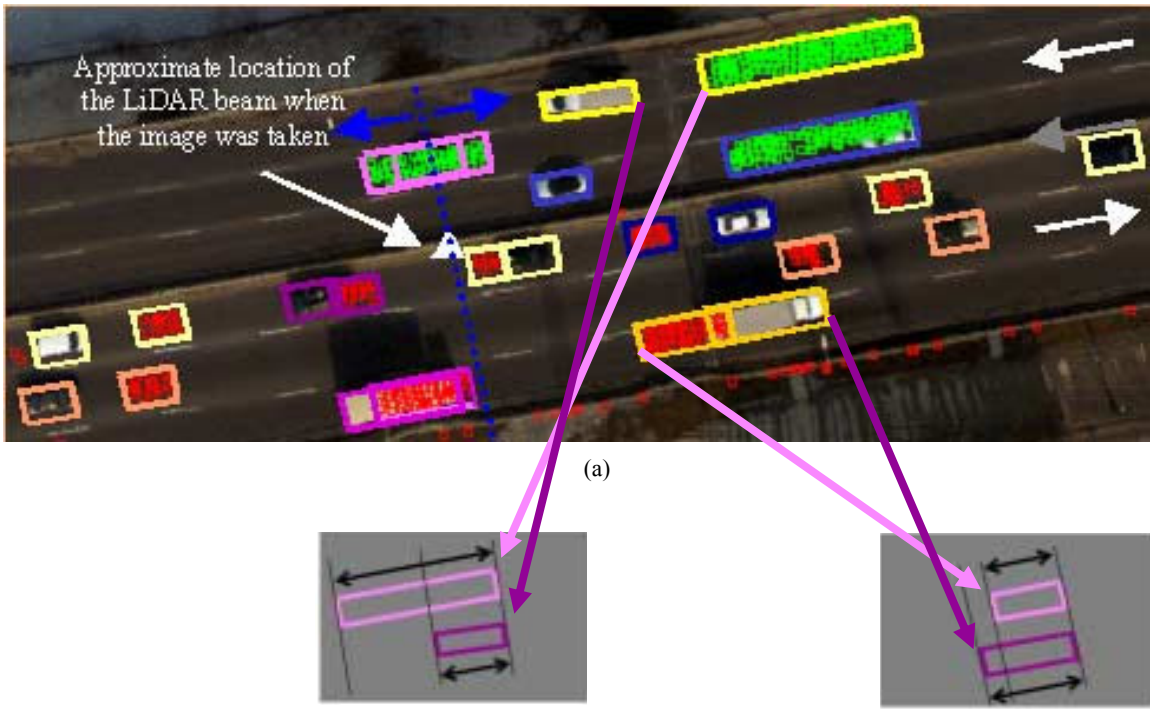

(a)

(b) (c)

Figure 1. Vehicles extracted from the LiDAR data and overlaid on the orthoimage; match of corresponding vehicles in the two datasets is marked with identical colors (a); also shown are vehicle elongation (b) and vehicle shortening (c).

Note that the LiDAR point clouds of the vehicles fall in front of the corresponding vehicles on the left side of the blue dotted line, and behind the corresponding vehicles on the right side of the line, as the LiDAR measured the vehicle either before or after the image was taken. Table 2 describes the corresponding vehicles' relative positions acquired by the two data types. Based on the known relative positions of corresponding vehicles, search areas for a matching procedure can be determined. The acquisition time of each LiDAR point as well as the image capture time is recorded in GPS seconds. The possible relative distance between the image and LiDAR vehicle positions could be calculated from the vehicle velocity and the acquisition time of the image and the LiDAR vehicle points (coarse vehicle velocity approximations could be obtained from vehicle velocity computation from image sequences or the minimum and maximum speed limits of the actual road type and so on). Note in Figure 1 that the relative distance between corresponding vehicles is getting bigger the farther of the triangle sign; similarly, the difference between the data acquisition time of the LiDAR sensor and digital camera is getting also larger.

ACCURACY ASSESSMENT OF THE VEHICLE VELOCITY ESTIMATION FROM THE COMBINED DATASETS

In order to assess the accuracy of vehicle velocity estimates from the combined datasets, we have to investigate the accuracy of the various components which are based on equation (1), the velocity of the LiDAR platform, the LiDAR-sensed vehicle length, and the true length of the vehicle. The LiDAR platform's speed is known with high accuracy; in the calculations they are considered as fixed values. The measured vehicle length from the LiDAR data (m) may not be very accurate due to the errors in the vehicle representation, and thus is considered with σ_m standard error. The accuracy of the true vehicle length derived from image measurements simply depends on the accuracy of single ground point determination from imagery. In the following, the accuracy of size parameter estimates from imagery and LiDAR data is discussed.

Accuracy of single ground point determination and vehicle size estimation from imagery

In our approach to extract vehicles from imagery, see (Toth et al., 2003b; Paska and Toth, 2004), the detection begins with image orthorectification, which produces good starting data for all the vehicle extraction and tracking processes. The orthoimagery provides advantages in many respects. First, by overlaying and subtracting images it makes easy the identification of moving objects from the images (vehicles on road surface). Second, since orthoimages are scaled to object scale, vehicle envelopes can be compared to actual dimensions making vehicle extraction more robust.

For orthorectification, exterior orientation parameters of images are usually provided from the GPS/INS solution. Once the image georeferencing is known, the images are orthorectified by using available DEMs, such as existing USGS DEM or in the case of simultaneous data acquisition of LiDAR with a digital camera, LiDAR will provide good quality, up-to-date elevation data. However, LiDAR provides a true DEM within its accuracy specifications only for stationary objects; moving objects appear distorted in the data set due to the facts described in the previous section.

The accuracy of single ground point determination was analyzed by error propagation assuming that all systematic errors have been removed a priori.

IO (Interior Orientation) parameters	3 (c, x_0, y_0)
	6 non-linear distortion parameters
EO (Exterior Orientation) parameters	3 positions (X_0, Y_0, Z_0)
	3 rotation angles (ω,φ,κ)
Boresight alignment between sensors (IMU and camera frames)	3 rotation angles ($\omega_b,\varphi_b,\kappa_b$)
DEM	Elevation data of the surface (Z)

Table 3. Required parameters to describe the mathematical relation between image and ground coordinates by single photo resection.

The accuracy of the ground coordinates of any objects determined from an image depends on the accuracy of the parameters shown in Table 3. The errors associated with each quantity will contribute to the error in the ground coordinates. The well-known collinearity equation (2) is used to propagate the uncertainties of the parameters to the data.

$$X = X_0 + (Z - Z_0) \cdot \frac{r_{11} \cdot x + r_{12} \cdot y - r_{13} \cdot c}{r_{31} \cdot x + r_{32} \cdot y - r_{33} \cdot c}$$

$$Y = Y_0 + (Z - Z_0) \cdot \frac{r_{21} \cdot x + r_{22} \cdot y - r_{23} \cdot c}{r_{31} \cdot x + r_{32} \cdot y - r_{33} \cdot c} \qquad (2)$$

where (x,y) are image coordinates, interior orientation parameters applied (x_0,y_0 and distortion), (X,Y,Z) are ground coordinates of the object, c is the focal length, (X_0,Y_0,Z_0) are the ground coordinates of the camera center, r_{ij} are the elements of the rotation matrix calculated from the camera attitude angles (boresight-corrected navigation angles).

The general error propagation for a function of n variables is given below (equation 3) provided that the various variable errors are independent.

$$\sigma_{w_i} = \sqrt{\left(\frac{\partial w_i}{\partial v_1}\right)^2 \cdot \sigma_{v_1}{}^2 + \left(\frac{\partial w_i}{\partial v_2}\right)^2 \cdot \sigma_{v_2}{}^2 + \ldots + \left(\frac{\partial w_i}{\partial v_n}\right)^2 \cdot \sigma_{v_n}{}^2} \qquad (3)$$

The partial derivative $\partial w_i/\partial v_n$ represents the change in the computed value w_i with respect to the measured value v_n, and σ_{Vn} represents the standard error assigned to the measured value. In the more general matrix format (4), where no assumption is made about variable correlations:

$$D(\overline{w}) = A \cdot D(\overline{v}) \cdot A^T$$

$$A = \begin{bmatrix} \frac{\partial w_1}{\partial v_1} & \frac{\partial w_1}{\partial v_2} & \cdots & \frac{\partial w_1}{\partial v_n} \\ \frac{\partial w_2}{\partial v_1} & \frac{\partial w_2}{\partial v_2} & \cdots & \frac{\partial w_2}{\partial v_n} \\ \cdots & \cdots & \cdots & \cdots \\ \frac{\partial w_m}{\partial v_1} & \frac{\partial w_m}{\partial v_2} & \cdots & \frac{\partial w_m}{\partial v_n} \end{bmatrix} \quad (4)$$

where $D(\overline{v})$ is the dispersion matrix, which contains the covariance (second moment) among all measured elements, A is the design matrix, and $D(\overline{w})$ gives the variances/covariances of the final results. The design matrix when calculating the accuracy of the ground coordinates of any objects determined from an image by single photo resection is given by (5).

$$A = \begin{bmatrix} \frac{\partial X}{\partial X_0} & \frac{\partial X}{\partial Y_0} & \frac{\partial X}{\partial Z_0} & \frac{\partial X}{\partial \omega} & \frac{\partial X}{\partial \varphi} & \frac{\partial X}{\partial \kappa} & \frac{\partial X}{\partial \omega_b} & \frac{\partial X}{\partial \varphi_b} & \frac{\partial X}{\partial \kappa_b} & \frac{\partial X}{\partial x} & \frac{\partial X}{\partial y} & \frac{\partial X}{\partial c} & \frac{\partial X}{\partial Z} \\ \frac{\partial Y}{\partial X_0} & \frac{\partial Y}{\partial Y_0} & \frac{\partial Y}{\partial Z_0} & \frac{\partial Y}{\partial \omega} & \frac{\partial Y}{\partial \varphi} & \frac{\partial Y}{\partial \kappa} & \frac{\partial Y}{\partial \omega_b} & \frac{\partial Y}{\partial \varphi_b} & \frac{\partial Y}{\partial \kappa_b} & \frac{\partial Y}{\partial x} & \frac{\partial Y}{\partial y} & \frac{\partial Y}{\partial c} & \frac{\partial Y}{\partial Z} \end{bmatrix} \quad (5)$$

Table 4 contains the typical accuracy range of the navigation, boresight, and interior parameters with their accuracy taken from calibration reports. In the following calculations, the accuracy parameters listed in Table 4 were considered.

Camera		Accuracy
Navigation errors (Applanix POS AV Model 510)	Position	5 – 20 cm
	Attitude	10 – 30 arc sec
Boresight misalignment	(Omega, Phi, Kappa)	10 – 30 arc sec
Errors in interior orientation parameters (DSS)	Focal Length (54.969 mm)	9 μm
	Principal Point	4.5 μm, 4.5 μm
Errors in image coordinate measurement		2 – 5 μm

Table 4. Accuracy of the orientation parameters and image coordinate measurements.

Table 5 shows the accuracy estimates of ground coordinates for two typical image point locations of the 4k by 4k image for various navigation and boresight misalignment errors, and for a common image measurement accuracy, focal length, and DEM accuracy. The size parameter is computed as the distance between two points given by their XY ground coordinates (assuming the road is horizontal). The accuracy of the size parameter estimation calculated by error propagation for different scenarios is included in Table 5. In the worst scenario, a 37-cm accuracy can be expected for the size parameter. In an average case, about 20 cm accuracy of the size estimation can be assumed.

x = 0 y = 0 [mm]	Navigation errors		Boresight misalignment	DEM (LiDAR)	Image coordinate measurement	Focal length	Accuracy of		
							positioning		size
	$\sigma_{Position}$ [cm]	$\sigma_{Attitude}$ [arc sec]	$\sigma_{Om,phi,ka}$ [arc sec]	σ_Z [m]	σ_x, σ_y [μm]	σ_c [μm]	σ_X [m]	σ_Y [m]	σ_Y [m]
H = 500 [m]	5	10	10	0.30	5	9	**0.08**	**0.08**	**0.11**
	10	20	20	0.30	5	9	**0.13**	**0.13**	**0.18**
	20	30	30	0.30	5	9	**0.23**	**0.23**	**0.32**

x = 15.36 y = 0 [mm]	Navigation errors		Boresight misalignment	DEM (LiDAR)	Image coordinate measurement	Focal length	Accuracy of		
							positioning		size
	$\sigma_{Position}$ [cm]	$\sigma_{Attitude}$ [arc sec]	$\sigma_{Om,phi,ka}$ [arc sec]	σ_Z [m]	σ_x, σ_y [μm]	σ_c [μm]	σ_X [m]	σ_Y [m]	σ_Y [m]
H = 500 [m]	5	10	10	0.30	5	9	**0.12**	**0.08**	**0.17**
	10	20	20	0.30	5	9	**0.17**	**0.13**	**0.23**
	20	30	30	0.30	5	9	**0.26**	**0.23**	**0.37**

Table 5. The accuracy estimates of ground coordinates of two typical image point positions, and the distance estimate (size) parameter estimation for different scenarios.

Uncertainties in size-parameter estimation from LiDAR data

The measured vehicle length from the LiDAR data may not be very accurate due to the errors in the vehicle representation: (1) the LiDAR pulse footprint size is not negligible, thus, the accuracy of the actual edge of the vehicle footprint determination depends on the size of the LiDAR footprint, (2) LIDAR point density; the distance between the points on the ground limits the accurate length estimation, and (3) the shadow effect, which does not influence the length parameter estimation directly, makes the vehicle orientation more ambiguous and the width parameter estimation less accurate. For examples illustrating these problems, see Figure 2.

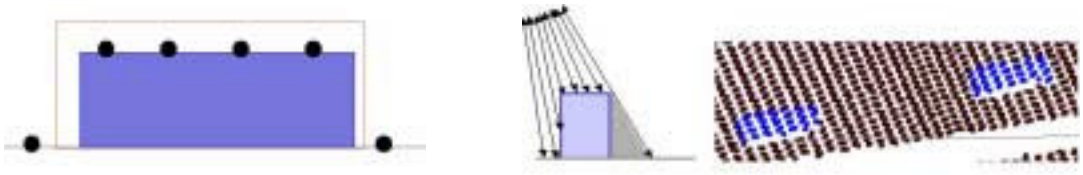

(a) (b)

Figure 2. Limitations in accurate parameterization of LiDAR-sensed vehicles: (a) data density and footprint size, (b) shadow effect.

Obviously, the denser the data the less uncertainty the vehicle length measured in the LiDAR data. When deriving the formula for vehicle velocity estimation, the assumption is made that the length of the vehicle is measured continuously by the sensor moving above the object. However, LiDAR measurement provides discrete points at some spacing, thus, resulting in an inaccuracy of the LiDAR-sensed length parameter.

Vehicle velocity estimation

The accuracy of the vehicle velocity estimation based on equation (3) is given by (6),

$$\sigma_{v_{veh}} = \sqrt{\left(-\frac{v_{LiDAR}}{m}\right)^2 \cdot \sigma_s^{\,2} + \left(\frac{s}{m^2} \cdot v_{LiDAR}\right)^2 \cdot \sigma_m^{\,2}} \qquad (6)$$

where V_{LiDAR} is the velocity of the LiDAR platform, m is the LiDAR-sensed vehicle length, and s is the true vehicle length; σ_{Vveh} , σ_m and σ_s are the accuracy of the vehicle velocity, LiDAR-sensed vehicle length, and the true vehicle length, respectively.

Figure 3 shows the standard deviation of vehicle velocities computed by equation (6) at different LiDAR-sensed lengths using the parameters listed in Table 6.

Figure 3	s [m]	σ_s [m]	σ_m [m]	Line color
(a)	5	0.30	0.30	Green
	5	0	0.30	Red
	5	0.30	0	Blue
(b)	4.3	0.30	0.30	Green
	5.3	0.30	0.30	Magenta
(c)	4.3	0	0.30	Red
	5.3	0	0.30	Magenta
(d)	4.3	0.30	0	Blue
	5.3	0.30	0	Magenta
(e)	5	0.10	0.30	Green
	5	0.20	0.30	Red
	5	0.30	0.30	Blue
(f)	5	0.10	0.10	Green
	5	0.20	0.20	Red
	5	0.30	0.30	Blue

Table 6. Summary of parameters considered in the computation of the standard deviation of vehicle velocities at different LiDAR-sensed lengths

From Figure 3a we can conclude that the vehicle velocity accuracy is more sensitive for the uncertainties of the size parameters at the shorter LiDAR-sensed lengths, i.e., the uncertainties in the size parameters (true vehicle length and LiDAR-measured length) has less impact when the LiDAR-sensed length is longer. The accuracy of the velocity estimation is better for vehicles traveling along the direction of the sensor motion, as their LiDAR-sensed measure is relatively long. In a similar way, if the car is traveling in the direction opposite of the LiDAR, its velocity estimate would be more accurate for lower speeds, since the shortening effect will be less severe. Moreover, uncertainties in the actual vehicle size have larger effects at the longer LiDAR-sensed lengths than that of the inaccuracy of the measured vehicle size, which rather increase the inaccuracy at the shorter LiDAR-sensed lengths. Figures 3b and 3c show that longer true size vehicles have bigger standard errors. Figure 3d illustrates that the true vehicle length would not affect the accuracy of velocity estimation if the LiDAR-sensed length estimation could be considered fixed. Figures 3e and 3f illustrate how the accuracy increases with decreasing uncertainties in the size parameters.

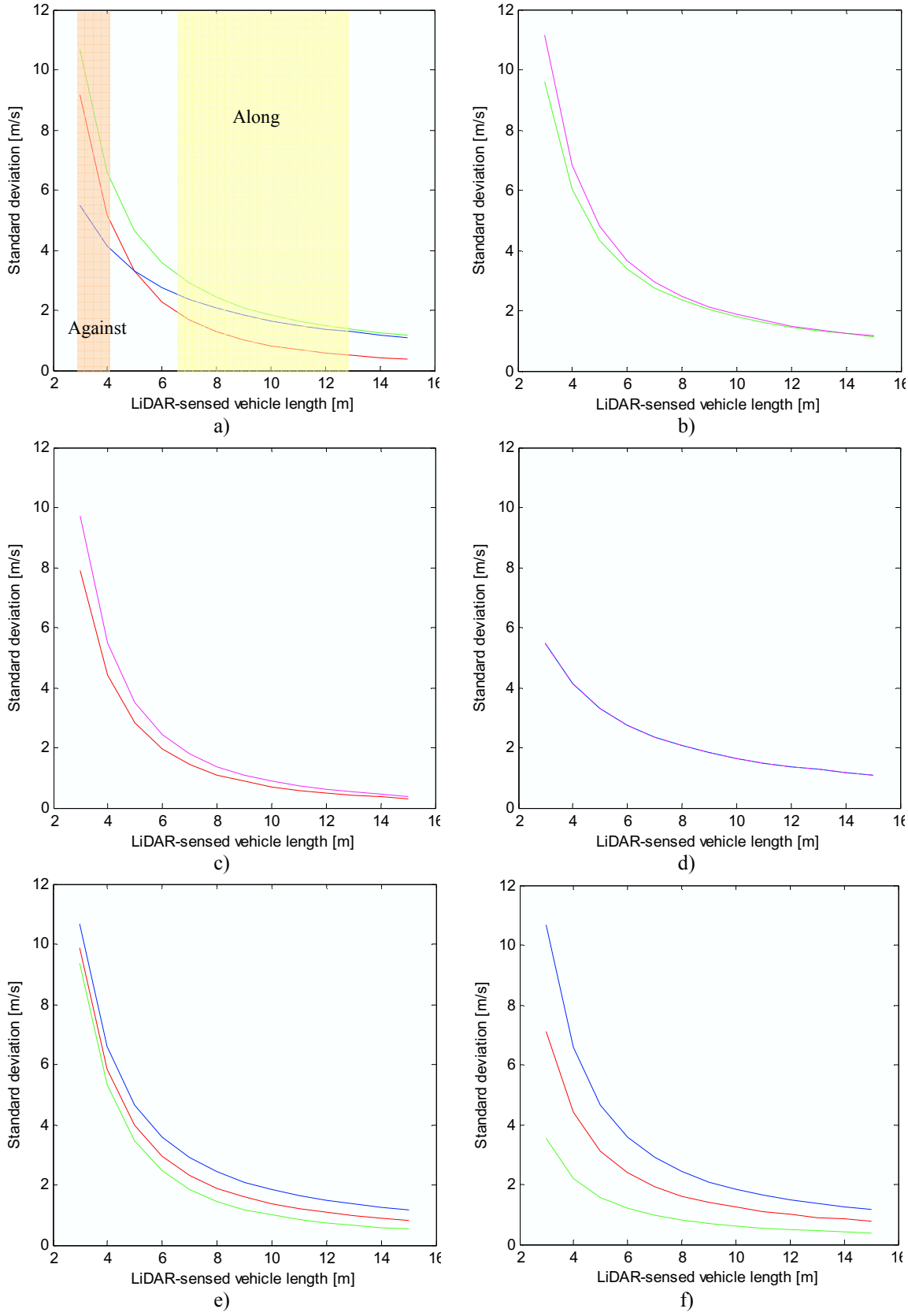

Figure 3. Accuracy of vehicle velocity estimation at different LiDAR-sensed vehicle length for scenarios summarized in Table 6.

CONCLUSION

Vehicle velocity estimation from LiDAR is based on the vehicle elongation and shortening of the moving objects due to the scanning mode of the data acquisition. The accuracy of vehicle velocity estimation depends on the vehicle's direction, true length, velocity, and on how accurately the true and LiDAR-sensed vehicle length could be estimated. The actual vehicle size is unknown in practice, and thus, the true lengths of the vehicles must be estimated from either the basic statistics of the vehicle categories, such as after classifying the extracted vehicles, or using additional information. A feasible approach to overcome the errors in the true vehicle length estimation due to generalization or possible misclassifications is if the actual length of the vehicles is determined from other sensory data, such as imagery collected simultaneously with the LiDAR. Our results have shown that combining LiDAR with complementary sensor data, such as simultaneously collected imagery, can provide a better base for velocity estimation, and thus allows for more reliable traffic flow parameter determination.

ACKNOWLEDGEMENTS

This research was partially supported by the NCRST-F and by the Ohio Department of Transportation. The authors would like to thank Optech International for providing the LiDAR datasets.

REFERENCES

Grejner-Brzezinska, D. A. and Toth, C., (2002): Modern Remote Sensing Techniques Supporting Traffic Flow Estimates, Proceedings, ION GPS, September 24-27, CD ROM, pp. 2423-2433.

Grejner-Brzezinska, D. A. and Toth, C. (2003a): Deriving Vehicle Topology and Attribute Information over Transportation Corridors from LiDAR Data, Proceedings, ION 59th Annual Meeting, June 23-25, Albuquerque, New Mexico, CD ROM, pp. 404-410.

Grejner-Brzezinska, D., C. Toth. (2003b): Airborne Remote Sensing: Redefining a Paradigm of Traffic Flow Monitoring, Proceedings, ION GPS/GNSS, Sept 9-12, Portland, Oregon, CD ROM.

Paska, E. – Toth, C., 2004. A Performance Analysis on Vehicle Detection from Remotely Sensed Imagery, Proceedings of the ASPRS Annual Conference, Denver, May 23-28, CD-ROM.

Ramprakash, V.L., (2003): Detection and estimation of Vehicular Movement on Highways using a LiDAR sensor, MS.C. Thesis, The Ohio State University.

Toth, C., Grejner-Brzezinska, D. and Lovas, T. (2003a): Traffic Flow Estimates from LiDAR Data, Proceedings, ASPRS Annual Conference, May 5-9, pp. 203-212, CD ROM.

Toth, C., Grejner-Brzezinska, D. A., Merry, C. (2003b): Supporting Traffic Flow Management with High-Definition Imagery, ISPRS Workshop on High Resolution Mapping from Space 2003, Hanover, Germany, October 6-8, CD ROM.

Toth, C. D. Brzezinska and S. Moafipoor (2004): Precise Vehicle Topology and Road Surface Modeling Derived from Airborne LiDAR Data, Proceedings ION NTM, June 7-9, Dayton, Ohio, CD ROM, pp. 402-408.

APPENDIX C

1. I_FLOW program installation instructions.
2. I_FLOW User's Manual.
3. I_FLOW executable and source code (only electronic version).

I_FLOW Installation Instructions

The source code of the L_Flow program is MATLAB. Therefore, the executable version of the program, L_Flow.exe, needs the support of MATLAB program. To install the software, you should install the MATLAB compiler in advance. About 300 Mb of space on the C:\ drive is required to install the MATLAB compiler. Please follow the below steps to set up the program:

1. Create a folder with the name [MCR] in C:\

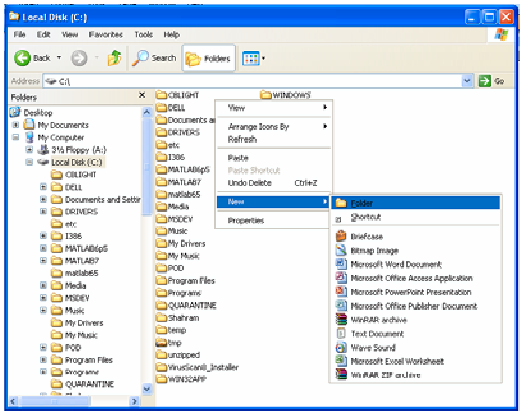

Fig. 1: Create a folder in the C:\ root

2. Copy the files of the CD on this folder

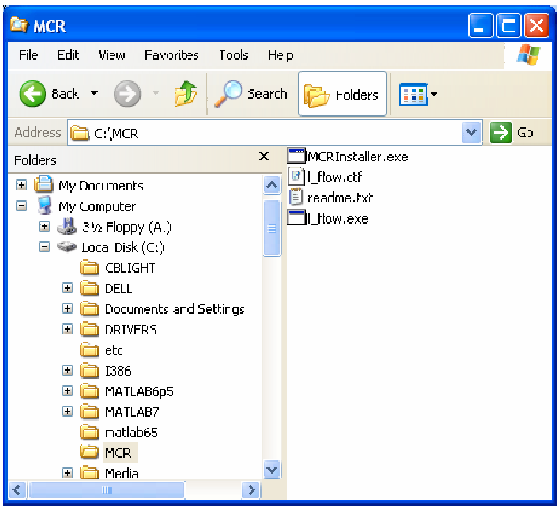

Fig.2: The files are transferred from the CD to the specific folder

3. Run MCRInstaller.exe from C:\MCR directory

   This file extracts all procedures needed to compile the MATLAB commands. By appearing a window with the logo of MATLAB, follows the below steps.

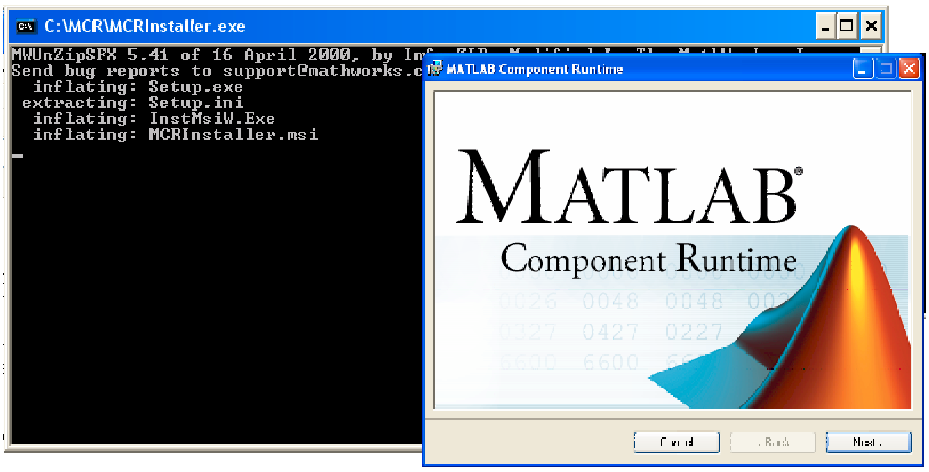

Fig.3: The first step of install the MATLAB compiler

- Press Next bottom three times.

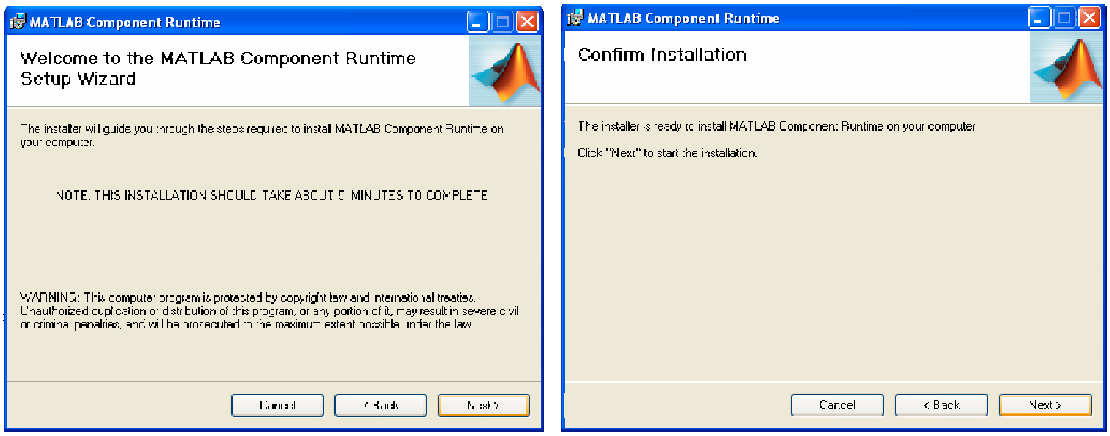

Fig.4: Press [Next] bottom in all appear windows

- It takes about 5 minutes to install. After it, you can press [Close] bottom. You are done.

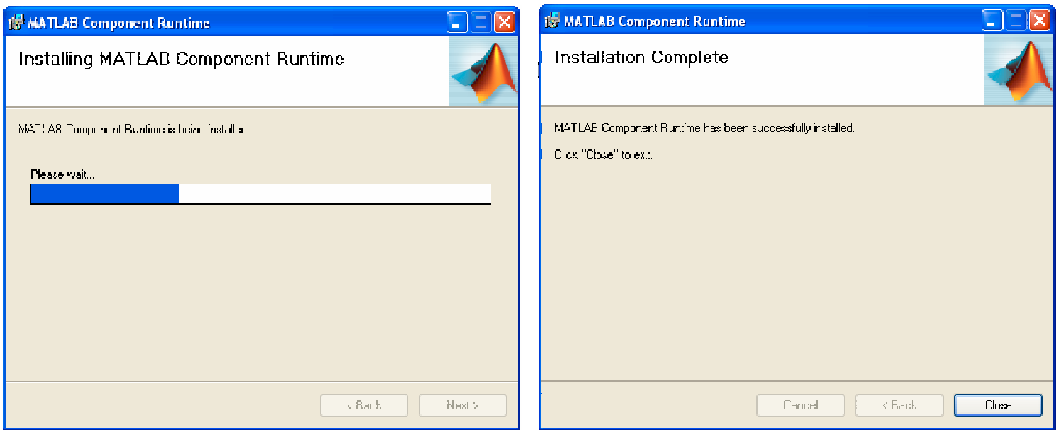

Fig.5: It takes about 5 minutes to install …

4. Run L_Flow.exe. The program is ready to run. Please return to the manual to learn about better handling the program.

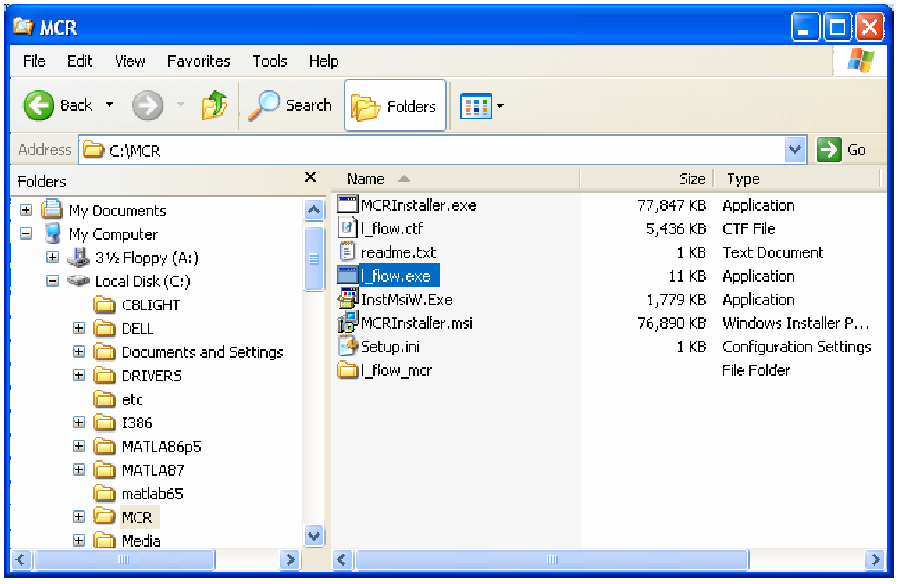

Fig.6: Run the L_Flow.exe to execute the program

Introdction

The L-FLOW is the software designed in the Center for Mapping, The Ohio State University to process the LiDAR data and estimate traffic parameters in terms of density and flow. It is supposed that the Lidar data is captured over a single transport corridor, and the prime object is to derive transportation features such as road and vehicles from it.

Our robust method for semi-automatic road extraction is based on supporting centerline information. This kind of information can be provided by either road spatial databases or user interaction. Vehicle extraction, vehicle modeling, vehicle classification and velocity estimation are the other paces achieved afterward to estimate traffic parameters. As conclusion, the main goal of this system was to overcome file size limitation, improve the efficiency of automated data segmentation, and provide robust solution for traffic parameters estimation.

This document which is divided into eight sections is designed to help the user learn to handle the input files, run the program, and manipulate the different procedures. Section 1 discusses the way of selecting the input files. Section 2 deals with checking the consistency of input files including all components needed to check before running the program. Section 3 illustrates the graphical representation of the data. The procedures of road extraction are explained in section 4. Section 5 discusses vehicle extraction and vehicle modeling algorithms. In section 6 and 7, the methods used to classify vehicles and estimate velocity are discussed respectively. In the last section, 8, the procedures of estimating the traffic parameters in basis of the results of the preceding steps are discussed.

For quick reference, a list of corresponding macros is included in the appendix I Moreover, a list of the tips is marked for almost all of the contents. These tips highlight the detailed descriptions of procedures and help to interpret and handle the program. Besides this manual in which we have explained the operation aspects of the program, the user can always use the paper reference. This reference is meant explaining intensely the theoretical background of each procedure in the framework.

1. User input files

The system is launched by executing the L_Flow.exe file. The user needs to load three files to execute the program: the LiDAR point clouds, the LiDAR intensity, and centerline files.

- **LiDAR point cloud (XYZ)**

The XYZ file should be an ASCII file in $(X,Y,Z)_{n*3}$ format.

- The LiDAR elevation files are distinguished by *.xyz extension
- There should be no blank or incomplete lines in the chosen file

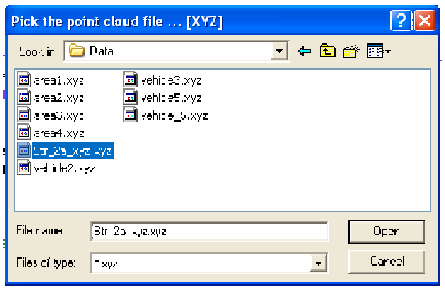

Figure 1 : Input point cloud file (XYZ)

- **LiDAR intensity data (XYI)**

The intensity file should be an ASCII file in $(X,Y,I)_{m*3}$ format.

- If there is no intensity information, press [Cancel] to go to the next step
- The program considers advertently the intensity information as independent data
- The LiDAR intensity files are distinguished by *.xyi extension
- There should be no blank or incomplete lines in the chosen file

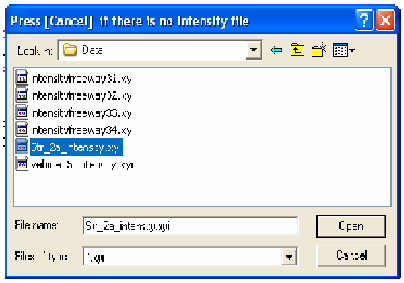

Figure 2 : Input intensity file (XYI)

- **Centerline points (CLP)**

The centerline file is an ASCII file of either $(X,Y)_{r*2}$ or $(X,Y,Z)_{r*3}$ format.

- The centerline files are distinguished by *.clp extension
- If the centerline (CL) points are 2D, the program turns them to 3D automatically
- There should be no blank or incomplete lines in the chosen file

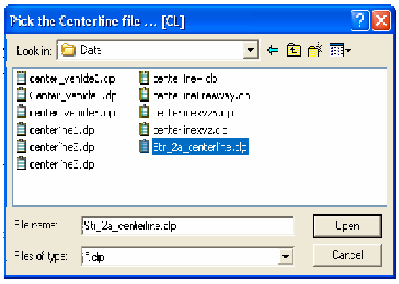

Figure 3 : Input centerline file (CLP)

2. Basic processing

Once the input files are selected, the consistency between LiDAR data and centerline file is checked. Despite of LiDAR data, point cloud and intensity, the centerline data is likely to exhibit more inconsistencies. To this end, the input centerline file is checked from different aspects, because our semi-automatic road extraction algorithm works by supporting centerline data.

Two options are proposed to supply the centerline file. The first one is to use the road spatial database, which is available for most of main highways and freeways in The States. The second one is user interaction by which a user inputs the seed points of a road. Generally, the centerline points should be drawn with accuracy better than 1 m, and be ordered in the file properly.

- A warning message is appeared If the XYZ and CL data do not cover each other

Figure 4: A warning message for unmatched input files

- To save the process details, the user can enter a name. In else, the entire process is saved in the default file [Report_1.txt].

```
Type output file name...press [Enter] for defualt name: Data_Set_1
```

Figure 5: The report of the system is saved in

2.1 Point cloud resolution

The point cloud resolution, Fig. 6, is represented by two terms: the horizontal and vertical components. These parameters are lately used in setting different thresholds.

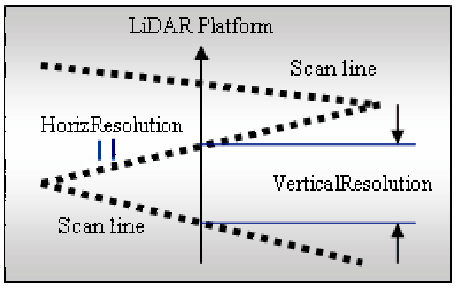

Figure 6: Point distribution and resolution terms

2.2 Alignment of the centerline points

The centerline points should be ordered properly. Fig 7 shows an example where the CL points are located improperly. The other common problems are wrong point number and wrong point coordinates, which should be fixed by operator ahead.

- For any misalignment, the location and number of the wrong CL point is reported
- The operator should fix the wrong point in the CLP file manually

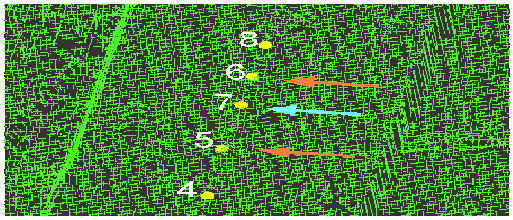

Figure 7 : The centerline points should be aligned

2.3 Minimum distance between centerline points

Once the user inputs seed centerline points, these points are manipulated in order to provide sufficient number of CL points along seed points. Small distances between CL would make the algorithm extracts road segments with high curvature; however, for highways or freeways with moderate curvature, a large distance may be allowed. If the distance is less than that the system requires, new points are interpolated and added to the CLP file. The experiments indicated that the distance between 10-15 m is sufficient for handling high curvature roads by considering processing time.

- The minimum default distance is 10 m. The operator can change this value in the macro [Control_CL_Points]

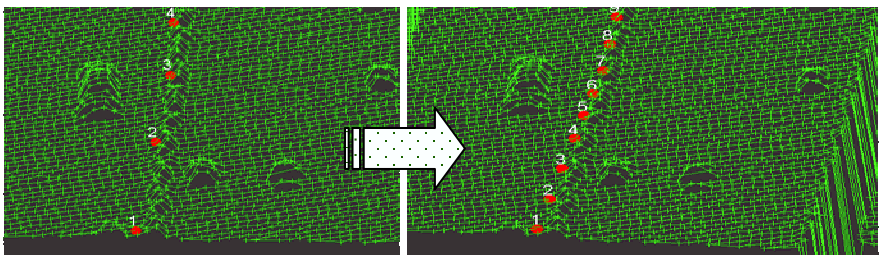

Figure 8 More centerline points need to be added to the CLP file

2.4 Determine the optimum number of centerline points

If the distance between centerline points is less than that the system requires, some of the selected points are eliminated from the CLP file. Fig. 9 shows an example in which the excess CL points are eliminated from the final list.

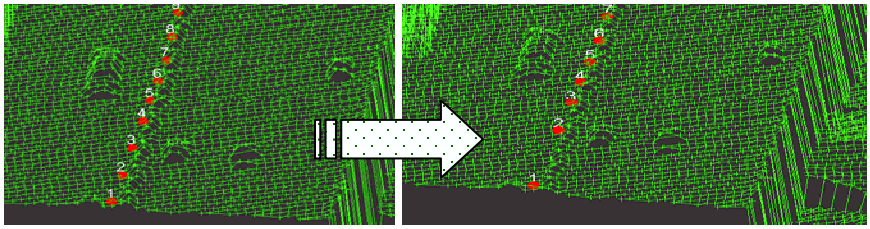

Figure 9 The extra points remove from the CLP file

2.5 Centerline projection

If centerline points are presented in 2D, they are projected into 3D.

- After fixing the centerline points, a new CLP file is recorded by the name of [CLP_filename_fix.clp] on the same path. Next time, by calling the old CLP file, the system automatically loads the new CLP file.
- For large data set, the interpolation process is time consuming. However, once the CL points are projected, they are saved in the new CLP file.
- Fig. 10 shows a sample output up to this point.

```
Horizontal Resolution : 0.49 [m]
Vertical Resoluton    : 0.62 [m]
-----------------------------------------------------------------
Centerline points are aligning  ....OK
The regular distance between CL points should be better than [10] meter
More centerline points should add to CL file .... OK
The number of the  Centerline points before sampling 25
The number of the  Centerline points  after sampling 23
Centerline Points are 3D ... OK
Length of the road segment is: [ 188.6 ] m
-----------------------------------------------------------------
```

Figure 10 A prototype output

3. Graphical representation of the input data

There are usually several outlier points in the XYZ data, and particularly in the elevation component, which prevent proper displaying of the data. Visual assessment is the best way to check these points. The proper graphical representation of the data is ready, after detecting and deleting these points. A simple filter based on average and standard deviation of the centerline elevation component, (μ_Z , σ_Z), Eq.1, is used to detect and remove the outlier points:

$$if \quad Z_i > (\mu_Z \pm 3 * \sigma_Z \quad \Rightarrow Point\ (i)\ is\ probably\ an\ outlier\ point \qquad (1)$$

- If the graphical representation shows some more outlier points, adjust the filter by changing the threshold e.g. $(\mu_Z \pm 2 * \sigma_Z)$. The operator can adjust the filter in the macro [plot_XYZ_CL]
- centerline points are superimposed on the main figure

- The Intensity data is not shown anywhere on the figure
- The graphical handling of oversized data sets is almost impossible. Consequently, for such a data set, the road area is just plotted.
- The graphical window is supported by MATLAB program. For more information about view utilities check the MATLAB help.

By proper displaying of data, Fig. 11, it can be concluded that everything is fine and it is time to arrive at the first step of traffic parameter estimation. The first stage is started by delineating the road surface from which vehicles can be extracted. To speed up traffic parameters estimation, particularly for long road lengths, an option, [Approximate], is proposed besides precise procedure [Precise]. As it can be comprehended, in the approximate mode, the road object is extracted and modeled approximately. This rough road modeling is reduced considerably the time of processing the data. i.e. from 1 hour to 1 min.

```
Approximate mode [A] ... Precise mode  [P]  :
```

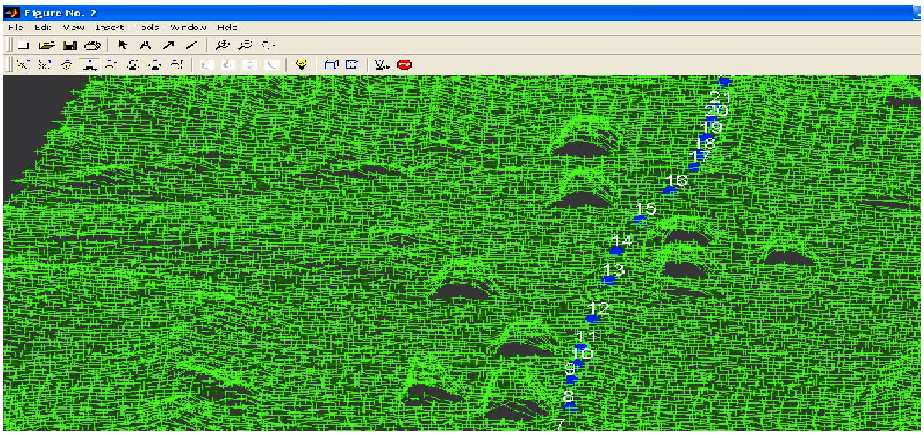

Figure 11: Graphical environment

- By choosing the [A] or [P] mode, the computations carry out in the individual way, but with the same methodology
- In [A] case, it can be expected obviously to have a rough estimate of traffic parameters

4. Roadoutlin e extraction

The road extraction algorithm is followed in two steps. In the first step, by exploiting centerline information, the XYZ data is segmented into two groups: a road group and a non-road group. In the second step, throughout the road group, the LiDAR scanlines which are represented roughly the cross profiles of the road are used to extract edges of the road.

- If the road boundaries are calculated earlier, the operator can enter [Y] and skip this step

```
Do you have any a prior RoaD Border file ... Press y for [Yes]  :
```

- The road boundary file is saved as [XYZ_file_name.rdb] in the same path

4.1 Roughly estimation of the road boundary

In conjunction with the forward movement of the aircraft, a wide strip of terrain is scanned as a result. The volume of this data is generally in the range of several megabytes, depending on the project size. This extent of data usually covers a vast area around the road surface; however, it is only the road surface which is important for us. Therefore, the first step of road extraction algorithm is approximation of the road location support centerline information. There are basically two ways to provide the approximation. First is using the intensity information, and second is using the XYZ data. Traditionally, intensity information has not been used in feature extraction from LiDAR data because of noisy of data. Therefore, the intensity can be used to derive roughly the road object whether the topography of the region is high and highways don't pass over one another. The second method is based on a geometry criterion in which a low order plane is fitted to the data.

- Technically, the road region is searched throughout the area about 35 m, around the centerline axes.
- If the road width is more than 35 m, the operator should change this threshold in the macro [Road_Coarse_Plane_Fitting]
- If the area is too smooth, there is no chance to estimate properly the road edges by analyzing the elevation data. In case the intensity data are available, the program switches to use the intensity information
- The result of intensity segmentation is not provided at once, more filtering are achieved to refine the classification as in Fig. 12
- The approximate road width is important in our algorithm. If this approximate is not calculated correctly for any reason, the operator can always enter the correct value while the program is running as Fig. 13

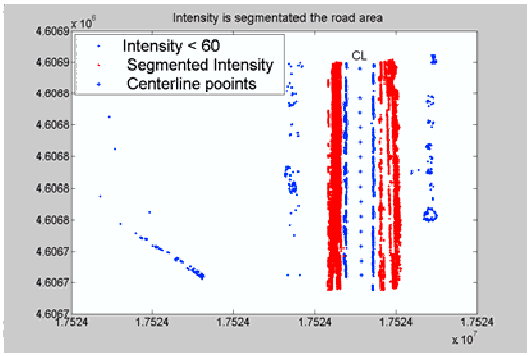

Figure 12: The intensity information could segment the road surface

```
Approximate road width ...
The approximate width of the [Right] side : 16.0 m
The approximate width of the [Left] side : 19.0 m
Press [Enter] to continue ...
      [Q]  to quit ...
      [N] to enter approximate road width:
```

Figure 13: A prototype message about confirmation of approximation

4.2 Scanline and cross profile formation

Basically the LiDAR scanlines represent the cross profiles of a road if the flight is parallel to the road direction. Otherwise, for reasons such as unparallel flight or breaks in the data, Fig.14, the cross profiles should be extracted from data. In both cases, the approximate road width bounds the profile length, and, the entire approximate road surface is finally covered with scanlines and interpolated cross profile as a wire-frame object. The intersection point of the centerline axis and each profile is split the profile to the left and right profiles. The next step is extracting road edges, median part and shoulder part, from these profiles.

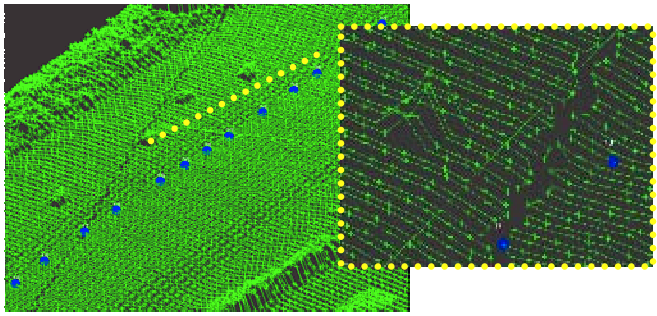

Figure 14: LiDAR scanlines may break and sweep irregularly road surface

- Cross profiles are typically perpendicular to the CL axes
- If the angle between a scanline and CL axes is lower than a threshold, plus, the number of the scanlines are larger than a threshold, the program uses the scanline profile to estimate the road features after compensating the angle influence
- If this angle is higher than the threshold, or the numbers of the scanlines are not sufficient to demonstrate the road surface on that particular pair of CL points, the program switches to interpolate cross profiles for just that CL segment. In addition, the numbers of those CL points are printed as Fig.15. For example, in this sample cross profiles are derived through CL pair, 9-10, 16-17, and 17-18
- In case of interpolation, the distance between cross profiles is determined by data resolution
- The interpolation of the cross profiles is very time consuming …

```
Scanlines ... Cross profiles ... 9
Scanlines ... Cross profiles ... 16
Scanlines ... Cross profiles ... 17
```

Figure 15: This message shows that cross profiles are interpolated for a pair of CL points

4.3 Road edges extraction

The median and shoulder locations are extracted from profiles by a technique called line fitting. In this procedure, a line with adaptive length is fitted to the points along each profile. This line shifts along the profile with a step corresponding to data resolution. To extract the road median, this line is moved from the inner part of the profile to the outer part, while for extracting the shoulder the line is moved from the outer to the inner edge in order to disregard all kinds of obstacles on the profile. The profiles are also smoothed

temporarily by a low-pass-filter to reduce effects of undesired objects as vehicles. Thereafter, the road edges are revealed based on analyzing the fitting error as if the line with the minimum fitting error and the semi-horizon attitude determines the road edge with accuracy better than data resolutions.

This algorithm is successful in extraction road edges only if the profiles closely represent the prototype of the road cross profile. But, there are lots of obstacles such as vehicles, natural variation, and objects on the road surface that violate this assumption. Fig.16 illustrates profiles with some toothed patterns due to these obstructions. This kind of problem is tried to fix by smoothing the profile, but there are also other situations in which the road edges are calculated inaccurately. Any miscalculation can be considered as a shift respect to centerline axes.

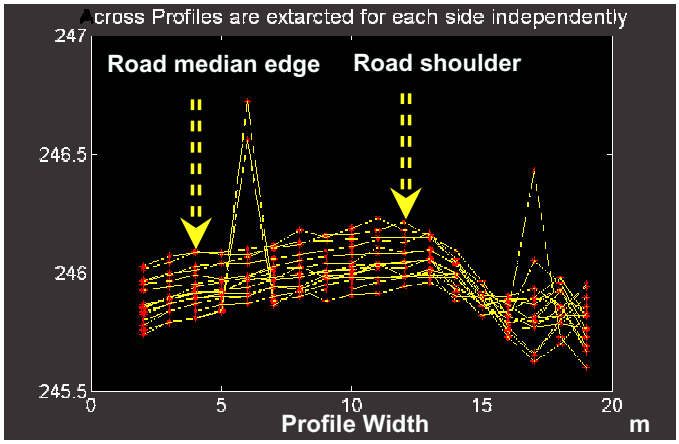

Figre 16: Scanlines represented the natural cross profiles

These shift edges are tracking and fixing in three steps. The first concern is that the road width, the distance between road median and road shoulder, is supposed to change gradually between each pair of centerline points. Therefore, the width between each pair of centerline points is almost kept invariable in order to not satisfy our assumption, but to bridge all possible miscalculations. By this way two average values, road median and road shoulder, are reported for each pair of centerlines as local width. The next concerns are dealing with observing the integrity of the whole road. Fig. 17 shows the overall problem:

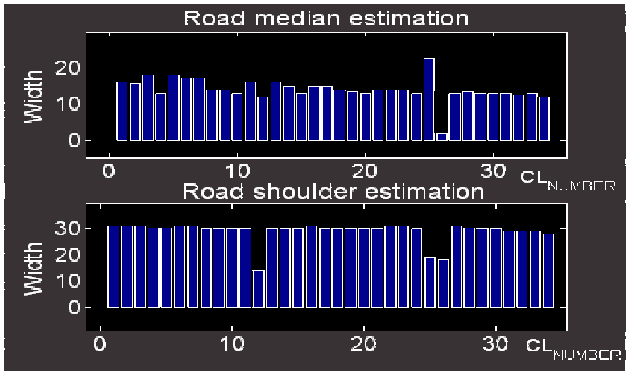

Figre 17 Adjust the road width

As can be seen in Fig. 17, there are still a few local road widths in terms of median and shoulder locations which are out of the range (CL number: 4, 8, 9, 12, 27, 28). The second concern is detecting these outlier estimations. By statistical analysis of the residuals, the values which are out of a defined range, adaptive threshold, are detected and substituted with an average value based on the neighboring estimations. Finally, a low order polynomial smoothes the road edges and provides a continuous form for road boundaries. Totally, the road boundaries of the right and left side are four smooth curves, median and shoulder edges on each side, which are printed and saved in road boundary file.

- The road edges on the Right/Left [R/L] sides are drawn with red and blue color respectively as Fig. 18
- The [R/L] side of a road is defined conventionally in basis of the order that the centerline points are setting up.
- The program saves the road edge results automatically at the file distinguished by [XYZ_file_name.rdb] on the same path.
- If the road is estimated in [A] or [P] mode, it is also saved with different name that is familiar for the program
- Once the road boundary is calculated, it can be always loaded to avoid running this procedure again (Section 4)

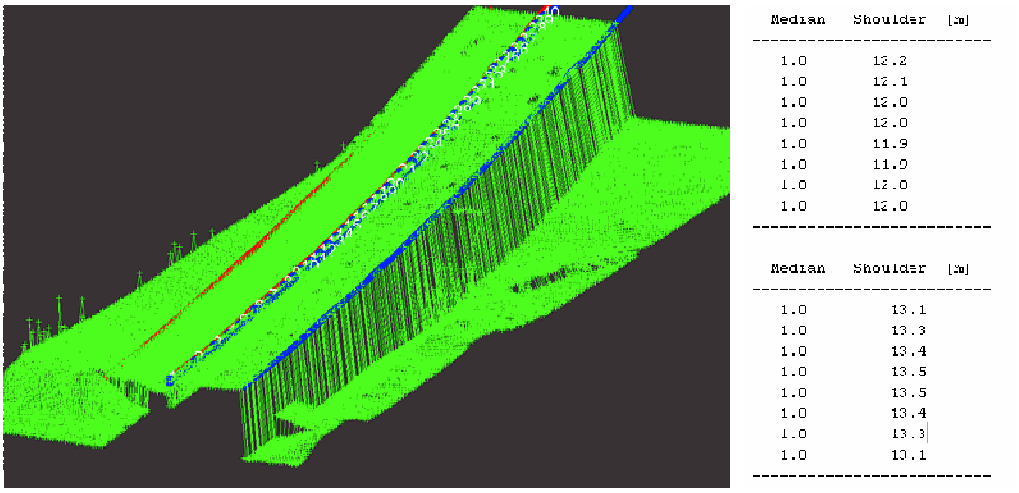

Figure 18 The road edges; right side with red color, and left side with blue color

5. Vehicle Extraction

After extracting the road surface, the right and left sides of the road, Fig. 19, delineate two regions from which the vehicles can be extracted. Vehicles, in the LiDAR context, are considered as structural objects having elevation higher than the local road surface. Therefore, our vehicle extraction algorithm is based on several rules established our knowledgebase system:

- A rational relative height with respect to the road surface
- Alignment with road direction
- A logical distance respect to the median edge

- Semi-rectangular shape
- Non-relationship with other objects
- Appropriate size (length, width, area, and volume)

Several steps are performed to detect and shape discrete point clouds into vehicles.

- If the vehicle procedure is performed before, the operator can load it and skip this step

```
Do you have any a prior Car file ... Press y for [Yes]  :
```

- Once the vehicles are extracted, a vehicle file is saved by the name of [XYZ_file_name.car] on the same path

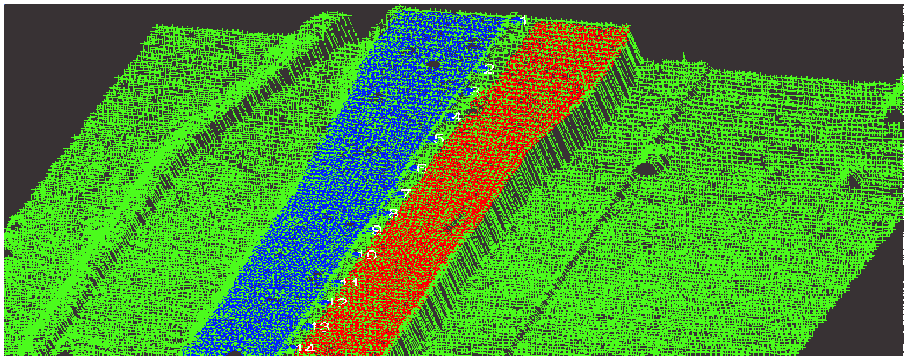

Figure 19 Road surface is ready to extract the vehicles

5.1 Searching candidate vehicle points

An adaptive elevation filter, in basis of plane fitting technique, regularly searches the road surface throughout a virtual grid covering the road area, and detects highest points in each cell. Our strategy to detect merely highest points in each grid is meant extracting those points belonging to vehicles confidently.

- As shown in Fig.20, the grid cells are laid perpendicular to the centerline axes and extended to the road edges from each side

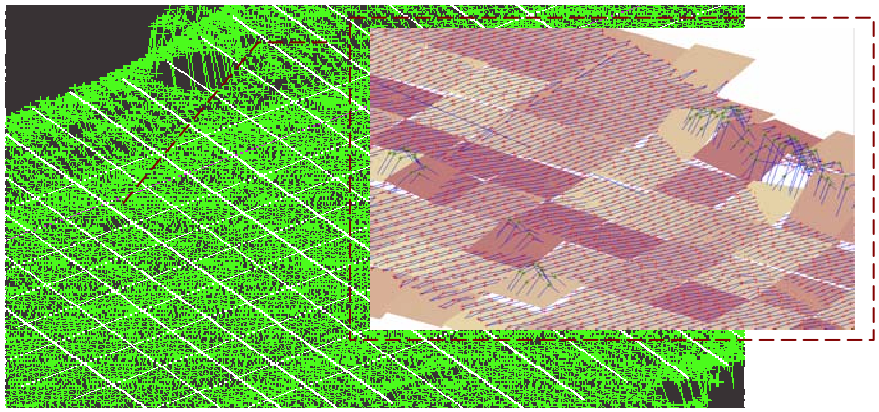

Figure 20 Searching regularly the road surface and detecting raised points

5.2 Cluster the raised points

To distinguish the raised points as individual vehicle object points, these points should be clustered. The clustering procedure is pursued in two steps. First, the clustering begins from each grid cell through the neighboring cells, and second, the clustering searches the further cells adaptively. The last one is adaptive because it is carried on by checking several factors in basis of our knowledge based instantaneously. After these steps, all points have a label and belong to an object as Fig.21.

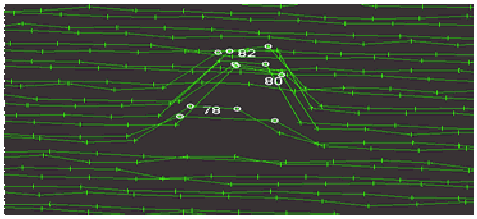

Figure 21: The raised points merge logically and shape individual objects

5.3 Shape the cluster objects

In order to clarify the points certainly belong to the vehicles, the highest points throughout the grid cells were derived and clustered (Fig.21). However, besides these points, there are also other points which should be added to the cluster to form a vehicle. To shape the vehicles, the vicinity of each cluster object is enlarged as Fig. 22. This new region sets up a new search area from which the shape of a vehicle can be "cast". This goal is addressed in the following stages:

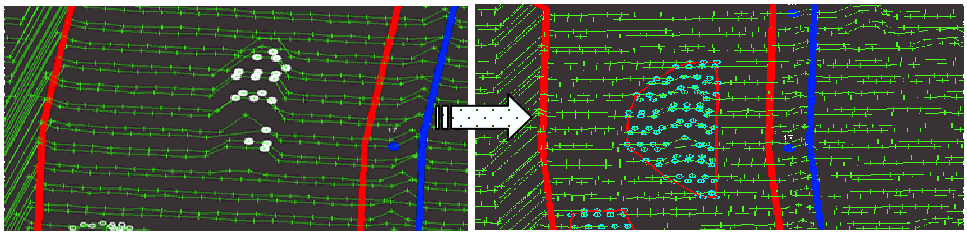

Figure 22: The new vicinity is searched for all points shaping a vehicle

- **Polish the area**

Polishing term in this context is meant to exploit a structural frame from the points in the new search region. To figure the frame out, an adaptive threshold is used to assess the elevation difference between each point and the local road surface. Whether the difference is more than that threshold, that point is considered as vehicle points.

Although by comprising all these points for an object, there are still some other points that shape the entire points set as a vehicle. These points, technically, are not reflected from the car. So far, the location of these points is on the intersections of the vehicle sides and the road surface. The cross profile analysis of the region can expose the location of these points. Fig. 23b illustrates the final form of a vehicle which is exploiting from the search area.

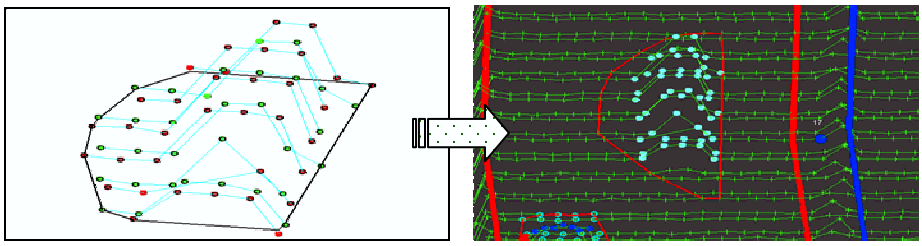

Figure 23: The enlarged area is polished to shape a vehicle

- **Remove non-vehicle objects**

Through all previous processing, there might be several non-vehicle objects extracted and modeled. Based on our experiments, these objects are usually generated close to the road edges, Fig. 24. Analyzing the parameters such as width, length, area, volume, or intensity could also help to detect these objects.

- An ordinary vehicle is recorded with the width about 0.3 – 4 m, length 0.7 – 50 m, and volume 0.5 - 1400 m^3

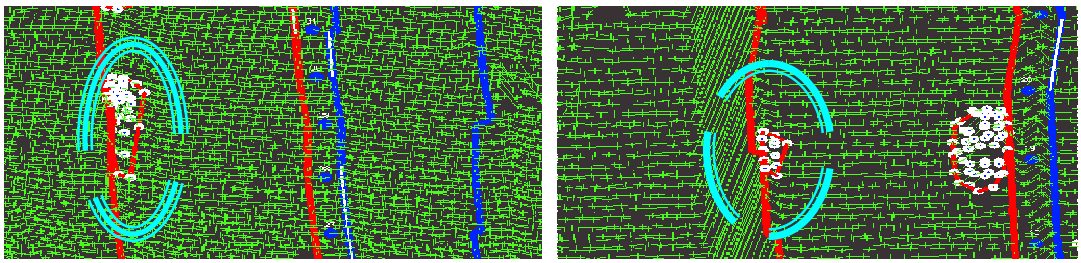

Figure 24: Controlling the vehicle attributes could detect the non-vehicle objects

- **Clean the duplicated and intersected vehicles**

If several vehicles move close to each other, the algorithm might identify them as overlap or intersected vehicles, Fig 25. Therefore, the last step is specified to deal with detecting and fixing these kinds of objects.

- If there are a couple of vehicles with relative distances less than data resolution, at least one of these vehicles would be advertently disregard so that there be individual vehicles
- The program saves automatically the vehicle extraction results in a file distinguished by [XYZ_file_name.car] on the same path. This file can be loaded as vehicle file (Section 5)

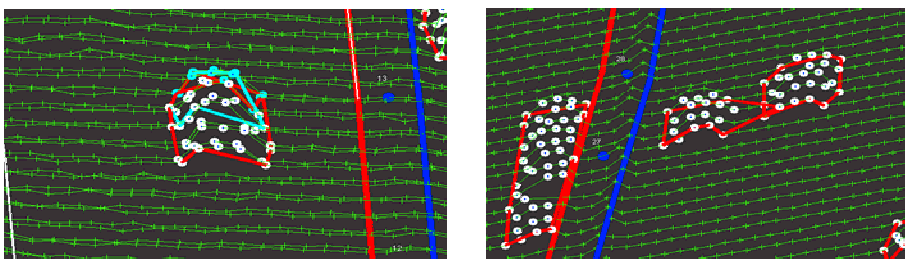

Figure 25: The overlaid objects are cleaned in the last step

6. Vehicle Classification

Four categories are chosen to classify the vehicles: passenger car, 3-axle-truck, 6-axle-truck, and other (multi purpose vehicle). The parameters used to set the object space up include length, width, area and volume called the vehicle parameters. A Principle Component Analysis, PCA is preferred to classify the vehicles. The feature space provided by PCA segments the vehicle parameters into four classes.

The classification performance was tested on different data sets using different coefficients. The results of these experiments determine the best coefficients in classification: Passenger<20, 20< MPV<60, 60<3-axle-Truck<140, and 6-axle-Truck > 140. The operator can always adjust these coefficients while the program is running as Fig.26. Fig. 27 shows the windows appeared after adjusting the new values. In this window the PCA feature space is plotted, and the operator can manually adjust the desire values. However, it is not recommended to change these coefficients if there is no apparent change in the system parameters.

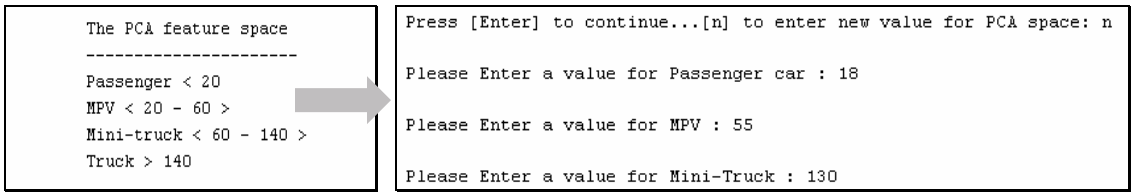

Figure 26: The operator can enter the new values for PCA coefficients

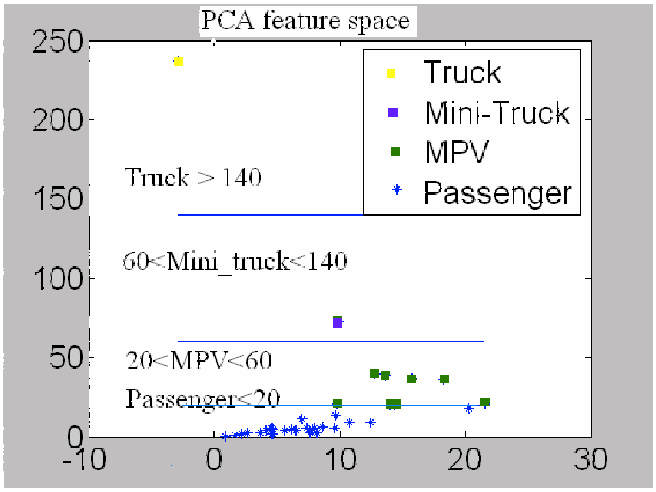

Figure 27 classification of the vehicles into four groups based on PCA

- The passenger cars, P, are plotted by cyan color (Fig. 28)
- The MPV vehicles, M, are plotted by white color (Fig. 28)
- The mini-trucks, B, are plotted by magenta color (Fig. 28)
- The trucks, T, are plotted by yellow color (Fig. 28)
- Changing the PCA coefficients affects directly the vehicle velocity procedure
- The vehicle attributes and vehicle point coordinates are printed, and saved at a file distinguished by [XYZ_file_name.veh] on the same path. The vehicle points are recorded in two forms: the raised points of the vehicle and all points shaping it

Num	Length	Width	Area	Volume	CL_Dist	Side	Type
1	3.0	2.6	4.5	6.1	12.4	R	P
2	3.4	3.3	6.3	3.3	13.1	R	P
3	13.7	3.2	37.9	262.6	13.9	R	T
4	12.7	3.4	38.6	244.6	11.8	R	T
5	13.9	3.4	42.7	195.0	9.6	R	T
6	3.0	2.6	6.6	1.6	8.4	R	P
7	7.3	3.4	20.3	119.6	8.3	R	B
8	7.3	3.1	19.4	104.9	12.1	R	B
9	3.3	3.0	5.6	3.6	8.3	R	P
10	9.0	3.5	26.8	82.1	12.2	R	B
11	3.1	2.7	5.1	2.4	11.8	R	P

Num	Z_Base	Azimuth [DegMin.Sec]	CL_Number	Inter.Angle [Min.Sec]
1	296.2	8639.5	19	5.5
2	297.0	9919.3	37	-8.3
3	298.0	9527.1	52	-4.3
4	298.2	9159.6	59	-0.5
5	298.1	8359.5	62	7.3
6	297.9	8410.3	65	7.2
7	297.7	8534.5	68	5.5
8	297.5	8627.2	73	6.1
9	297.4	9057.6	73	6.1
10	296.9	9151.2	85	0.3
11	296.7	9053.1	88	1.3

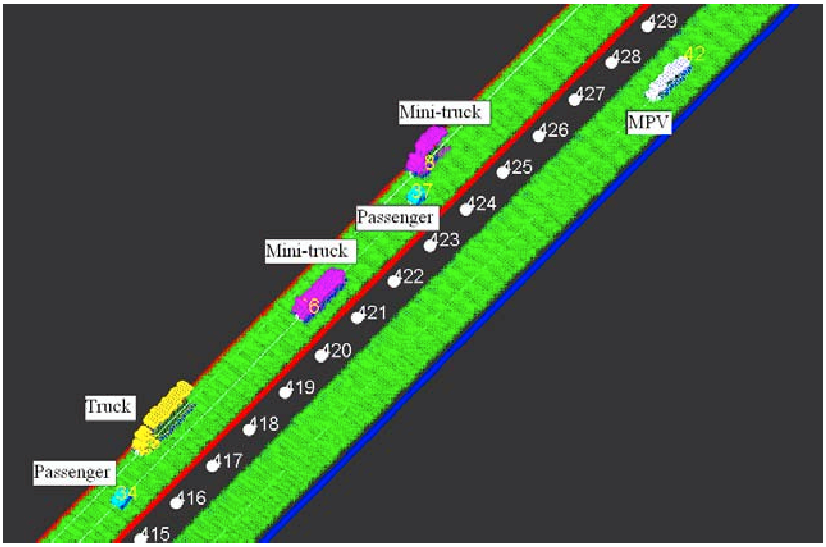

Figure 28 classification of the vehicles into four groups based on PCA

7 Velocity estimation

During data capturing, due to the continuous scanning of the platform, the vehicles record shorter or longer than their original size depending on the relative motion direction. This variation helps us to determine the vehicle velocity. Through the four vehicle categories, the passenger cars and trucks have almost known size. Therefore, velocity estimation algorithm is in based on analyzing the passenger and truck size variations (particularly the length component). Apparently, if there were no passenger or truck vehicles, the velocity couldn't be estimated. Indeed, besides the length, there are several other information needed to estimate the general velocity value:

- The average length and standard deviation of passenger car market share in The USA is about: $\mu = 4.68 \quad m, \quad \sigma = 0.35 \quad m$
- The average length and standard deviation of truck market share in The USA is about: $\mu = 23 \quad m, \quad \sigma = 2 \quad m$
- The individual speed of each vehicle is usually not of interest, as mainly the average velocity of a group of vehicles is needed to obtain traffic flow data

- **LiDAR platform direction**

As it can be seen from Fig.29, the average azimuth derived from coordinates of middle points of scanline is used to estimate the platform direction. The yellow points on the Fig.27 indicate the location of middle points of the scanlines in the instance.

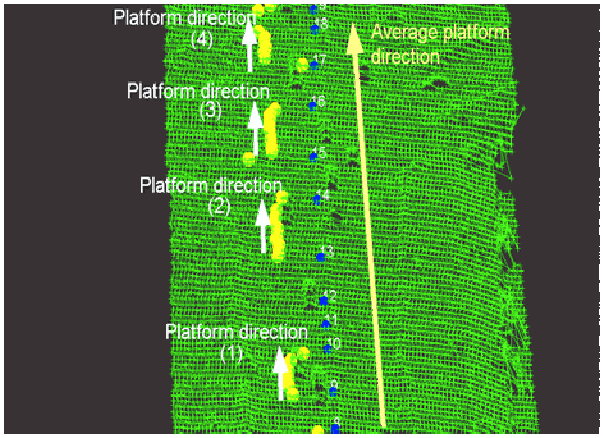

Figure 29 The LiDAR platform direction

- **Alongside direction**

Provided the sensor flies parallel to the road, on the alongside direction the vehicles appear longer than the original size. Consequently, a simple evaluation of the average lengths of a prototype car passing on the two sides of the road, Fig. 30, can expose the alongside direction.

- Statistically, a hypothesis test confirms the meaningful of average lengths
- The truck sizes is also confirmed the alongside direction
- To visualize the alongside direction If the alongside direction is on the right side, the color of the centerline points is chosen as red color, and for left side, the color will be turned to blue (section 4.3)
- There might be cases in which there is no passenger car or truck on one of the road side. In this case, the alongside direction cannot be estimated [R/L]. Under this situation, the velocity still can be estimated.

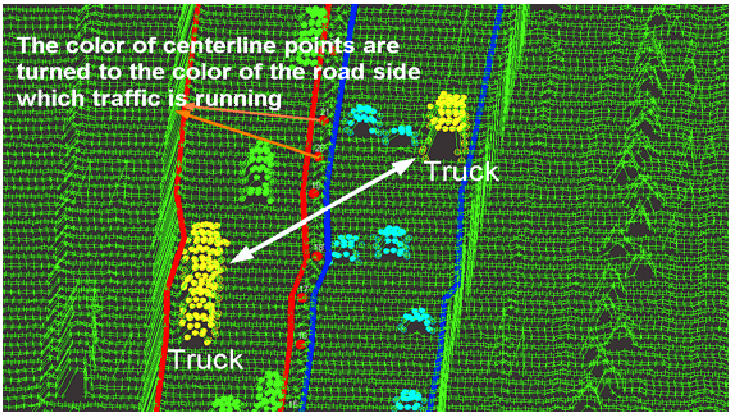

Figure 30 The alongside direction is determination in basis of average length

- **Intersection angle of platform and vehicle directions**

The angle between platform (or scanline) and vehicle affects the velocity magnitude. As can be seen from Fig 31, if the platform flies parallel to the road direction, the intersection angle is almost appeared as a right angle. Fig. 32 shows another sample data with information needed to calculate the intersection angle.

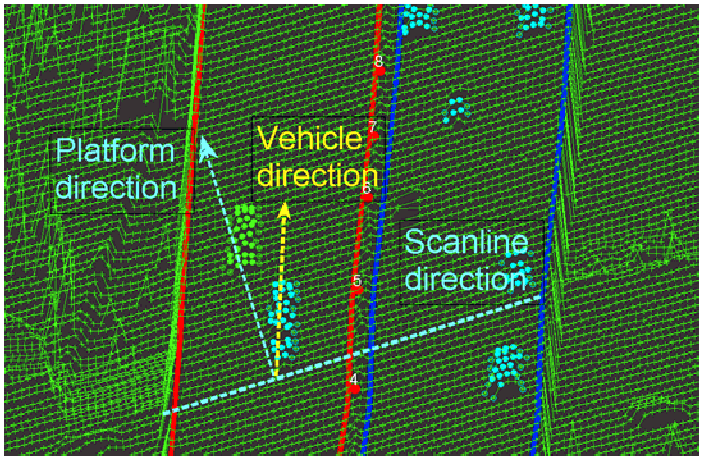

Figure 31: Intersection angle (deviation from right angle)

```
The centerline direction is: [ 268.43 ] Deg
The platform direction is: [ 219.60 ] Deg
The Again Direction is [ Right ] side
The Intersec. angle between Vehicle and LiDAR direction: [ 21.25 ] Deg
```

Figure 32: A prototype report about velocity determination

Once the stated parameters are provided, the general velocity can be estimated. Equation 2 discusses velocity estimation based on the intersection angle between platform and vehicle directions, θ, the actual size of the vehicle, *s*, and the measured size of the vehicle, *m,* in two different scenarios: alongside and againstside direction.

$$V_{Vehicle} = \frac{m-s}{m\cos(\theta)} V_{LiDAR}\Big|_{along} \quad , \quad V_{Vehicle} = \frac{s-m}{m\cos(\theta)} V_{LiDAR}\Big|_{against} \qquad (2)$$

Fig.31 illustrates a prototype report on statistical analysis of velocity estimation in basis of two types of the vehicles, passenger car and truck, respectively. The first column shows the calculated velocity, the second column is the number of extracted cars, the third is the number of the cars which are well-matched with the model in eq. 2. Indeed, the program uses this group of vehicles to estimate the velocity. The forth column shows the standard deviation of the velocity estimated, and the last is the error propagation model in basis of eq. 2. As can be seen in Fig. 33, due to lack of enough number of the passenger cars on the right side, the corresponding velocity isn't calculated. The same situation is happened for the left side of the road, where there is no truck. The final result is provided by getting average from general velocity derived by passenger cars and trucks.

```
        Vel.[mile/h]    #P    #P[used]   std(Vel)[mile/h]   Error[mile/h]
       --------------  -----  --------   ----------------   --------------
Right:        5.0         3        1            0.0          20.6  Acceptable
 Left:       62.1        20        8           13.0          16.7  Acceptable

        Vel.[mile/h]    #T    #T[used]   std(Vel)[mile/h]   Error[mile/h]
       --------------  -----  --------   ----------------   --------------
 Right:       77.0         1        1            0.0           4.2  Acceptable
  Left:        1.0         0        1           50.0          50.0   Unacceptable

 Final   Vel.[mile/h]    std(Vel)[mile/h]
       --------------  ----------------
 Right:       77.0             4.2
  Left:       62.1            16.7
```

Figure 33: Velocity estimation in basis of passenger cars, P, and trucks, T

- The operator must enter the platform velocity, V_{LiDAR}

```
Lidar Sensor Velocity  [m/s] :
```

- If the operator press [Enter] key in response to above question, the previous entered value is loaded automatically
- Provided the alongside direction is not concluded, [R/L], there is still the chance of velocity estimation based on the existed information.
- The vehicles are also sorted into related lanes based on the lane width of 2.7 m. Fig. 34 shows an example of a prototype data set in which the vehicles types on each lane plus the distance of that lane with respect to CL axes is reported

```
The Vehicle types are [ PPPPPPPP ]
The mean CL_Distance of the lane [1] is [ 3.99 ]

The Vehicle types are [ PPPPP ]
The mean CL_Distance of the lane [2] is [ 6.59 ]

The Vehicle types are [ PPPPMPPP ]
The mean CL_Distance of the lane [3] is [ 10.29 ]
```

Figure 34: The vehicles are placed in different lanes

- The default lane width can be adjusted in the macro [Divided_Side_To_Lane]
- If the number of vehicles in each lane is great enough, the general velocity can be calculated for each lane particularly. Fig.35 shows an example of calculation the velocity for different lanes on the right and left side of a road.

```
Velocity [ Right ] side at Lane [ 1 ] : 48.0 mile/h
Velocity [ Right ] side at Lane [ 2 ] : 53.0 mile/h
Velocity [ Right ] side at Lane [ 3 ] : 41.0 mile/h

Velocity [ Left ] side at Lane [ 1 ] : 65.0 mile/h
Velocity [ Left ] side at Lane [ 2 ] : 31.0 mile/h
Velocity [ Left ] side at Lane [ 3 ] : 62.0 mile/h
```

Figure 35: velocity estimation in basis of vehicles located on different lanes

- The lane velocity is applicable only if it is in the border of the average speed
- The velocity error is also calculated and reported for different lanes
- Generally, the velocity error of againstside is larger than the alongside direction
- If the number of vehicles on any side of the road is not enough to estimate the velocity, the operator can always enter a value as the velocity for that side, or set it equal to the calculated velocity of the opposite side, Fig. 36.

```
------------------------------------------------------------------------
The velocity of [Left] side cannot be determined ...
To estimate the flow parameter, it is needed to have a velocity value
Do you want to use the velocity of the [Right] side [Yes] , [No] ? n

Please enter the right velocity value [mile/h]: 60

------------------------------------------------------------------------
```

Figure 36: If there is no vehicle, the velocity can be entered by operator

8 Traffic flow estimation

Once all vehicles have been successfully extracted from the road region, sorted into their own lanes, classified, and their general velocity have been calculated, the traffic stream is ready to evaluate for each lane in terms of density and flow.

- **Density Parameter**

Traffic density is defined as the number of the vehicles present over a unit length at a given instant time. So, the next step is to calculate the average space of vehicles along a given lane. On the other hand, density is primarily calculated for each lane separately. For the left and right side, the summation of densities from all lanes of each side provides the final density estimate. Eq. 3 shows the model of density estimation:

$$D = \sum_{j=1}^{L} \left(\frac{n_j}{\sum_{i=1}^{n_j - 1} S_i} \right) \qquad (3)$$

where, L is the number of road lane on each side, n is the number of vehicles on the lane, and S is the distance between the vehicles moving in the same direction. Furthermore, this distance is measured between corresponding points (front to front) of consecutive vehicles.

- The density error is also calculated and reported for each lane

- **Flow Parameter**

Flow can be defined as the number of vehicles passing a given point during a given period of the time, typically one hour.

$$Flow = Density * Velocity \quad (4)$$

By multiplying the density of each lane with corresponding velocity, the flow is calculated for that lane. For the left and right side, the summation of flows from all lanes of each side provides the final flow estimate. Fig.37 shows the final report of traffic stream parameters.

- The traffic flow error is usually larger on against side direction

Density at Lane(1) :	58	+ -	0.1	[Vehicle/mile]
Density at Lane(2) :	87	+ -	0.1	[Vehicle/mile]
Density at Lane(3) :	74	+ -	0.1	[Vehicle/mile]
Flow at Lane(1) :	2581	+ -	873.0	[Vehicle/hour]
Flow at Lane(2) :	4089	+ -	1309.5	[Vehicle/hour]
Flow at Lane(3) :	3478	+ -	1113.8	[Vehicle/hour]

Density at Lane(1) :	66	+ -	0.1	[Vehicle/mile]
Density at Lane(2) :	44	+ -	0.2	[Vehicle/mile]
Density at Lane(3) :	66	+ -	0.2	[Vehicle/mile]
Flow at Lane(1) :	3498	+ -	487.3	[Vehicle/hour]
Flow at Lane(2) :	2200	+ -	325.0	[Vehicle/hour]
Flow at Lane(3) :	3399	+ -	487.3	[Vehicle/hour]

```
------------------------------------------------------------------------
The Density on the Right side:  176 + - 0.289,    [Vehicle/mile]

The Density on the Left side:  219 + - 0.217,    [Vehicle/mile]

The Flow of the Right side:     9097  + -  761.96,     [Vehicle/hour]

The Flow of the Left side:     10148  + -  1928,     [Vehicle/hour]
------------------------------------------------------------------------
```

Figure 37 The final report includes the density and flow parameters as well as corresponding errors values